FEB 27 1986
830-H-14
NAS 1.26:175005
COMPLETED
143.

NASA Contractor Report 175005

Aerodynamic Properties of Turbulent Combustion Fields

ORIGINAL

Chia-Chun Hsiao and A.K. Oppenheim
University of California, Berkely
Berkely, California

November 1985

Prepared for the
Lewis Research Center
Under Grant NAG 3-131

NASA
National Aeronautics and
Space Administration

ABSTRACT

Flow fields involving turbulent flames in premixed gases under a variety of conditions are modeled by the use of a numerical technique based on the random vortex method to solve the Navier-Stokes equations and a flame propagation algorithm to trace the motion of the front and implement the Huygens principle, both due to Chorin. A successive over-relaxation hybrid method is applied to solve the Euler equation for flows in an arbitrarily shaped domain. The method of images, conformal transformation, and the integral-equation technique are also used to treat flows in special cases, according to their particular requirements.

Salient features of turbulent flame propagation in premixed gases are interpreted by relating them to the aerodynamic properties of the flow field. Included among them is the well-known cellular structure of flames stabilized by bluff bodies, as well as the formation of the characteristic tulip shape of flames propagating in ducts. In its rudimentary form, the mechanism of propagation of a turbulent flame is shown to consist of (i) rotary motion of eddies at the flame front, (ii) self-advancement of the front at an appropriate normal burning speed, and (iii) dynamic effects of expansion due to exothermicity of the combustion reaction. An idealized model is used to illustrate these fundamental mechanisms and to investigate basic aerodynamic features of flames in premixed gases.

The case of a confined flame stabilized behind a rearward-facing step is given particular care and attention. Solutions are shown to be in satisfactory agreement with experimental results, especially with respect to global properties such as the average velocity profiles and reattachment length. Velocity fluctuations are found to compare quite well with experimental data, exhibiting discrepancies which can be plausibly ascribed to three-dimensional effects and the scarcity of the numerical data sample. The unconfined turbulent flow behind a circular flameholder is calculated to study the detailed mechanism of flame stabilization. The process of vortex shedding and the development of the Von Karman vortex street at a high Reynolds number are described in terms of the vorticity field and the instantaneous streamline pattern. Although the flame front is stabilized on the outer contours of eddies, the classical alternating large scale structure of the wake is destabilized by the expansion due to the exothermicity of combustion. The parametric study of flame propagation indicates that the flame spread and the burning rate are relatively insensitive to the Reynolds number in the range under consideration, whereas the product of the normal burning speed and the normalized density ratio increment across the front, expressing the action of the flame as a velocity source, is of crucial importance.

Acknowledgement

The authors wish to express their gratefulness to Professor Alexandre J. Chorin for his generous advise and many valuable suggestions, and to Professor Ahmed F. Ghoniem for the valuable help he provided in the course of this work. They are also most appreciative of the guidance they received from Dr. Cecil John Marek, the Director of the program at NASA Lewis Research Center, under which the project was supported as Grant NAG 3-131. Additional support for this work was also received from the Office of Energy Research, Office of Basic Energy Science, Engineering, Mathematics, and Geosciences Division of the U.S. Department of Energy under Contract No. DE-AC-03-76SF00098.

TABLE OF CONTENTS

NOMENCLATURE v

1. Introduction 1

2. Numerical Model 8

  2.1 Turbulent Non-reacting Flows 8

    2.1.1 Solutions of the Euler Equation 10

      2.1.1.1 Method of Images 11

      2.1.1.2 Conformal Transformation 11

      2.1.1.3 Integral-Equation Methods 13

      2.1.1.4 Finite-Difference Methods 15

        2.1.1.4.1 The Cloud-in-Cell Method 15

        2.1.1.4.2 The Successive Over-Relaxation Method 16

    2.1.2 Viscous Effects 21

      2.1.2.1 Diffusion Equation and Random Walk 22

      2.1.2.2 Vorticity Generation at Boundaries 23

  2.2 Turbulent Reacting Flows 25

    2.2.1 Flame Front Location: the SLIC Method 26

    2.2.2 Self-Advancement and Huygens Principle 26

    2.2.3 Velocity Field of Reacting Flows 27

3. Rudiments of Flame Aerodynamics in Premixed Gases 30

  3.1 Three Fundamental Mechanisms 31

  3.2 Flame Propagation in a Duct with Closed End 36

4. Confined Flame: A Turbulent Flame Stabilized Behind a Rearward-Facing Step 41

  4.1 Configuration and Computation Parameters 44

  4.2 Vorticity Field 46

4.3 Flame Development 47
4.4 Mean Velocity Profiles 48
4.5 Reattachement Length 49
4.6 Turbulence Intensities 50
4.7 Conclusions 53
5. Unconfined Flame: A Turbulent Flame Stabilized by a Circular Flameholder 55
5.1 Numerical Parameters and Formulations 57
5.2 Vorticity and Flow Development 61
5.3 Vortex-Shedding Process 62
5.4 Streamlines, Pathlines and Streaklines 64
5.5 Flame Development 65
5.6 Conclusions 67
Figures 69
References 119

Nomenclature

A_t : Area

a : coordinate of a point on the real axis of the ζ - plane

α : radius of a cylinder

b : coordinate of a point on the real axis of the ζ - plane

c : coordinate of a point on the real axis of the ζ - plane

D : molecular diffusivity

d : diameter of a cylinder

F : differential transformation function

f : volume fraction of burned gases in a cell

G : Gaussian distribution function

H : width of the duct

h : mesh size

I : number of grid points in x - direction

i : $\sqrt{-1}$

J : number of grid points in y - direction

K : coefficient of transformation function

k : thermal conductivity

k : turbulence kinetic energy

Le : Lewis number, defined as D / k

M : total number of grid points for finite-difference calculation

N : total number of vortex elements

n : unit normal vector

P : pressure

p : coordinate of a point on the surface of a bluff-body

q : coordinate of a point outside the body

Re : Reynolds number, defined as Ul/ν

r_f : position vector of flame front

r_o : core radius of a vortex blob

r_s : core radius of a source blob

S_u : laminar flame speed

s : unit vector tangential to streamline

T : nondimensional time

Δt : nondimensional time step

U : mean velocity

u : velocity vector

u : velocity component in x - direction

V : density ratio across flame front

v : velocity component in y - direction

W : complex velocity

x : x - coordinate in the physical plane

y : y - coordinate in the physical plane

z : $= x + i\,y$, complex coordinate

α : an interior angle of a polygon in the physical plane

β : an interior angle of a polygon in the physical plane

Γ : strength of a vortex

γ : an interior angle of a polygon in the physical plane

Δ : strength of a source blob

δ : boundary-layer thickness

ε : local rate of expansion

ζ : complex coordinate in the transformed plane

η : random displacement

ϑ : angle measured counter-clockwise from x - axis to the tangent of the wall

λ : a parameter used to determine the over-relaxation coefficient

ν : kinematic viscosity

ξ : vorticity

ρ : density

σ : standard deviation

Φ : velocity potential

φ : equivalence ratio

Ψ : stream function

ω : over-relaxation coefficient

subscript

b : burned medium

c : combustion

f : flow field

i : x index of grid point

j : y index of grid point

k : index of grid point along the wall

max : maximum value

n : normal component

p : potential component

s : effect due to source blobs

u : unburned medium

v : effect due to vortex blobs

w : value at wall

∞ : value at infinity

superscript

n : index of time step

$*$: conjugate of a complex number

o : degree

$'$: fluctuation

CHAPTER 1

Introduction

Turbulent reacting flows have attracted lots of attentions in recent years. This is because that they not only involve all kinds of chemical reactions, energy transports and complicated fluid mechanical turbulence, thus making them challenging, but also because there are still a number of unresolved problems in this field due to the complicities. In premixed turbulent combustion, the thermal conduction and diffusion from the hot products to preheat the reactants can be augmented both indirectly by distortion of flame surfaces and directly by turbulent mixing. The mean reaction rate is thus more strongly influenced by the turbulence than by chemical kinetics factor, so that premixed turbulent combustion is primarily a complex fluid mechanical problem.

Ever since Damkohler's (1940) classical theoretical and experimental study of turbulent flames in premixed gases, the wrinkle laminar flame idea, which considers large-scale turbulence as simply distorting the flame without affecting its structure or propagating speed, has been playing a very important part in today's research of turbulent flame. When the radius of curvature of a steady distorted flame is considerably larger than the width of the thermal structure of the flame, a flame model which simply treated the flame as a hydrodynamic discontinuity of density and assumed that the propagating speed relative to the gas along the flame did not vary, has been proposed (Landau, 1944, Sivashinsky, 1976), the latter studies a number of flame problems with great deal of success.

Vortex method was used to calculate inviscid flows at the early stage (Rosenhead, 1931, Takagi, 1964, and Clements, 1973). Later, it was developed (Chorin, 1973) to include the viscous effect by vorticity generations at boundaries and random walks to simulate the diffusion process in a statistical sense. Without resorting to closure modeling of turbulence and introducing numerical diffusivity by traditional finite-difference method, the random vortex method is able to compute the evolution and interaction of he turbulent flow field at high Reynolds number. It has thus been used to calculate the two-dimensional turbulent flows quite successfully (Ashurst, 1979, Cheer, 1982, Ghoniem et al, 1982, Chen et al, 1983 and Hsiao et al 1984).

Since the diffusion equation is adroitly handled by random walks of vortex elements, the remained problem is the solving of the Euler's equation. The vorticity of the flow field is represented by a number of vortex blobs. There are many ways of finding the velocity field induced by vortex blobs in a specific domain. Some examples of the methods used to handle the zero normal velocity condition will be outlined and discussed in our numerical model. Their applicability to different flow configurations and evaluations of each method will also be given.

To preserve the grid-free principle of the vortex method, the method of images, conformal transformation and the integral-equation method can be applied to solve the inviscid flow field without imposing grids in the computational domain. The velocity fields are found by direct interactions of all vortex blobs. The computational time is thus proportional to N^2, where N is the number of vortex elements. For most practical cases, transformation functions have to be evaluated by complicated numerical integration and the source-density functions of the integral-equation method along body surfaces also have to be determined by solving a set of linear algebraic equations. These not only bring additional difficulties and errors into the numerical method, but also increase computational efforts dramatically.

A most straightforward way to deal with all kinds of geometries is the finite-difference method. The so-called fast Poisson solvers (Buzbee et al, 1970, Swarztrauber et al, 1975) are frequently used to find the stream functions or velocity potentials at grid points. The velocities can then be obtained by differentiation and interpolation. Since the existing numerical codes in solving Poisson equation can not be very generally applied to any flow domain, the successive over-relaxation method is suggested here to solve the Poisson equation in arbitrary-shape domain because of its easiness of programming and the competitive efficiency.

Recently, Oppenheim and Ghoniem (1983) were able to deduce three fundamental mechanisms of turbulent flame propagation, including rotary motion of eddies with different length scales, flame advancement in the normal direction, and volumetric expansion due to exothermicity, from many interesting flame phenomena in premixed combustion. These three mechanisms are also the basic components governing flame propagation in our numerical model. The interaction between flame fronts and turbulent eddies can result in the distortion of the flame, so that the surface area is markedly increased. On the other hand, the entrainment mechanism of the recirculation zone or large-scale structures can enhance the mixing by bringing more fresh reactive mixtures into products. The result is an increase in the reaction rate. While the volumetric expansion due to combustion reaction not only modifies the flow field, such as the reduction of the recirculation zone and the divergence of streamlines outside flame boundaries, but also changes the flame shape by the feedback action of local velocity.

Flame propagation in a closed volume has somehow different natures from that in an open volume. The former is always accomplished by a continuous rise of system pressure. This will cause a temperature rise in the mixture so that the reaction rate or flame propagation speed also increases. The compression of the reactive mixtures and the flow field generated by the combustion can result in several very interesting phenomena of flame deformation. The cause of the so-called "tulip" shape flame in an enclosed duct is still an unresolved problem. By assuming a slowly propagating flame so that the pressure rise in the enclosed vessels can be instantaneously balanced over the entire volume, Sivashinsky (1979) was able to derive a hydrodynamic theory to describe a centrally-symmetric flame in an enclosed volume. Majda and Sethian (1984) also accomplished a theory of zero-Mach-number combustion using a different approach. They applied it to study the flame propagation of the swirling flow inside a square vessel.

Unfortunately, these theories have not been able to apply to problems which will demonstrate certain interesting features of flame propagation in a closed domain, such as the deceleration of the flame motion, the deformation of flame shape and the detailed flow field result from the reaction. Before proceeding to a more complete theory or a detailed numerical model, we will use an ideal potential flow model in Chapter 3 to present , we think, the essence of the cause of the tulip-shape flame from a purely hydrodynamic point of view. The individual or combined effects of the three fundamental mechanisms of flame propagation will be used to illustrate the interpretation.

The turbulent shear layer behind a rearward-facing step in a channel has been extensively investigated for both reacting and non-reacting flows in connection with their significance for a number of practical engineering systems and the simplicity of the case where the separated flow region is fixed. Summaries of experimental studies of non-reacting flows with this specific geometry can be found in the review papers by Eaton & Johnson (1981) and Durst & Tropea (1982). Some numerical solutions of this flow configuration can be also found in the publications of Durst & Rastogi (1979), Ashurst (1979), Ghoniem et al (1982), Dai et al (1983) and Walterick et al (1984). Many things have been learned about the two-dimensional mechanism of flow separation and reattachment. The existing data of mean flow properties and turbulence characteristics of such flows, although still spread out a finite range, are sufficiently satisfactory to compare with other kinds of flows and to be used for checking numerical models and computer codes.

The study of the reacting flow for a rearward-facing step combustor was first performed by Ganji & Sawyer (1980) using high speed schlieren photography. They discovered that the reacting flow is dominated by large scale coherent structures in mixing layers. Pitz & Daily (1983) then measured the detailed flow properties and turbulence statistics up to the fourth moment. They found a shift of the peak positions of the turbulence intensity profiles toward the recirculation zone and a reduction of the reattachment length for reacting flow. The streamwise velocity PDFs were also shown to be double-peaked in the reacting shear layer near the step. Meanwhile, Ghoniem et al (1982) developed a numerical model using random vortex method and a flame propagation algorithm by Chorin (1980) to simulate the turbulent flow field behind the rearward-facing step. They obtained a qualitative description of the large scale structure of the turbulent flow as well as the salient feature of the flame front in agreement with the experimental results obtained by Ganji & Sawyer.

Since the upstream flow conditions have been found to have a significant effects on the flow development behind the step, the computational domain is extended to cover the contraction inlet section for a more complete simulation of the experiment. The mean flow velocities and turbulence intensities will be computed in addition to the development of vorticity field and flame fronts. The comparison between numerical results and experimental data will also be carried out.

A circular cylinder is the simplest geometry of bluff bodies. The investigation of the wake behind a cylinder have been done on flows at different Reynolds numbers (Taneda, 1952, Roshko, 1961, Gerrard, 1966, Mair & Maull, 1971 and Perry et al, 1982). A recent experimental study by Cantwell & Cole (1983) gave detailed entrainment and transport processes in the near wake region at very high Reynolds number. However, the vortex-shedding mechanism in the formation zone behind the cylinder is still not well understood.

Flame stabilized by a rod holder is also an extensively studied subject (Peterson & Emmons, 1961, Cheng & Ng, 1983, Katsuki et al, 1983 and Yoshida & Tsuji, 1984) in combustion area. Beside all the turbulence statistics, the flame stability and turbulence-combustion interaction seem to be the two most frequently studied topics. It was conjectured that the vortex-shedding process in the near wake region triggers the wrinkles of flame front downstream.

The connection between the study of non-reacting flow and reacting flow in the wake region is poor. Owing to the lack of proper flame model, most research works of this subject have been concentrating on the experimental measurement of velocity, temperature and density fluctuations (Kilham & Kirmani, 1979, Susuki et al, 1979 and Dandekar et al, 1982). Their results, although quantitative in nature, are insufficient to the understanding of the mechanism of flame wrinkling and turbulence-combustion interaction. It has been suggested that the qualitative features of the flame shown by flow visualization would be useful to explore the possible interrelationship between the flame structures and the observed behavior of the turbulence statistics and correlations.

Our numerical model, being capable of simulating large scale structures in the flow field and providing a phenomenological description of the flame shape and flame-flow interaction, seems to be a proper tool in serving a link between the quantitative measurements and the observed flame structures. In Chapter 5 the detailed investigation of the flow development and vortex-shedding process for non-reacting flow is conducted, first, to demonstrate the flow phenomena in the wake region. The flame front which starts from the rear stagnation point of the cylinder follows the motion of turbulent eddies and advances into its normal direction in the meantime. The volumetric expansion, which is a major factor of modifying the flow field, is also counted. The resulting flame front and flow field due to the combined effect of these three fundamental mechanisms can certainly let us proceed to the further understanding of the unconfined flame stabilized by a circular cylinder.

Chapter 2

Numerical Model

The numerical model used here is in principle based on that developed by Ghoniem et al (1982) in the paper studying turbulent flow in a combustion tunnel. The model uses random vortex method to calculate turbulent flows and is currently applied to two-dimensional cases only, thus an important vorticity-maintenance mechanism in turbulence known as vortex stretching is absent in our analysis. To investigate the aerodynamic features of the turbulent combustion, the flame front is treated as an infinitely thin interface separating incompressible premixed reactants from the products. The normal burning speed along flame front is assumed to be as a prescribed constant. Effects of chemical kinetics and flame structure are therefore not taken into account. Turbulent transport and flame propagation are linked together by the velocity field. Flame front is convected by the local velocity while the dynamic effect due to exothermicity of combustion is modeled by volumetric sources located along flame fronts according to amount of burning to augment the flow field.

2.1. Turbulent Non-reacting Flows

Turbulent flows have been studied for more than a century, but no general approach to the solution of problems in turbulence exists (Tennekes & Lumley, 1970). However, equations which are used to describe the turbulence in fluids are generally accepted to be continuity equation and

Navier-Stokes equation. In two-dimensional incompressible fluids they can be expressed in the non-dimensional form as

$$\nabla \cdot u = 0 \tag{2.1}$$

$$\frac{Du}{Dt} = -\nabla p + \mathrm{Re}^{-1} \nabla^2 u \tag{2.2}$$

with boundary condition

$$u = 0 \tag{2.3}$$

where u is velocity, p is pressure and Re is Reynolds number, while D/Dt is material derivative, ∇ is del operator and ∇^2 is the Laplace operator.

In most turbulent-flow calculations, the Reynolds number is usually so large that traditional finite-difference method is difficult to apply especially near boundaries where velocity gradients are large. The random vortex method which involves the simulation of the process of vorticity generation and disposal, developed by Chorin (1973), has been found to be able to overcome these problems and calculates turbulent flows of high Reynolds numbers with plausible accuracy without resorting to closure models. Governing equations under consideration are vorticity transport equations

$$\frac{D\xi}{Dt} = \mathrm{Re}^{-1} \nabla^2 \xi \tag{2.4}$$

and

$$\nabla^2 \Psi = -\xi \tag{2.5}$$

$$u = \frac{\partial \Psi}{\partial y} \quad ; \quad v = -\frac{\partial \Psi}{\partial x} \tag{2.6}$$

where $\xi = \nabla \times u$ is vorticity and Ψ is stream function.

The solution procedure of above equations is based on fractional steps, according to which the vorticity equation can be split into a sum of convection component (the Euler equation) and diffusion component (diffusion equation). The result obtained by adding up solutions to these two equations in succession has been proven to converge by Chorin et al (1978) and Hald (1979).

2.1.1. Solutions of the Euler Equation

Inviscid flow field is solved by discretizing the vorticity field into a number of vortex blobs. To get rid of the singularity at the center of a point vortex, the vorticity of each blob is constructed to have small but finite support. The motions of vortex blobs are described by the inviscid Euler equation

$$\frac{D\xi}{Dt} = 0 \quad or \quad \frac{\partial \xi}{\partial t} + (u \cdot \nabla)\, \xi = 0 \tag{2.7}$$

and

$$\nabla^2 \Psi = -\xi \tag{2.8}$$

In an infinity flow domain without any boundary, the velocity field can be easily found by summing up all velocities induced by vortex blobs according to Biot-Savart's law

$$u_v - i\, v_v = \sum_{j=1}^{N_v} \frac{i\Gamma_j}{2\pi} \frac{|z - z_j|}{\max(|z - z_j|, r_o)} \frac{1}{(z - z_j)} \tag{2.9}$$

where $i = (-1)^{1/2}$, $z = x + iy$ and r_o , Γ_j are the core radius and the strength of the vortex blob respectively. In most practical cases, however, rigid walls exist in the flow domain. The zero normal velocity condition

$$u \cdot n = 0$$

has to be satisfied at boundaries. There are several different ways of solving the above equations. Four examples of these methods which will be used together with vortex method to solve the inviscid flow are presented in following sections.

2.1.1.1. Method of Images

If the geometry of the boundary is simple such as an infinity plate or a circular cylinder, the inviscid flow solution can be obtained by the method of images. The solution of a uniform potential flow past a circular cylinder can be found by the circle theorem (Milne-Thomson, 1971). For every vortex blob in the flow domain, there will be a corresponding vortex blob with equal strength and opposite sign at its image location. The normal velocity component induced by each pair of vortices at the boundary can thus cancel out each other. Inviscid flow solutions obtained by the use of this method always turn out to be exact and in analytical closed forms. They are usually used as basic solutions of conformal transformation methods as we will discuss in the next section. This method will be used in Chapter 5 to calculate the flow field behind a circular flameholder. The mathematical formulation of this method will be outlined in detail there.

2.1.1.2. Conformal Transformation

For the flow in a duct, around a corner or past an elliptic cylinder, the inviscid flow solution can no longer be simply obtained by the method of images. By expressing two-dimensional coordinate in the form of complex variables, conformal transformation can then be employed to transform a given geometry into an upper half plane or a circle for which solutions are already known. Several well-known examples in this category are Schwarz-

Christoffel transformation which transforms a closed polygon into an upper half plane, Joukowski transformation (Milne-Thomson, 1971) which transforms an airfoil or an elliptic cylinder into a circle and Theodorsen's method (Theodorson, 1932) which transforms a single arbitrary-shaped body into a circle. Among these methods, Schwarz-Christoffel transformation is especially useful in our numerical model because it can be easily used to apply to a variety of combustion configurations such as a sudden-expansion duct, a backward-facing step and a cavity. The method transforms a given polygon in the physical plane (z-plane) into an upper half plane (ζ -plane) by the following differential equation,

$$F(\zeta) = \frac{dz}{d\zeta} = K(\zeta-a)^{\frac{\alpha}{\pi}-1} \cdot (\zeta-b)^{\frac{\beta}{\pi}-1} \cdot (\zeta-c)^{\frac{\gamma}{\pi}-1} \cdots \qquad (2.10)$$

where α , β , γ ... are interior angles of a simple closed polygon of n vertices

so that $\alpha + \beta + \gamma + \ldots = (n-2)\,\pi$.

the parameters a,b,c, ... ,$a < b < c$, are the coordinates of n points on the real axis in the ζ -plane corresponding to n vertices in the z-plane.

K is a constant to be determined ; it may be a complex number.

The relation between z and ζ can be found by integrating equation (2.10). The result usually takes an integral form and has to be evaluated by numerical integration except for some particular geometries (for example, a parallel duct and a splitter plate) for which analytical formula can be obtained. The velocity field in the physical plane is evaluated by first calculating in the transformed plane and then multiplying the transformation function obtained above.

This method is easy to apply. In some cases, however, integration constants become very difficult to find and the numerical integration is difficult to perform accurately (Sand, 1984). For some specific geometries such as a double-sided sudden expansion duct used in a dump combustor, the transformation function has the form of a strong exponential increase or decay regarding channel length (Giovaninni, 1984). This restricts the dimension of the flow domain which we are interested in due to the limitation of computer accuracy.

When conformal transformation is used to find the inviscid flow solution with vortex method, it can reserve the grid-free principle of the random vortex method and is thus devoid of numerical diffusivity. But the deformation of the shape of vortex blobs due to conformal mapping is speculated to create certain amount of inaccuracies.

2.1.1.3. Integral-Equation Methods

The previous two methods can only be applied to two-dimensional flow about a single body. For flow about a three-dimensional body or two-dimensional multiple bodies, integral-equation method seems to be an excellent way to find the potential flow solution. The ideal of this method is to reduce the problem to an integral equation by a singularity (source-density or vortex-density) distribution on the surface of the body. According to Hess & Smith (1967), the resulting integral equation for the source-density distribution σ (p) is

$$2\pi\sigma(p) - \int_s\int \frac{\partial}{\partial n}\left(\frac{1}{r(p,q)} \right)\sigma(q)ds = -n(p) \cdot U_{\infty} \qquad (2.11)$$

where n denotes a derivative in the direction normal to the boundary surfaces at point p, q is a point outside the body and U_∞ is the velocity at infinity. The conditions under which a solution of the above equation can be obtained are general. The shape of the body does not need to be analytic and may consist of several disjoint surfaces. Detailed solution procedures and theories of two- or three-dimensional flows can be found in the works by Kellogg (1929) or Hess & Smith (1967).

Since this method is used to solve for the potential flow only, the total inviscid velocity u in equation (2.7) has to be decomposed into a rotational velocity component u_v and a potential velocity component u_p by the well-known orthogonal decomposition,

$$u = u_v + u_p \tag{2.12}$$

where

$$u_p = \nabla \Phi_p$$

and

$$\nabla \times u_v = \nabla^2 \Psi_v = -\xi \tag{2.13}$$

$$\nabla \times u_p = \nabla^2 \Psi_p = 0 \tag{2.14}$$

the boundary condition becomes

$$u \cdot n = (u_p + u_v) \cdot n = 0 \tag{2.15}$$

or

$$u_p \cdot n = -u_v \cdot n \tag{2.16}$$

The rotational velocity component u_v can simply be found by summing up all velocities induced by vortex blobs according to equation (2.9) while the potential velocity component u_p can be evaluated by applying equation (2.11). The method was used by Chorin (1973) to find the potential velocity in his study of flows past a circular cylinder and it will also be used in our future studies.

2.1.1.4. Finite-Difference Methods

When the flow domain has a more complicated geometrical form, finite difference method offers a most straightforward way to approximate partial differentiation operators to solve the problem. Equation (2.8) can be directly discretized by using central-difference to approximate the Laplace operator

$$\frac{1}{h^2}(\Psi_{i-1,j} + \Psi_{i+1,j} + \Psi_{i,j-1} + \Psi_{i,j-1} - 4\Psi_{i,j}) = \xi_{i,j} \qquad (2.17)$$

where i, j are indices of meshes and h is the mesh size.

2.1.1.4.1. The Cloud-in-Cell Method

In order to retain the Lagrangian description of the vorticity field but solve the Poisson equation for the velocity field on a Eulerian mesh, a method called cloud-in-cell was used by Christiansen (1973) and Baker (1979) in research on the interaction of regions of vorticity and the roll-up of vortex-sheet. This method uses area weighting scheme to redistribute vorticities inside a given mesh cell to the four mesh points at the corners and solve equation (2.17) by fast Poisson solvers. The velocity of each vortex blob is then determined by central-difference differentiation of stream function and bilinear interpolation to convect itself in the Lagrangian coordinate. The major advantage of this method is the reduction of computational time from $O(N_v^2)$ of direct calculation to $O(N_v) + O(M\log M)$, where N_v is the number of vortex elements and M is the number of grid points. This is especially useful when the number of vortex elements reaches a very high value. However, the method introduces some additional numerical errors due to the anisotropic nature of the vorticity distribution and interpolation. The angular moment of vorticity also does not conserve. For detailed discussion of this method and error considerations, see papers by Christiansen (1973) and Baker (1979) as well as the review by Leonard (1980).

2.1.1.4.2. The Successive Over-Relaxation Method

There are some cases for which good accuracy is desired and the number of vortex elements is not too large. To prevent the anisotropic nature of the vorticity distribution, one can solve only potential flow component by the finite-difference method and calculates the rotational velocity component by direct vortex interactions. The equation to be solved for potential velocity is

$$\nabla^2 \Phi_p = 0 \qquad (2.18)$$

with boundary condition

$$\frac{\partial \Phi_p}{\partial n}\Big|_w = u_p \cdot n \Big|_w = -u_{vn} \qquad (2.19)$$

or they can be expressed in terms of stream function as

$$\nabla^2 \Psi_p = 0 \qquad (2.20)$$

and

$$\frac{\partial \Psi_p}{\partial s}\Big|_w = u_p \cdot n \Big|_w = -u_{vn} \qquad (2.21)$$

where n is the unit vector normal to the wall while s is the unit vector along streamline and u_{vn} is the velocity induced by vortex blobs in the normal direction.

By using five-point approximation for Laplace operator, the finite-difference form of equation (2.18) and (2.20) can be obtained in the same form as equation (2.17) except that the right hand side of the equation equals to zero instead of ξ_{ij} . Equation (2.18) and (2.20) can be solved by either direct methods (e.g. Fourier method (Dorr, 1970), EVP method (Roache, 1971)) or iterative methods (e.g. SOR method (Young, 1954) and ADI method (Peaceman & Rachford, 1955)). Among these methods, the SOR (successive over-relaxation) method seems to be the easiest one to understand and to program with compatible efficiency for complicated flow domains. It is thus chosen here to solve the Laplace equation for the potential velocity.

By viewing equation (2.18) and (2.20), the potential velocity u_p can be solved either from velocity potential or from stream function. Since equation (2.21) will give us the Dirichlet boundary condition which is easier to deal with numerically, we would determine to solve the Laplace equation in terms of stream function. According to the successive over-relaxation method, equation (2.20) can then be written in the discretized form as

$$\Psi_{i,j}^{n+1} = \Psi_{i,j}^{n} + \frac{\omega}{4}\left[\Psi_{i-1,j}^{n+1} + \Psi_{i,j-1}^{n+1} + \Psi_{i+1,j}^{n} + \Psi_{i,j+1}^{n} - 4\Psi_{i,j}^{n}\right] \qquad (2.22)$$

where superscript n, n+1, refer to number of iterations and ω is the over-relaxation parameter

The boundary condition (equation (2.21)) can also be written in the finite-difference form as

$$\frac{\Psi_{k+1} - \Psi_{k}}{\Delta s} = -u_{vn} \qquad (2.23)$$

or

$$\Psi_{k+1} = \Psi_k - u_{wn} \cdot \Delta s \tag{2.24}$$

where subscript k and k+1 are indices of successive grid points along solid walls and Δ s is the spatial increment between two points.

The iteration of the SOR method will converge only when the value of the over-relaxation parameter ω is between 0.0 and 2.0. In a complicated region, there is no analytic formula for predicting the optimal value of ω. It thus has to be determined by numerical experiments. However, the analytic formula for the problem in a rectangular domain of I x J grid points derived by Frankel (1950),

$$\omega_o = 2\left[\frac{1 - \sqrt{1 - \lambda}}{\lambda}\right] \tag{2.25}$$

where

$$\lambda = \left[\frac{\cos\left(\frac{\pi}{I - 1}\right) + \cos\left(\frac{\pi}{J - 1}\right)}{2}\right]^2 \tag{2.26}$$

is used to estimate the optional parameter ω for the initial guess.

The formula of equation (2.22) can be used to calculate stream functions for the interior grid points in the flow domain as long as the shape of the mesh remains a square. In the case of a sloping wall or a curve boundary, grid cells near the boundary become irregular-shaped (see Figure 1), the finite-difference approximation of Laplace operator has to be modified in order to handle the irregularity of grid cells. A second-order Taylor series expansion is utilized in order to approximate the partial differentiation operator as :

$$\frac{\partial^2 \Psi}{\partial x^2} = \frac{2}{h^2}\left[\frac{\Psi_{i-1,j}}{1+\vartheta_R} + \frac{\Psi_R}{\vartheta_R(1+\vartheta_R)} - \frac{\Psi_{i,j}}{\vartheta_R}\right] \tag{2.27}$$

$$\frac{\partial^2 \Psi}{\partial y^2} = \frac{2}{h^2}\left[\frac{\Psi_{i,j+1}}{1+\vartheta_B} + \frac{\Psi_B}{\vartheta_B(1+\vartheta_B)} - \frac{\Psi_{i,j}}{\vartheta_B}\right] \tag{2.28}$$

thus

$$\begin{aligned}\nabla^2 \Psi = \frac{\partial^2 \Psi}{\partial x^2} + \frac{\partial^2 \Psi}{\partial y^2} = \frac{2}{h^2}\Bigg[&\frac{\Psi_{i-1,j}}{1+\vartheta_R} + \frac{\Psi_R}{\vartheta_R(1+\vartheta_R)} + \\ &\frac{\Psi_{i,j+1}}{1+\vartheta_B} + \frac{\Psi_B}{\vartheta_B(1+\vartheta_B)} - \left(\frac{1}{\vartheta_B} + \frac{1}{\vartheta_R}\right)\Psi_{i,j}\Bigg]\end{aligned} \tag{2.29}$$

where $\vartheta_R = |CR|/h$

$\vartheta_B = |CB|/h$

Ψ_B is the stream function at point B calculated by equation (2.24)

Ψ_R is the stream function at point R calculated by interpolation.

The discretized Laplace equation used in the SOR method for irregular grids becomes then :

$$\begin{aligned}\Psi_{i,j}^{n+1} = \Psi_{i,j}^{n} + \frac{\omega}{2\left(\frac{1}{\vartheta_B} + \frac{1}{\vartheta_R}\right)}\Bigg[&\frac{\Psi_{i-1,j}^{n+1}}{1+\vartheta_R} + \frac{\Psi_B^{n+1}}{\vartheta_B(1+\vartheta_B)} \\ &+ \frac{\Psi_R^{n}}{\vartheta_R(1+\vartheta_R)} + \frac{\Psi_{i,j+1}^{n}}{1+\vartheta_B} + \left(\frac{1}{\vartheta_B} + \frac{1}{\vartheta_R}\right)\Psi_{i,j}^{n}\Bigg]\end{aligned} \tag{2.30}$$

In order to calculate the stream function at each grid point on the boundary, the velocity induced by vortex blobs normal to the wall u_{vn} needs to be evaluated. When the boundary is parallel to x- or y- axis, the normal velocity component is simply the y or x component of the total induced velocity. In the case of a sloping wall or a curve boundary, it can then be simply found by coordinate transformation as

$$u_n = u \sin\vartheta + v \cos\vartheta \qquad (2.31)$$

where ϑ is the angle measured counter-clockwise from the x-axis to the tangent of the boundary at certain grid point, and u, v are velocity components in the x and y direction respectively.

For internal flows, besides boundary conditions at walls, inlet and outflow condition, also have to be specified in order to be able to solve the Laplace equation. The inlet flow condition is usually given and its value can be directly assigned to inlet grid points. But outlet flow condition is often not known *a prior*. It has to be evaluated with the entire flow field at the same time. Thus, instead of using a prescribed velocity profile, a less restrictive condition $\partial \Psi / \partial x = 0$ is suggested here as the boundary condition at the exit of the duct. This condition has been reported (Paris & Whitaker, 1965), and is also found in our study to be quite successful in obtaining accurate results, as we will discuss in Chapter 4.

For external flow such as would occur around a blunt body, the flow domain often extends to infinity. In this case boundary conditions at the upper and lower boundaries of the computational domain have to be specified. Since the mesh size used in the potential flow calculation does not have to be very small, one can always specify an undisturbed velocity condition at upper and lower boundaries far enough from the body. For a parallel flow past a blunt body we can use $U = U_\infty$, where U_∞ is the velocity upstream , or constant stream functions as boundary conditions.

Once all boundary conditions have been specified, one can start to iterate either equation (2.22) for square meshes or equation (2.30) for non-square meshes by successive over-relaxation method until Max $| \Psi_{ij}^{n+1} - \Psi_{ij}^{n} | < \tau$,where τ is the desire accuracy and I, J are the number of grid points in x- and y-direction respectively. The number of iterations required for each time step will depend on the specific geometry under consideration. For the backward-facing step with a contraction inlet, as will be studied in Chapter 4, it ranges from 20 to 40 depending on velocity fluctuations of each time step.

The potential velocity component of each vortex blob may be found by differentiating stream function with central difference and by interpolating velocities at grid points at four corners of a mesh using area weighting method (Figure 2)

$$u_p = \sum_{i=1}^{4} u_i \frac{A_i}{h^2} \tag{2.32}$$

The total convection velocity of each vortex blob is then obtained by adding rotational velocity u_v to the potential velocity u_p according to equation (2.12).

2.1.2. Viscous Effects

In addition to the zero normal velocity boundary condition of an Euler flow, the tangential velocity component also has to vanish for viscous flow due to finite value of fluid viscosity. The no-slip boundary condition is satisfied by creating vorticities at rigid walls to cancel non-zero tangential velocities. The diffusion equation

$$\frac{\partial \xi}{\partial t} = \mathrm{Re}^{-1} \nabla^2 \xi \tag{2.33}$$

is present here together with the Euler equation in order to constitute the complete vorticity transport equation. These two major components of viscous effects in our model are now briefly discussed as follows :

2.1.2.1. Diffusion Equation and Random Walk

The diffusion process of vorticity in viscous flow is characterized by the diffusion equation with Re^{-1} as the coefficient. The solution of diffusion equation in free space is a Gaussian distribution of mean zero and variance 2t / R

$$G(x,t) = \sqrt{\frac{\mathrm{Re}}{4\pi t}} \exp\left(-\frac{\mathrm{Re}\, x^2}{4t}\right) \tag{2.34}$$

For conventional time-dependent flow calculation, the time interval (0,t) is always split into n small time steps, each with interval $\Delta t = t / n$. Since the vorticity field in our model is represented by a number of vortex blobs, we can let them undergo random walks which are independent Gaussian random variables with mean zero and variance $2 \Delta t / \mathrm{Re}$. This is because two-dimensional flow random displacements in two directions are also independent to each other. The final displacement after n time steps thus also has a Gaussian distribution with mean zero and variance 2t / Re. Thus the distribution of vortex blobs at time t is given by equation (2.34) and it satisfies the diffusion equation. The location of each vortex blob at next time step can be found by

$$x_i^{n+1} = x_i^n + \int u_i \, dt + \eta_{ix} \tag{2.35}$$

$$y_i^{n+1} = y_i^n + \int v_i \, dt + \eta_{iy} \tag{2.36}$$

where η_{ix} , η_{iy} are Gaussian distributed variables with zero mean and variance $2 \Delta t / R$.

Since the computational time required for velocity calculation at certain location is proportional to N^2, where N is the number of vortex blobs, a higher order time integration usually requires the evaluation of velocities at certain intermediate time steps and thus increases computational time dramatically. It is certainly not worth pursueing if higher accuracy is not critical. First order Euler's time integration is often used to carry out the displacement calculation of vortex blobs.

2.1.2.2. Vorticity Generation at Boundaries

In Chorin's paper (1973) of random vortex method, the tangential velocity at boundary is eliminated by creating vortex blobs of total vorticity $\xi = u_w h$ at each equally spaced check point along the wall, where u_w is the tangential velocity at wall and h is the space between check points. By doing this, the rate of convergence near boundary is slow and the computation effort is substantial especially in interior flow problems. Therefore, a vortex sheet approximation of boundary layer was developed (Chorin, 1978) to overcome these problems.

According to boundary layer approximation, the velocity gradient in streamwise direction is small compared with that in the normal direction. The vorticity equation is thus simplified as

$$\frac{\partial \xi}{\partial t} + (u \cdot \nabla)\,\xi = \mathrm{Re}^{-1}\,\frac{\partial^2 \xi}{\partial y^2} \qquad (2.37)$$

where

$$\xi = -\frac{\partial u}{\partial y} \qquad (2.38)$$

The diffusion component of vorticity equation becomes one-dimensional, therefore, only random walk in y-direction is needed to simulate the diffusion process of vorticity. Detailed formulations of convection velocity inside boundary layer resulting from above equations have been derived by Chorin (1978). Vortex sheets are designed to induce velocity field only below themselves. Each time step new vortex sheets are generated at walls according to amount of vorticities needed to satisfy the no-slip condition. They are then subject to random displacements of zero mean and variance 2 $\Delta t / Re$ in y-direction. In order to attain certain computational accuracy, a maximum vorticity Γ_{max} allowed is selected for vortex sheets. This results in generating several vortex sheets at certain check points along walls.

Since boundary layer approximations are valid only inside the boundary layer of which the thickness is of the order of $O(Re^{-1/2})$, vortex sheets approximation can be applied in that small region only. The numerical boundary-layer thickness δ is chosen to be a multiple of standard deviation $(2 \Delta t / Re)^{1/2}$ in order to minimize the loss of vortex blobs across boundaries (Chorin, 1978). When vortex sheets move outside the boundary-layer, they are turned into vortex blobs and induce rotational flow outside. On the other hand, when vortex blobs move into boundary-layer, they are changed to vortex sheets and follow the motion of boundary-layer flow. As we stated above, vortex sheets only induce velocities below themselves. Therefore, when calculating velocities at certain points, we don't have to include the effects induced by vortex sheets unless the point of interest is inside the numerical boundary layer. The computational effort is thus tremendously reduced especially in internal flows for which the number of vortex sheets is large.

2.2. Turbulent Reacting Flows

As a consequence of all the complexities associated with turbulent flow in the presence of chemical reactions, the analysis must be based on an array of simplifying assumptions. In particular, we are interested here in the case of a perfectly premixed reacting medium where chemistry is so fast that combustion is controlled primarily by turbulent transport. As already stated earlier, flame front is modeled as an interface between premixed reactants and burned products that is significantly thiner than smallest turbulent length scale. Thus the only effect of turbulence on the flame is manifested in wrinkling its front while its integral features remain unchanged. According to Ghoniem et al(1982), under such circumstances, the flame motion is described as follows

$$\nabla \cdot u = \varepsilon(r_f) \qquad (2.39)$$

and

$$\frac{\partial r_f}{\partial t} = S_u \cdot n + u \qquad (2.40)$$

where r_f is the position vector of the flame front, S_u is normal burning speed assumed to be a prescribed constant and n is the unit vector normal to flame front, while

$$\varepsilon(r_f) = u_s \cdot \delta(r - r_f)$$

$$u_s = \frac{1}{2}(V - 1)\, S_u$$

models the local rate of expansion by volume sources. In the about $V = v_b / v_u$ is the specific volume ratio across the flame front.

2.2.1. Flame Front Location : the SLIC Method

The non-reacting flow is described in the Lagrangian coordinate by following the motions of vortex blobs, while the flame front is traced at the same time in every time step.

The shape of flame front in a turbulent flow always exhibits such a complicated characteristics that it is difficult to represent it by a single interpolation function, especially when cusps occur. Quite often, one finds also the appearance of the so-called unburned "islands" and "pockets" (Bray, et al, 1984) behind the flame front due to the entrainment of the unreacted medium. Therefore the flame, which is not even simple-connected becomes more difficult to describe by an analytical function.

The method used here to determine the location of the flame front is based on the SLIC(Simple Line Interface Calculation) algorithm (Noh & William, 1976 and Chorin ,1978). According to this the flow domain is first divided into a number of square cells. Volume fraction of burnt medium inside each cell f is calculated and the geometry of the interface is deduced from the value of f in the cell and its four neighbors. Interface geometries inside cells of partially burned are classified into four cases : (i) vertical interface, (ii) horizontal interface ,(iii) corner and (iv) neck, as illustrated in Figure 3.

2.2.2. Self-Advancement and Huygens Principle

Since no explicit function is given to describe the shape of flame front, the normal direction of every point along the flame front cannot be simply determined. The self-advancement of the flame in its normal direction is computed by an implementation of the Huygens principle. Interface inside the cell is moved at a constant flame speed into eight different directions, each 45° apart. The maximum value among eight new f numbers is chosen to be the resulting volume fraction. New values of volume fraction f are used to determine the interface geometries and locations. The change of volume fraction f inside each cell is also recorded to evaluate the strength and core radius of source blobs.

An example of flame propagation in its normal direction can be easily obtained by igniting premixed reactants inside a rectangular duct at the center of its end wall. The shape of flame front remains a semi-circle until it reaches side walls. It then becomes flatter and flatter due to the increase of radius of curvature. In Figure 4, we display the numerical simulation of this case for every 20 time steps. Numerical parameters used are h = 0.05, Δt = 0.1 and $S_u = 0.25$, where h is the cell size, Δt is time step, and S_u is the prescribed laminar flame speed.

2.2.3. Velocity Field of Reacting Flows

The dynamic effect of exothermicity during the combustion process was properly modeled by the use of volumetric source blobs located along flame front. The strength and core radius of each source blob is evaluated according to the change of volume fraction f in the cell by normal burning. The velocity field induced by source blobs in free space is described by

$$u_s^* = \sum_{j=1}^{N_s} \frac{\Delta_j}{2\pi} \frac{|z - z_j|}{\max(|z - z_j|, r_s)} \frac{1}{(z - z_j)} \tag{2.41}$$

where Δ_j is the strength of the source blob

r_s is the core radius of the source blob.

A source blob is in concept analogy to a vortex blob, or in terms of complex function, a source blob is a vortex blob with imaginary strength. Equation (2.41) has the same form as equation (2.9), except that the velocity field produced by source blobs is potential and curl free, while that induced by vortex blobs is rotational, but divergence free.

If the method of image or conformal transformation can be used to find the solution of the flow field, a similar way used in section 2.1.1.1 and 2.1.1.2 for vortex blobs can also be applied to source blobs with the exception that image source blobs do not change signs of their strengths. When integral-equation or finite-difference method is applicable, the velocities induced by source blobs have to be added to the total velocity in equation (2.12) as

$$u = u_v + u_p + u_s \tag{2.42}$$

and

$$\nabla \times u_v = \nabla^2 \Psi_v = -\xi \quad \& \quad \nabla \cdot u_v = 0 \tag{2.43}$$

$$\nabla \times u_p = \nabla^2 \Psi_p = 0 \quad \& \quad \nabla \cdot u_p = 0 \tag{2.44}$$

$$\nabla \times u_s = \nabla^2 \Psi_s = 0 \quad \& \quad \nabla \cdot u_s = \varepsilon \tag{2.45}$$

The boundary condition for solving potential velocity becomes

$$u \cdot n = (u_p + u_v + u_s) \cdot n = 0 \tag{2.46}$$

or

$$\begin{aligned} u_p \cdot n &= -(u_v + u_s) \cdot n \\ &= -(u_{vn} + u_{sn}) \end{aligned} \tag{2.47}$$

The potential flow component can then be solved by methods outlined in section 2.1.1.3 and 2.1.1.4 . Total velocities of reacting flows can be obtained by adding up u_s in equation (2.41) and u_v in equation (2.9) to u_p. The overall procedures for calculating reacting flows are depicted in Figure 5 by block diagrams.

Flame propagation is usually initialized by a point ignition or a line ignition. Sometimes a region with completely burned products is introduced in order to save the computational time of establishing a continuous front. Initial interfaces inside cells are moved by the normal burning speed and local convection velocity according to equation (2.40) in two fractional steps. The number of cells used in the reacting flow calculation may be large. In order to reduce the computational effort, flow velocities are calculated only when either cells themselves or at least one of their eight neighboring cells are active. A cell is considered to be active at the specific time step when the change of volume fraction of burned products in it during the normal burning process is finite. This algorithm lets us move flame front every time step correctly, without going through all cells in the computational domain.

Chapter 3

Rudiments of Flame Aerodynamics in Premixed Gases

Non-steady flame propagation in a variety of combustion configurations have exhibited many interesting features which include the coherent structures in reacting flows, the breakdown of laminar flames and cellular structures of flame front stabilized by a bluff body. Each of these phenomena involves a large set of complicated mechanisms which are difficult to deal with, even individually.

In premixed combustion fluid mechanics plays an important role in determining the reaction rate, flame shape and other combustion processes. By relating the salient features of flame propagation to the aerodynamic properties of the flow field, we are able to deduce three fundamental mechanisms which physically are capable of interpreting most flame phenomena in premixed gases, and mathematically are particularly connected with our numerical model.

While the detailed calculations of turbulent flow fields and the development of flame front in both confined and unconfined regions will be carried out in Chapter 4 and 5, we will, first, in this chapter use an ideal potential flow model to illustrate the individual or combined effects of these fundamental mechanisms on the flame propagation in simple geometries. Extensions are possible to cover most aerodynamic features in premixed gases. The formation of tulip shape flame in a closed duct serves as another example of our illustrations.

3.1. Three Fundamental Mechanisms

The flow fields of most practical combustion systems, whether turbulent or laminar, often consist of rotational flows of various length scales. The rotational flow field which may result from wall effects or density gradient across flame front can always be represented in the form of vortices. These small or large vortex structures in reacting flows have the effect of entraining more fresh reactants into to the reaction zone and then modifying the mixing and reaction rate of combustion process. The rotary motion of eddies thus plays an important role in the determination of flame shapes.

Combustion is a process associated with the transformation from reactants into products at a certain reaction rate. The normal burning velocity of flame front has a strong dependency on local properties of reacting gases as well as the structure of the flame front. Accordingly, no unique function has yet been found to describe the relation between the normal burning velocity and its dependent variables with satisfactory results. However, models which assume constant burning velocity are found to be very successful in describing many flame propagation phenomena. The effect due to constant normal burning is also considered here to be one of the basic mechanisms in the investigation.

The dynamic effect of thermal expansion result from chemical reaction is modeled by volumetric sources located along flame front as described in previous sections. These volumetric sources not only affect the flow field but also modify the shape of flame front due to the interaction between them..

The three fundamental mechanisms of flame propagation -- (i) rotary motion of vortex structures; (ii) self-advancement of flame front at a prescribed constant normal burning speed; and (iii) the concomitant action of volumetric sources along flame front used to model the thermal expansion, have already been brought up by Oppenheim & Ghoniem (1983). We would like to use these mechanisms to investigate some aerodynamic features of flame propagation in premixed gases in more detail.

In this section the simple case of a straight flame front normal to the walls of a parallel duct is used to study the deformation of the flame front due to the individual or combined effects of three fundamental mechanisms stated above. To make the problem even simpler, we assume the flow field is potential, i.e.

$$\nabla^2 \Phi = 0 \qquad (3.1)$$

where

$$u = \nabla \cdot \Phi \qquad (3.2)$$

with boundary condition

$$\frac{\partial \Phi}{\partial n} = 0 \qquad (3.3)$$

The velocity field induced by a potential vortex located at the center of the duct is formulated by the Schwarz-Christoffel transformation. The transformation function of a parallel duct is found to be

$$F(\zeta) = \frac{dz}{d\zeta} = \pi\zeta \qquad (3.4)$$

The relation between z and ζ can be easily obtained by integrating the above equation as

$$\zeta = \exp(\pi z) \tag{3.5}$$

or

$$z = \frac{1}{\pi}\log\zeta \tag{3.6}$$

For a potential vortex with strength Γ located at z_0 in physical plane, the complex velocity in the transformed plane is specified by

$$\begin{aligned} W(\zeta) &= -\frac{i\Gamma}{2\pi}\left[\frac{1}{\zeta-\zeta_o} - \frac{1}{\zeta+\zeta_o}\right] \\ &= -\frac{i\Gamma\zeta_o}{\pi(\zeta^2+\zeta_0^2)} \end{aligned} \tag{3.7}$$

where

$$\zeta_o = \exp(\pi z_o) \tag{3.8}$$

The velocity field in the physical plane can then be obtained by taking the conjugate of the product of the transformation function and the complex velocity as

$$\begin{aligned} u(z) &= W^*(z) = \left[W(\zeta)F(\zeta)\right]^* \\ &= -\left[\frac{i\Gamma e^{\pi z_o}\, e^{\pi z}}{e^{2\pi z} + e^{2\pi z_o}}\right]^* \end{aligned} \tag{3.9}$$

where ( )* denotes the conjugate of a complex number. To perform the computations in terms of nondimensional parameters, we choose the coordinate system shown in Figure 6.a. The height of the duct H is chosen to be 1.0, thus the coordinate of the vortex is $z_0 = 1/2$. The strength of the vortex Γ is set to be 2.0 so that velocity at the nearest wall points induced by the potential vortex is equal to unity. The normal burning velocity is taken as

$$S_u = 0.4$$

while the density across the flame front is

$$V = \frac{v_b}{v_u} = 3.0$$

where subscript u and b denotes the unburned and burned gas respectively. The source strength per unit length of the flame front is

$$u_s = \frac{1}{2}(V - 1)\, S_u = 0.4 \qquad (3.10)$$

and the time step is taken to be

$$\Delta t = 1.7857 \times 10^{-3}$$

in order to satisfy Courant condition in the computation of flame propagation.

Figure 7 displays the deformed flame fronts and velocity vectors on both unburned and burned sides after 80 computational time steps. The scale of velocity vectors is shown at the right corner below the first plot. The dash line represents the initial flame front while solid lines show the contours of deformed flame fronts.

Figure 7.a applies to the case of the distorted flame front due to the rotary motion of the vortex alone. A large deformation of the flame shape as well as an increase of flame area resulting from the interaction of the flame with the vortex element can be observed from the figure. When the normal burning speed is added to the motion of the flame front, the velocity fields on both sides of flame front of course remain unchanged, while the flame front advances in its normal direction, smoothes out the wrinkles and forms a cusp as the result shown in Figure 7.b.

If the flame front in Figure 7.b is compared with that of the initial straight interface propagates at the same flame speed without the vortex motion, one finds that the burning rate, which is defined here as the number of burned cells consumed per time step, of the former case is about two times higher than the latter. The increase in the flame area due to the stretch of vortex motion obviously augments the burning rate. That turbulent burning velocity is larger than the laminar one due to the wrinkling of flame front by the interactions of turbulent eddies has been observed in most turbulent combustion.

Figure 7.c displays the flame front due to the combining effects of all three fundamental mechanisms. The basic flame shape remains unchanged from Figure 7.b except that flame front advances more into the unburned gas by the augmented flow field. Velocity vectors on the unburned side are found to have significant changes due to effects of volume sources. The directions of the velocity vectors also indicate the divergence of streamlines outside flame fronts.

While the velocity vectors on the burned side are found to be unchanged by the action of distributed volume sources. This is because, as interpreted by Oppenheim & Ghoniem (1983), that physically the domain of burned gases contains a point of zero translation velocity, and mathematically the domain of burned gases in the transformed plane is closed by the flame front, continuous volume sources distributed along the front thus do not change the flow field inside.

To illustrate this interpretation, the computation of flame front and velocity vectors with same conditions in the transformed plane are performed. Figure 8 is the corresponding results of Figure 7 in the ζ - plane. The enlargement of the inner portions of Figure 8 is shown in Figure 9. The scale of velocity vectors of each figure is also shown at the right hand corner below the first plot. The closed feature of the burned gases can be clearly noticed in the figure.

Although the calculation is done in a confined region, similar results as those shown in Figure 6 - 8 in an unconfined domain can also be obtained except that the zero normal velocity boundary condition is excluded. Thus the flame front does not necessarily remain a right angle with duct walls. Cusps will still exist at the flame front and form singularities in the flow field. The result is similar to the cellular structures of confined or unconfined flames stabilized by a bluff-body holder. A phenomenological sketch by Oppenheim (1983) (Figure 10) is also found to be simulated well by our numerical model.

3.2. Flame Propagation in a Duct with Closed End

The phenomena of flame propagation in a tube have been investigated for over a century (Mallard & Le Chatelier, 1883, Maxworthy, 1962, Zel'dovich 1980). Most of the experimental or theoretical works have concentrated on the steady plane flame and result in very complete mathematical theories (Sivashinsky, 1983) in this area. The phenomena of non-steady flame propagation have also been studied by many researchers; however, results are less satisfactory.

One of the interesting features of non-steady flame propagation in a closed duct is the formation of the so-called "tulip shape" flame. If the length of the duct is not too long, it has been found (Ellis, 1928, Guenocho 1964, Steinet et al, 1982 and Dun-Rankin et al, 1984) that, when the premixed reactants inside a closed duct are ignited at one end, the flame initially exhibits a semi-cylindrical shape and then flattens into a planar front after it reaches side walls. As the planar front propagates further downstream with a noticeable decrease in burning rate, cusps begin to form along the front. The center cusp of the front then becomes more and more pronounced and finally develops to a "tulip" shape flame as the flame approaches the closed end.

Since no quantitative results have been obtained on this problem, the causes of tulip shape flame remain controversial at this time. Flame stability, pressure wave and flame driven flow field are three most prevailing speculations about this interesting phenomenon.

The measured maximum flow velocity induced by the flame in a closed channel is found to be of the order of several meters per second. The Mach number in this case is small, thus pressure wave will not have a significant effect on either the flow field or the flame front. For stoichiometric methane/air mixture, the Lewis number, which isfined as $Le = D/k$, approximately equals 1.0. The value is near the thermo-diffusive instability threshold of flame fronts, hydrodynamic instability therefore becomes a dominant factor. According to Markstein's theory, the flame is unstable to long-wave disturbances but is stable to short-wave ones. The dimensions of ducts or tubes used in experiments are always small. The planar flame front bounded by narrow walls can thus prevent the appearance of long-wave disturbances and becomes hydrodynamically stable.

We therefore believe that the flow field driven by the flame is the major cause of the "tulip" shape flame. As experimental photography showed, at the initially stage of flame propagation the effect of flame driven flow is small. The flame behaves like a free-propagating front until it "feels" the existence of the end wall and then flattens. This early part of flame propagation can be easily explained or modeled by the Huygens Principal as we discussed in last section.

The transitional flame front is modeled here by the use of a simple conceptual model. It considers a planar flame front propagating in a duct toward the closed end wall. The coordinate system used for the computation is shown in Figure 6.b. In view of the symmetry of the flame, the computation is performed only on the upper half of the duct. According to Zel'dovich's analysis (1980), the flow field ahead of the flame is potential while that on the burned side is rotational. The inviscid flow model used in the last section is also chosen here to calculate the flow field. The rotational flow part is simulated by creating a large scale vortex behind the flame.

To calculate the velocity field in the duct, the Schwarz-Christoffel transformation is used to map the computational domain into an upper half plane. The transformation function for the geometry under consideration is found to be

$$F(\zeta) = \frac{dz}{d\zeta} = -\pi\sqrt{\zeta^2 - 1} \qquad (3.11)$$

After integration, we have the relation between z and ζ, as

$$\zeta = \cosh[\pi(i - z)] \qquad (3.12)$$

Assumed the location of the vortex at the physical plane is z_0, the complex velocity in the transformed plane can be found by the formula in equation (3.7) with $\zeta_0 = \cosh[\pi\,(i-z_0)]$. The velocity field in the physical plane is then obtained by

$$
\begin{aligned}
u(z) = W^*(z) &= \left[W(\zeta)\,F(\zeta)\right]^* \\
&= \left[\frac{i2\pi\Gamma\zeta_o}{\zeta^2-\zeta_o^2}\sqrt{\zeta^2-1}\right]^*
\end{aligned}
\qquad (3.13)
$$

For the sake of convenience, the width of the duct H is also chosen to be the reference length. In order to allow the planar front to have enough distance to develop into a tulip shape, the flame is initially located at 2.5 H away from the end wall. The vortex is then located at the center of the half duct and 0.5 H behind the flame front. The strength of the vortex is chosen to be -2.0 so that the velocity at the nearest wall point is equal to unity. For consistency, the values of laminar flame speed and density ratio are chosen to be the same as those used in the last section, i.e. $S_u = 0.4$ and $V = 3.0$

If the location of the vortex is fixed in space with time, the effect of rotary motion acts on the flame front will be gradually reduced as the flame keeps on propagating downstream. In order to keep up the effect of the vortex, a constant velocity with the magnitude 7.5×10^{-3} to the right is chosen to impose on the motion of the vortex after a number of numerical experiments. Computational time step Δ t is taken to be 1.7857×10^{-2} to satisfy the stability condition.

Figure 11 displays the development of flame fronts and locations of vortices at the 40th, 120th and 200th time step. The initial flame front is represented by a dash line while solid lines delineate the contour of flame fronts at subsequent time steps. Figure 11. a, b & c. are results of three cases corresponding to Figure 7. a, b & c, i.e. the effect(s) due to (a) the rotary motion of vortex alone; (b) rotary motion and self-advancement in normal direction, and (c) all three fundamental mechanisms.

By the action of the rotary motion alone , flame fronts are stretched and exhibit peculiar shapes. The added flame advancement in the normal direction smoothes out the front and forms flame shapes similar to the tulip flame observed in experiments. When the effect of thermal expansion is modeled, the axial motion of flame front is found somehow retarded and the fold of the front is deeper into the burned gases. This is because that the domain of unburned gases surrounded by the flame front and duct walls is now closed. The flow field induced by distributed sources along flame front thus only affect the velocity field on the burned gases without modification of that on the unburned gases.

Velocity vectors and flame fronts at the 200th time step are shown in Figure 12, while Figure 13 shows the corresponding plot in the transformed plane.

Although the model used in this section is only phenomenological and over-simplified, we believe that we have already demonstrated some important features of the unsteady flame propagation in a closed duct by such a simple model. A more detailed numerical model which calculates the flow field induced directly by the changes of pressure and density from the exothermicity of chemical reaction in a closed domain is currently underway. The location of flame front is determined by following the flow velocity produced by itself. Meanwhile, the experimental measurements of the detailed flow field by the LDA technique is also in process. We hope all of these efforts will bring us to a better understanding of the formation mechanism of tulip shape flame.

Chapter 4

Confined Flame:
A Turbulent Flame Stabilized Behind a Rearward-Facing Step

Combustion of premixed gases in the wake of a rearward-facing step has recently attracted deservedly broad attention, as manifested by experimental investigations of Ganji & Sawyer (1980), Pitz & Daily (1983), Shepherd, et al (1982) and El-Benhawy, et al (1983), as well as by the numerical studies of Ghoniem, et al (1982) and Ashurst (1981). The reason for this lies in the following unique interesting features of the system:

(1) it provides proper means for mass and heat recirculation, a process of particular advantage to lean combustion, enhancing thermal efficiency and reducing pollutant emission;

(2) it promotes strong interaction between the turbulent flow field and the combustion process, forming a closed loop feedback mechanism;

(3) it exploits the intrinsic flow instability to stabilize the flame;

(4) it enhances mixing, leading to the establishment of close coupling between the combustion process and flow instabilities.

However,because of the same reason, the instability of the flame is of crucial important since it is so dependent on various operating conditions, such as equivalence ratio, inlet flow velocity, pressure, and temperature. As the flame is stabilized by the recirculation, bringing hot products into close contact with the reaction zone furnishing thereby a continuous supply of heat for ignition of fresh mixture, the turbulent field plays a major role in determining the geometry of the flame front. On the other hand, the expansion associated with the conversion of reactants into products acts to modify the turbulent field, e.g. the recirculation (reattachment) zone length is reduced to almost one half of its value in the non-reacting flow due to gas acceleration across the flame front. Meanwhile, the free-stream flow and the recirculation vortex interact with the set of trailing eddies of the mixing layer dominated by large scale structure, enhancing the interaction between combustion products and reactants and acting locally as a heat exchanger that augments the temperature of the reactants. There is a wide range of frequencies detectable in the energy spectrum of the mixing layer corresponding to the size and motion of these eddies. However, some frequencies can become dominant if the mixture quality is adjusted, resulting in flow instabilities that cause the flame to oscillate (Keller, et al, 1982). This process emphasizes the close coupling between fluid mechanics and combustion in the system under study, as well as the major role of the vortical flow structure that has to be, therefore, properly taken into account by the model.

The combined effect of the three fundamental mechanisms of a turbulent flame, including turbulent eddies, laminar flamelets, and volumetric expansion, as discussed in last chapter, elucidate a variety of phenomena related to flame stability, effects of confinement and geometrical obstacles, flame acceleration and its effect upon flow instability. However, attempts to study theoretically these processes and to reproduce the outcome of their interaction have been plagued by lack of proper models of turbulent flow, difficulties associated with representing chemical reactions in a fluctuating field (Mellor & Ferguson, 1980), and numerical instabilities which are introduced when dynamic effects of combustion are expressed in terms of the expansion across the flame front (Williams, 1974). The crux of the problem lies in the effect of the Arrhenius exponential term in the kinetic rate equations that describe the chemical reaction. Thus attempts to incorporate turbulent fluctuations in the combustion process using statistical decomposition of thermodynamic variables leads to non-convergent solutions. Moreover, conventional numerical methods used in these studies are influenced by artificial viscosity inhibiting the growth of nature flow instabilities at high Reynolds numbers, tending to "laminarize" the flow (McDonald, 1979). On the other hand, the use of grids to calculate the flow variables imposes a limit on the spatial resolution of the results and may require the added complicity of adaptive modifications around zones of large gradients with the concomitant effects of numerical diffusivity.

Conventional artificial modeling of turbulence is avoided by the use of the random vortex method to evaluate the fluctuating field and the interaction of turbulent eddies. Our numerical model stresses the unsteady and highly fluctuating nature of the flow field associated with turbulent flames, as well as the dynamic effects due to exothermicity combustion in a flow system. It was used originally to study the evolution of the vorticity field and the development of the flame front behind a step in a relatively short channel. Presented in this chapter are solutions we obtained for a long channel incorporating a smooth contraction followed by an abrupt expansion. This relates to essential geometrical features of the combustion tunnel used for experimental studies. In order to treat the appreciably large flow field, we had to use a Cray computer with the numerical code properly vectorized for this purpose. Besides the vorticity field and flame front kinematics, the results include here the detailed average velocity profiles and turbulence intensity profiles, in comparison with experimental results of Pitz & Daily

(1983).

4.1. Configuration and Computation Parameters

The overall configuration of the rearward-facing step combustor used by Pitz & Daily is shown in Figure 14 with all dimensions properly labeled. The vorticity field and flame development behind the rearward-facing step, without considering any information about inlet section and step geometry, was modeled by Ghoniem, et al (1982). Their results (see Figure 15) have been in agreement with the experimental schlieren cinematographys recorded by Ganji & Sawyer (1980).

In order to simulate the reacting flow in greater detail, the computational domain is extended to cover the entire step and the upstream inlet section. The width H_i and the velocity U_i at the inlet of the duct are chosen to be the characteristic length and velocity respectively. Since the reattachment length of the shear layer behind a step is approximately about 6 to 8 step heights H_o, we here choose the duct length behind the step to be 10 H_o (or 5 H_i) to prevent the untractable outflow boundary condition in the incomplete recirculation zone. The duct length upstream the step is chosen to be $2H_i$ and the geometry of the step is tried to match the experimental shape as closely as possible without introducing too many computational complicities. The computational configuration of the rearward-facing step is shown in Figure 16. For premixed propane-air reactants with equivalence ratio $\varphi = 0.57$ the density ratio across the flame front is approximately equal to 6.0 and the measured laminar flame speed is about 0.02 U_o, where U_o is the mean velocity at the step.

The computation was performed at two Reynolds numbers Re = 22,000 and 37,000, based on the inlet flow velocity U_i, its width H_i and the kinematic viscosity of the reactants ν, in order to match the experimental conditions of Pitz & Daily. At zero time step, the flow field is initialized by a potential flow with a velocity $U_i = 1$ uniform at the inlet section with a vortex sheet layer of thickness $\delta = 3\,\sigma$, where $\sigma = (2\,t/Re)^{1/2}$ is the standard deviation of the set of random displacements mentioned in section 2.2.2, on each wall of the channel. The sheet is discretized along each wall into a number of finite-length vortex elements, each of $h = 0.2$ in length. A maximum strength $\Gamma_{max} = 0.05$ for each vortex sheets is chosen to control the error in simulating the diffusion process of vorticity; therefore, at each point, there will be four sheets generated for each unit wall velocity u_w. The disposal of vortex sheets and sheets-blobs transformation will then follow the algorithm described in our numerical model.

The Euler flow for this specific geometry was solved by the SOR-vortex method. The flow domain was discretized for this purpose into square meshes, each of $h_f = 0.05$ in size. The optimal value of relaxation parameter was found to be $\omega_o = 1.87$. To reach 1×10^{-3} accuracy of function under consideration, the number of iteration for each time step are found to range between 20 and 40.

As vortex sheets are continuously created on the walls, the vorticity field of shear layer behind the step and boundary layer along walls start to grow; accordingly, the number of vortex blobs increase with time. Vortex blobs are disregarded once they move beyond the exit section of the channel due to the finite computational domain. The number of vortex elements finally oscillate around a constant value and the flow and vorticity field are then considered to reach a stationary state.

We start our reacting flow calculation when the flow field has been considered fully developed. Previously, a point ignition source was provided at the corner behind the step to study the development of reacting flow from distributed flamelets to flame front (Ghoniem et al, 1982). The number of time steps required to establish a continuous flame front is sometimes over 100. Computational cost of this portion is always expensive, especially when the number of vortex elements reaches several thousands. Therefore, instead of expressing the initial condition in terms of a point ignition, the flame front is introduced as an interface extending along the horizontal centerline throughout the flow field in the combustion section to save some computational efforts.

For the sake of convenience, the mesh size used in the flame front calculation matches that used in non-reacting flow, i.e., $h_c = h_f = 0.05$. The time step for the reacting flow calculation is then properly reduced to satisfy the Courant stability condition.

4.2. Vorticity Field

To visualize the flow field all vortex blobs used in the computation are plotted as small circles while line segments display vectorial properties of their velocities. The developing vorticity fields of Re = 22,000 and Re = 37,000 are displayed in Figure 17 & 18 respectively from T = 0.0 to 10.0 for every twenty time steps. The vorticity fields exhibit large scale structures associated with the generation of finite-size eddies that grow by entraining fluid from the inviscid portion of the flow field. The coherence is manifested by continuous paring of eddies as they propagate downstream. The structure of the mixing layer is located between the free stream of the incoming flow and the recirculation zone. For step height equal to one half of the channel width, the mixing layer is likely to interact with the boundary layer at the upper wall as they both grow downstream. The mixing layer for this specific configuration is certainly affected by the presence of the upper wall as we can also see in Figure 17 and 18.

4.3. Flame Development

Figure 19 depicts the flame front contour and the vorticity field of the reacting flow after T = 11.0 for every 0.2 nondimensional time. The flame front initialized by a horizontal line across the middle of the combustion section, soon follows the flow field and bounds the large scale eddies of the mixing layer which provide, through their stirring action, a good contact between the products in the recirculation zone and the incoming reactants.

The vorticity field of reacting flow still clearly exhibits the large scale structures which are coherent and grow as they move downstream. This suggests that heat release which results in expansion and increase in kinematic viscosity of the gas mixture in the mixing layer does not considerably affect the vortex shedding behind the step. However, the number of vortex elements which have a resemblance to eddies in the turbulent flow field decreases because of the actions of source blobs. This "laminarization" phenomenon in reacting flows (Takagi et al, 1980) results from the increase in viscosity of hot products can be modeled without modifying Reynolds numbers in the computational parameters.

4.4. Mean Velocity Profiles

Velocity profiles at the step and eight equally-spaced cross sections downstream are calculated by averaging the results of 20 consecutive computational time steps. The vorticity field under consideration is shown in Figure 20 and 21, for the cases of Re = 22,000 and 37,000 respectively. Since the flow has reached a stationary state and the incoming flow is steady, time-averaging is identical to ensemble averaging. While the flow field is continuously perturbed by the random samples used in the random walk modeling of diffusion, the growth and decay of instability is governed by the non-linear interaction due to convection.

The comparison between our numerical results and experimental data of Pitz & Daily for the nonreacting and the reacting cases of both Reynolds numbers are displayed in Figure 22 and 23. The results are quite satisfactory. Since the flow behind the step has a definite separation point and is dominated by large eddy structure, which is well reproduced by our method, while the fluctuations associated with high Reynolds number flow conditions are not encumbered by numerical diffusivity, the agreement between the numerical and experimental profiles is especially good in the isothermal case. The discrepancies of mean velocity profiles near the step are properly due to the fact that the number of vortex blobs in the mixing layer is still too small to simulate the large velocity gradient across the layer. This claim can be seen clearer in the reacting flow case where the number of vortex blobs in the shear layer are reduced by the effect of source blobs, the deviation of numerical results from experimental data as a result becomes larger.

Since the reacting flow behind the step is also dominated by the large scale structure that causes wrinkling and stretching of the flame front when entraining the reactants into the combustion zone, our numerical model also yields quite satisfactory results for mean velocity profiles in the reacting case. The increase of flow velocity in the reaction zone due to thermal expansion is properly modeled by volumetric sources along flame front. Our phenomenological model of flame propagation has certainly the capability of predicting the complicated reacting flow field without solving detailed chemical kinetics and energy equation.

4.5. Reattachment Length

The reattachment length is the length measured from separation point of flow field to the reattachment point where the dividing streamline returns to the wall. Its value is often expressed in terms of step height and varies as a function of some flow parameters such as expansion ratio, Reynolds number and boundary layer informations at the step (Eaton and Johnson, 1981)

In the non-reacting case, the reattachment length as deduced from the mean velocity profiles is about eight step heights for both Reynolds numbers, being slightly longer than the data obtained by Pitz & Daily. However, when compared with other experimental data collected by Durst and Tropea (1982), our results even seem to have closer matches in terms of Reynolds number and expansion ratio (Figure 24).

For reacting flow, the length is decreased to between five and six step heights as a consequence of the expansion due to combustion. The recirculation is also reduced accordingly while the maximum reverse velocity and recirculation rate is increased.

4.6. Turbulence Intensities

Turbulence intensities are important parameters in the study of turbulence. These quantities are difficult to evaluate not only by analytical modeling but also by experimental measurements. Even for rearward-facing step, there is a substantial variation between experiments in the values of the turbulence intensity. The variation is probably caused as much by experimental uncertainty as by real difference in the flows. According to the review by Eaton & Johnson (1981), the maximum value of streamwise turbulence intensity $\overline{(u'^2)}^{1/2} / U_o$ lies from about 0.16 to 0.21 for most experiments while the peak value of the shear stress $-\overline{u'v'} / U_o^2$ is estimated to be in the neighborhood of 1.25×10^{-3} .

Figure 25 provides the comparison between the experimental and numerical values of streamwise turbulence intensity $\overline{(u'^2)}^{1/2} / U_o$ in both non-reacting and reacting case. The peak value occurs, as expected from the velocity field, at three places : on both walls and at the start of the mixing layer. Turbulence due to high shear is continuously generated there, giving rise to maximum levels, followed by decay downstream. The maximum value of $\overline{(u'^2)}^{1/2} / U_o$ of our numerical results in the shear layer region is about 0.16, which is at the lower edge of most experimental data. We also have very obviously large intensities on both walls, while the experiment data do not show peaks there. The measured intensities also have very nice profiles which develop with the shear layer. However, the maximum turbulence intensity obtained by Pitz & Daily, $\overline{(u'^2)}^{1/2} / U_o |_{max} = 0.28$,seems to overpredict the value by comparing with other measurements. This leads to a large discrepancies in the comparison of the maximum value.

While numerical results resemble the trend of experimental data, its profiles exhibit more irregular shape in the shear layer region and the discrepancy becomes particularly apparent downstream. The results also show an early decay of the peak value at 2 to 3 step heights upstream the reattachment point. All of these deviations might be in part, due to the following reasons :

(i) the relatively small size of the sample used in evaluating the numerical averages : this is particularly apparent when higher moments of the solution are evaluated. Computing them is equivalent to time differentiation, emphasizing errors in deviations from the mean. Higher moments such as skewness and flatness factor thus were not calculated.

(ii) the influence of the boundary condition at the exit. This can be attributed to two factors : (a) the deletion of vortex blobs at the outflow section to save computational time and (b) the boundary condition $\partial \Psi / \partial x = 0$ or $v = 0$ used to evaluate the potential flow velocity. The fluctuating component of the velocity is artificially reduced, as manifested by the fact that the comparison is more favorable near the step than towards the end of the channel.

(iii) the less accuracy of the vortex blob method near the boundaries where large number of vortex blobs are generated and accumulated. The overlapping of vortex blobs cause large fluctuations of streamwise velocity.

(iv) three-dimensional effect : Experimental results indicate that turbulence intensity grows around the mixing layer close to the separation zone. This is apparently due to three dimensional effects by which energy is drawn from the main flow into turbulent fluctuation by vortex stretching, an effect beyond the scope of our purely two-dimensional model.

In Figure 26 we present the comparison between the experimental and numerical values of transverse turbulence intensity $(\overline{v'^2})^{1/2} / U_o$, in both the reacting and non-reacting case. Our results have better agreement in this direction. The transverse turbulence intensity of numerical calculation is shown to have the similar trend and comparable magnitude as $(\overline{u'^2})^{1/2} / U_o$. while the experimental results show a smaller transverse intensity than the streamwise one (Etheridge & Kemp, 1978).

Since the no-slip boundary condition in our numerical model is satisfied by creating new vortices every time step, the random displacements of vortex elements and the transformation between blobs and sheets in the region of high vorticity density decidedly induce considerable fluctuations of streamwise velocity. The transverse velocity v, on the other hand, is automatically equal to zero when inviscid flow solution is obtained. Therefore, the streamwise turbulence intensities obtained by methods based on vortex dynamics are always found to have a very large value near walls (Dai et al, 1983, Ashurst, 1980) and the transverse turbulence intensities have smaller values and converge earlier to zero near walls.

The discrepancy between experimental turbulence intensities and numerical results was also reported by Briggo, et al (1976), who used a Reynolds stress closure model and a law-of-the-wall boundary condition to compute the same flow field. Their results either under- or over- predicted the streamwise component of turbulence intensity, depending on the rate of velocity generation on the step. A recent publication (Walterick, et al, 1984) on the numerical calculation of the turbulent flow behind a backward-facing step, showed a very good prediction of experimental turbulence intensities. They used the k - ε model with a special modeling of pressure-velocity correlation to match the experimental data. While most of the existing turbulence model requires artificial modeling of some correlation in the averaged Navier-Stokes equation, our method can at least qualitatively predict turbulent intensities without all these artificial informations.

4.7. Conclusions

1. The flow field is dominated by the presence of large scale eddies that separate the incoming reactants from the recirculation zone embodying the combustion products. The far-field effects of the eddies enhance the entrainment of fresh reactants into the mixing zone.

2. The flame front is stabilized on the contours of the eddies and acts as a contact surface between the reactants and the products; as a consequence, it propagates almost tangentially to the local flow direction.

3. The average velocity profiles for both the non-reacting and the reacting case are satisfactorily predicted; thus, without modeling the effect of turbulent fluctuations, the method provides realistic information about the overall dynamic behavior of the flow field.

4. The prediction of turbulence intensity is less satisfactory because of the small size of the sample, and the three-dimensional effects which were not included in our calculations.

5. The length of the recirculation-zone is accurately predicted in both the isothermal and the reacting flowand is relatively independent of the Reynolds number.

Our results indicate that the random vortex method is capable of simulating the large scale, mean behavior of turbulent flow in a two-dimensional field. Turbulent intensity is under-predicted because three-dimensional effects are not taken into account. A large ensemble of data as well as a precise specification of inlet conditions in terms of vorticity distributions are required to accurately evaluate high moments of the velocity field. The flame model we adopted was quite adequate to provide information about the front geometry as well as the dynamic effect of combustion on the turbulent flow field. Some of these conclusions were speculated upon by Peters and Williams (1980) after Ghoniem, et al published their first paper on the model. It is our hope that the new results presented here will promote further constructive debate on the subject.

Chapter 5

Unconfined Flame :
A Turbulent Flame Stabilized by a Circular Flameholder

Inserting rods in the stream of combustible mixtures is another way of stabilizing the flame. The near-wake region behind the rods is capable of recirculating combustion products and continuously igniting the fuel mixture. Fluid mechanics plays an important role in this process. The investigation of the detailed flow field in the wake region behind the circular flame holder can surely give us a better understanding of the mechanisms of flame stabilization.

Two-dimensional turbulent flow behind a circular cylinder has been studied with the vortex method by Chorin (1973) and Cheer (1980) for only a relatively short computational time and Reynolds number up to 10^3. Both their results have shown very interesting initial flow structures. They also predicted accurate drag and lift coefficients with experimental data. Another numerical method based on the QUICK method was used by Davis & Moore (1982) to study flows behind rectangular cylinders. They obtained a series of impressive streakline and isovorticity plots. The computed lift, drag and Strouhal number were also found to compare well with experimental data for Reynolds number below 1000.

Recently, Perry, et al (1982) took advantage of the movie made by Prandtl to obtain the instantaneous streamline patterns behind a circular cylinder for the flow of Reynolds number about 100. A simple model for steady vortex shedding was deduced from those streamline patterns. The salient features of the flow pattern was also interpreted by using properties of critical points. They conjectured that the vortex shedding process behind a circular cylinder is insensitive to Reynolds number.

The visualization of the flow field in experiments are always accomplished by continuously injecting dyes, gas bubbles or small particles upstream the test section. A collection of experimental works of flow visualization can be found in the album by Van Dyke (1980). Numerically, the simulation can be done by releasing a number of passive particles at fixed points upstream the body every time step and tracing their positions at consecutive time steps. Streakline plots at any specific time step can be simply obtained by displaying the instantaneous locations of all particles which have been released. The results of streakline plots obtained earlier by Fromm & Harlow (1963) and recently by Davis & Moore (1982) have attracted a considerable amount of attention.

Although streaklines can be used to give an idea of where the vorticity resides in a flow field, they can tell us very little about the surrounding flow field and the entrainment process. Instantaneous streamlines, which are difficult to be obtained experimentally but are easier to be calculated numerically, can serve this need. The particle paths, on the other hand, describe the trajectory history of specific particles. It gives us the duration of time that particles reside in a given region, thus has application in the areas of chemical reaction.

In this chapter, calculations are extended to a longer computational time to study the development of Karman vortex street at high Reynolds numbers up to twenty diameters downstream. The instantaneous streamlines in the formation zone are used to study the vortex shedding process after the flow is impulsively started. Streaklines and particle pathlines are also computed.

Flame stabilization is an important process in the practical design of combustion chamber. Theories emanating from Spalding (1957) and Zukoski & Marble (1956) in this area are found to correlate data well. Wright & Zukoski (1958) also investigate flame spreading behind flame holders in a confined duct and found that flame spreading is independent of free-stream velocity, temperature, equivalence ratio and flame speed as long as the flow is turbulent and subsonic.

In an unconfined region, flame stabilized behind a circular cylinder always shows a symmetrical wrinkling V-shaped fronts (Petersen & Emmons, 1961, Cheng & Ng, 1983 and Yoshida & Tsuji, 1984). It was found the wrinkles have relatively large mean wavelength compared to the integral scales of the unburned gas turbulence. Although turbulence intensities of unburned gas decrease downstream, the amplitude of wrinkles increases. It has been suggested (Yoshida & Tsuji, 1984) that laminar flame instability plays an important role in the mechanism of flame wrinkling.

Instead of investigating the flame stability and blow-off limit, the results presented in this chapter are primarily concerned with the hydrodynamic effects on flame shape and burning rates in the near wake region behind a circular flame holder. Several different values of burning speed, density ratio and Reynolds numbers are used to investigate their effects.

5.1. Numerical Parameters and Formulations

For simple geometry like a circular cylinder in our case, the inviscid flow component can be easily evaluated by the method of images. The potential flow solution of a uniform flow past a cylinder is obtained by the circle theorem (Miline-Thomson, 1970) as

$$W_p(z) = U_\infty \left[1 - \frac{a^2}{z^2} \right] \tag{5.1}$$

where U_∞ is the velocity of the uniform flow at infinity and a is the radius of the cylinder.

In non-reacting flows, for every vortex blob in the flow domain, there is a corresponding image vortex of reverse strength at the inverse point a^2 / z^* to cancel out the normal velocity component at the surface of the cylinder (Figure 27). Usually a vortex with equal strength at the center of the cylinder is also needed to conserve the vorticity. According to Cheer (1980) this vortex should be omitted in order to satisfy the zero total vorticity condition at infinity. The complex velocity induced by all vortex blobs can be obtained as

$$W_v(z) = \sum_{j=1}^{N_v} \frac{i\Gamma_j}{2\pi} \left(\frac{|z - z_j|}{\max(|z - z_j|, r_o)} \frac{1}{z - z_j} - \frac{\left| z - \frac{a^2}{z_j^*} \right|}{\max\left(\left| z - \frac{a^2}{z_j^*} \right|, r_o \right)} \frac{1}{\left(z - \frac{a^2}{z_j^*} \right)} \right) \tag{5.2}$$

In reacting flows, image source blobs have same signs and strengths as their corresponding ones along flame front. The complex velocity induced by all source blobs can be formulated in a similar way as:

$$W_s(z) = \sum_{j=1}^{N_s} \frac{\Delta_j}{2\pi} \left(\frac{\left| z - z_j \right|}{\max(\left| z - z_j \right| r_s)} \frac{1}{z - z_j} - \right.$$

$$\left. \frac{\left| z - \frac{a^2}{z_j^*} \right|}{\max\left(\left| z - \frac{a^2}{z_j^*} \right| , r_s \right)} \frac{1}{\left(z - \frac{a^2}{z_j^*} \right)} \right) \tag{5.3}$$

The total inviscid flow solution thus can be obtained by adding up above equations. For the sake of convenience, the diameter d and the uniform flow velocity U_∞ are chosen as the characteristic length and velocity for nondimensionalization. The time scale is therefore nondimensionalized with respect to d / U_∞ .

To calculate the boundary-layer flow near the surface of the cylinder, the surface is divided into two parts : the upper and the lower semi-circle. Each part is then discretized into a number of equally spaced segments. Since it is easier to compute the flow field in a universal coordinate, each semi-circle is transformed into a line segment according to the following formula

$$x' = a \cdot \left[\pm\pi - \tan^{-1} \frac{y}{x} \right] \tag{5.4}$$

$$y' = \sqrt{x^2 + y^2} - a \tag{5.5}$$

where superscript ' denotes the coordinate after transformation ; + and - sign in equation (5.4) apply to the upper and the lower semi-circle respectively. The front stagnation point of the cylinder then becomes the leading edge of a flat plate. Vorticities are created and disposed following the algorithm described in section 2.1.2.2. After the velocity field in the boundary layer and the locations of all vortex sheets are obtained, the coordinate is then transformed back to the physical domain in order to check if there are any vortex sheets moved from the upper semi-circle to the lower one or vice versa. Transformation between vortex sheets and vortex blobs as well as locations of newly generated vortex blobs can also be found.

Since the recirculation zone behind the circular flameholder acts as an constant ignition source, the reacting flow calculation is initialized by a line ignition source behind the cylinder. A delay of ten computational time steps after the flow is impulsively started is used to start the motion of the flame so that the flame front can interact with leading vortices.

The combustion domain behind the cylinder is divided into a number of square cells. The size of each cell is chosen to be $h_c = 0.25$, so that the The size of each cell is chosen to be about the same as the distance between check points along the surface of the cylinder such that the computational time step of flame propagation can match that used for the calculation of turbulent flow field. The spatial resolution of flame front is also required to be high enough to identify the flame contour without doing any additional interpolation. The number of cells in each direction is properly selected to ensure that the flame front does not spread out of the computational domain. The laminar flame speed normalized with respect to uniform flow velocity S_u has the value of from 0.02 to 0.04. The density ratio V across flame front also varies from 6.0 to 11.0 for any study of their effects on the flame propagation. Reynolds numbers of 10^4 and 10^3 are used in the reacting flow calculation.

5.2. Vorticity and Flow Development

The flow is initially started with a uniform velocity $U_\infty = 1$. Vorticities represented by vortex blobs are gradually generated at walls to satisfy no-slip condition and are carried downstream as time goes on. Figure 28. (a)-(d) displays the vorticity field in the wake region at $Re_d = 10^4$, where $Re_d = U_\infty d/\nu$,from nondimensional time 1 to 20 for every 10 computational time steps. Each point in the figure represents the location of a vortex blob while the line segment associate with the point represents the velocity vector of the vortex blob as before. These plots of vorticity field not only show the vorticity distribution of the turbulent flow, but also give us a streakline like picture of the flow structure as we will discuss in the later section.

The flow first develops symmetrically after impulsively started. It then becomes asymmetric when the vortices shed from upper part of the cylinder start to interact with the vortices of opposite sign shed from lower part of the cylinder. Vortices are then carried downstream by the convection velocity and grow by entraining surrounding inviscid fluid. As the defect velocity in the wake region becomes smaller downstream, the celerity or the propagating velocity of each vortex center gradually increases to the free stream velocity. The centers of vortex structures become difficult to identify in the figures. However, their positions can be found by subtracting the local flow velocity to the free-stream velocity or the predicted celebrity of each vortex center (Cantwell & Coles, 1983). It can also be noticed from the figure that as the flow propagates downstream, the vorticity field spreads out wider and wider due to the viscous diffusion (or random walk). The number density of vortex blobs inside the large scale structure also becomes smaller. This implys that the circulation of large scale structures decays as the structures move downstream.

5.3. Vortex-Shedding Process

For flows at low Reynolds number, the Von Karman vortex street has already been recorded by many investigators (Taneda, 1952). It was found that the flow pattern still exhibits regular structures up to Reynolds number of the order of 10^5 . However, the detailed vortex shedding process behind the cylinder is still not well understood. Recently, Perry et al (1982) made an effort to investigate the vortex shedding process for the flow past a cylinder or a vertical plate at low Reynolds numbers experimentally. In this section, the process will be studied for higher Reynolds numbers by our numerical model.

In order to inquire into the vortex-shedding process, the instantaneous streamlines in the vortex formation zone for Reynolds numbers of 10^4 and 10^5 are calculated. Numerically streamlines can be obtained either by integrating the instantaneous velocities

$$\Psi (z) = \int u \, dy = - \int v \, dx \tag{5.6}$$

or by directly taking the imaginary part of the complex potential Ω (z) = Φ (z) - i Ψ (z). For a uniform non-reacting flow past a circular cylinder, the stream function can be formulated as

$$\begin{aligned} \Psi (z) = {} & U_\infty y \left(1 - \frac{a^2}{| z |^2}\right) + \sum_{j=1}^{N_v} \frac{\Gamma_j}{2\pi} \left[\frac{| z - z_j |}{max(| z - z_j | , r_e)} + \right. \\ & \left. \log\left(\frac{max(| z - z_j | , r_e)}{a} \right) - 1 \right] \end{aligned} \tag{5.7}$$

A continuous streamline is obtained by connecting all the points which have same values of stream function in the flow field. Results in Figure 29 and 30 show that after the flow is impulsively started, two symmetric separation bubbles begin to grow behind the cylinder. As a consequence of the hydrodynamic instability, one of these two bubbles becomes bigger than another as shown in Figure 29.a and 30.a. At T = 2, the bigger one starts to detach from the surface of the cylinder and moves downstream. The so-called "alleyway" forms between two cavities. As the front cavity is gradually carried downstream, its size becomes smaller and finally opens up as shown in Figure 29.b and Figure 30.b.

Meanwhile, another cavity starts to leave from another part of the surface and propagates downstream. The sizes of cavities are about the same as the diameter of the cylinder for two Reynolds numbers under study. This is different from the experimental results of low Reynolds numbers obtained by Teneda (1952), for which the size of each cavity can grow to as big as three diameters.

Mostly, cavities will become smaller and finally open up before they reach two diameters downstream. Saddle points then cease to exist and streamlines become wave-like afterward. It could sometimes happen that cavities will entrain more fluids and grow in size again (see Figure 30.b). The cavities in this case can remain closed for a longer time.

By comparing the instantaneous streamlines in Figure 29 and 30 with those obtained by others (see, for example, Perry et al, 1984 and Cantwell & Coles, 1983), one can find that the vortex shedding process behind a bluff body at high Reynolds number has the same qualitative picture as that at low Reynolds number except that the vortex formation region reduces in size. Separation cavities with two different rotating directions shed alternatively from the back surface of the cylinder. They form centres, saddle points and alleyways in the wake region. The centres in the cavities do not necessarily match foldings of vortex sheets, while the valleys of the wave-like vorticity field always correspond to the saddle points.

5.4. Streamlines, Pathlines and Streaklines

The unsteady feature of the flow can be examined by the differences among streamlines, pathlines and streaklines. A streamline is a space curve which is tangent everywhere to a velocity vector, a pathline is the trajectory of a fluid particle of fixed identity, while a streakline is the instantaneous locus of points that connect the location of all particles which have passed through a fixed point in the flow field. They are all identical in a steady flow.

Instantaneous streamlines at T = 20, as observer stays stationary with respect to the cylinder, are shown in Figure 31.a. They exhibit wave-like shapes except in the vortex formation zone. Figure 31.b shows the corresponding streamlines as observer stays stationary with respect to the incoming flow. Centers of vortices do not arrange themselves on two rows with a definite spacing ratio as that occurs at lower Reynolds numbers. Instead, two neighboring vortices of same rotation tend to get closer, while another two neighboring vortices of opposite sign are going apart. We can therefore observe two vortices separate another two of opposite sign in an alternative way. Two neighboring vortices of same sign also have the tendency to merge into a single vortex as shown in Figure 31.b. The strong interaction of two vortex streets at high Reynolds number was also observed by Papailiou and Lykoudis (1974) in their experimental investigation of a turbulent wake.

Streaklines are calculated by releasing 12 passive particles every computational time step at 12 equally spaced locations upstream the cylinder. Results of the instantaneous locations of all released particles are shown in Figure 32 for T = 5.0, 10.0, 15.0 and 20.0 respectively. Streaklines are found to be quite chaotic in the wake region, but are continuous and smooth in the outer part of the flow. This is consistent with most of the experimental results (Van Dyke, 1980).

By comparing Figure 28 with Figure 32, one finds that the chaotic region of streaklines exactly matches the place where vorticities are distributed. It was also found by Davis & Moore (1982) in their calculation of flows behind rectangular cylinders that streaklines exactly match the plots of isovorticity. This is not surprising because vortices (or eddies) are the fundamental elements of turbulence.

Figure 33 presents 12 particle pathlines by following their motions from time T = 0.0, 5.0, 10.0, 15.0 to T = 20.0 respectively. Consecutive points represent their instantaneous positions at the following time step. Distances between consecutive points along the same pathline are thus proportional to their instantaneous velocities. Particles will have larger residence time if they have ever been brought into the wake region by the flow field.

5.5. Flame Development

Development of turbulent flame behind a circular flameholder are studied by igniting the flow at the 10th computational time step after the flow is started. Results of flame fronts and the corresponding vorticity fields are shown in Figure 34. The flame first propagates symmetrically with a slower motion near the center line of the cylinder due to the effect of defect velocity. At T = 3 the first vortex structure, which just shed from the surface of the cylinder, starts to stretch the flame front and entrains unburned mixtures into the burned region. After some time part of the entrained unburned mixtures are surrounded by burned products and form islands and pockets inside the flame contours. These unburned islands not only increase the burning area, but also widen the flame spreading angle by pushing out flame fronts as a result of the volumetric expansion. The burning rate is also increased by flame wrinkling and entrainment mechanism of turbulent eddies. Computations are performed from non-dimensional time T = 0.0 to 15.0. Although the flame front is still in its developing stage, the tendency of the flame front to develop into a V-shaped flame can be seen from Figure 34.

Figure 35.a - 35.e provide the comparison of the instantaneous vorticity field and velocity vectors between non-reacting and reacting flows from T = 11.0 to 15.0. Local velocities in the wake region are found to be quite fluctuating for both cases. The velocity vectors of reacting flows outside the flame boundary indicate the divergence of streamlines. This is in agreement with the experimental results reported by Cheng & Ng (1982). The vorticity field of the reacting flow has a considerable deterioration of order in the vortex sheet and it is also shown to be more diffused than that of the non-reacting flow.

Several other cases of flame development are also studied by varying values of normal burning velocity, density ratio and Reynolds number. Results of flame fronts at T=15.0 for each case are shown in Figure 36. By increasing density ratio and burning speed, flame fronts are found smoother and no more unburned pockets exists inside burned region. Figure 37 shows the results of burning rates for each case. Burning rates for all other cases are found to be larger initially and then are caught up by the case with smaller density ratio and flame speed. This is due to the fact that flame area is reduced by the smoothing effect of larger thermal expansion. According to Figure 37, Reynolds number has only very little effect on the burning rate. But flame front at higher Reynolds number can follow the shape of large scale structures better than that at lower Reynolds number because of higher turbulence intensities. In our flame model, viscosity changes due to combustion are not taken into account. Its value can change dramatically due to temperature increase and this is probably one of the reasons why symmetrical flame structure is not accurately modeled by our numerical method.

5.6. Conclusions

1. Periodic vortex street structure exists up to the largest Reynolds number under study (1×10^5), however, the vortex pairing and diffusion process cause some irregularities in vortex spacings.

2. The size of separation bubble behind the cylinder at high Reynolds number is found to be about the same size as the diameter of the cylinder. The closed cavity behind the cylinder can sustain only for a short period of time.

3. The size of cavities always reduces downstream and finally opens up. However, the cavity may have the chance to entrain more fluids inside itself and grows in size.

4. Vortex shedding process in the formation zone has the same qualitative picture as long as the Reynolds number is below the critical value.

5. Although the flame front is stabilized at the outer contour of eddies, the alternating large scale structures are destabilized by the thermal expansion of combustion process. The growth of the amplitude of wrinklings is associated with the growth of the large coherent structures by the diffusion process.

6. Since the inertial force dominates the flow fields under investigation, Reynolds number has little effect on the flame propagation except that the flame shape can follow the large scale structures better at higher Reynolds number.

7. Large normal burning velocity and density ratio does not necessarily have higher burning rate and spreading angle of flame fronts because they tend to smooth out the flame shape and decrease the burning area. On the other hand, flame propagation with smaller burning velocity will tend to have wrinkler flame front due to stronger interactions of turbulent eddies. The unburned pockets inside the flame front , which will push the flame more outward when they become burned, can also increase the burning rate of the reacting flow.

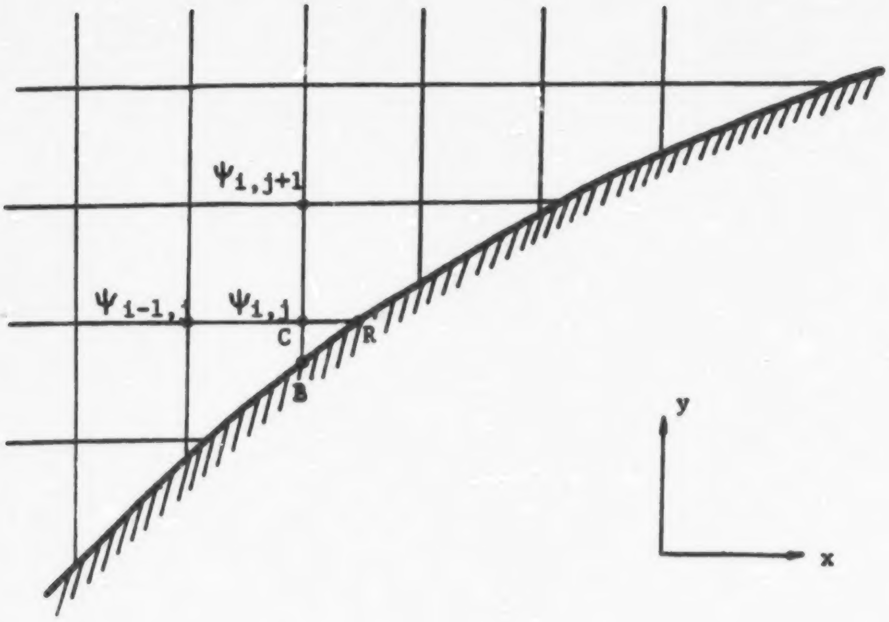
$\Psi_{i,j+1}$
$\Psi_{i-1,j}$
$\Psi_{i,j}$
C
R
B
y
x

Fig. 1 Configuration of grid points near a curve boundary.

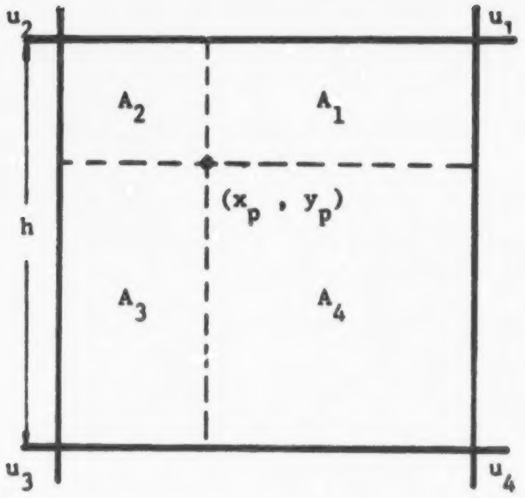
u_2
u_1
A_2
A_1
(x_p, y_p)
h
A_3
A_4
u_3
u_4

Fig. 2 Area weighting scheme for velocity interpolation

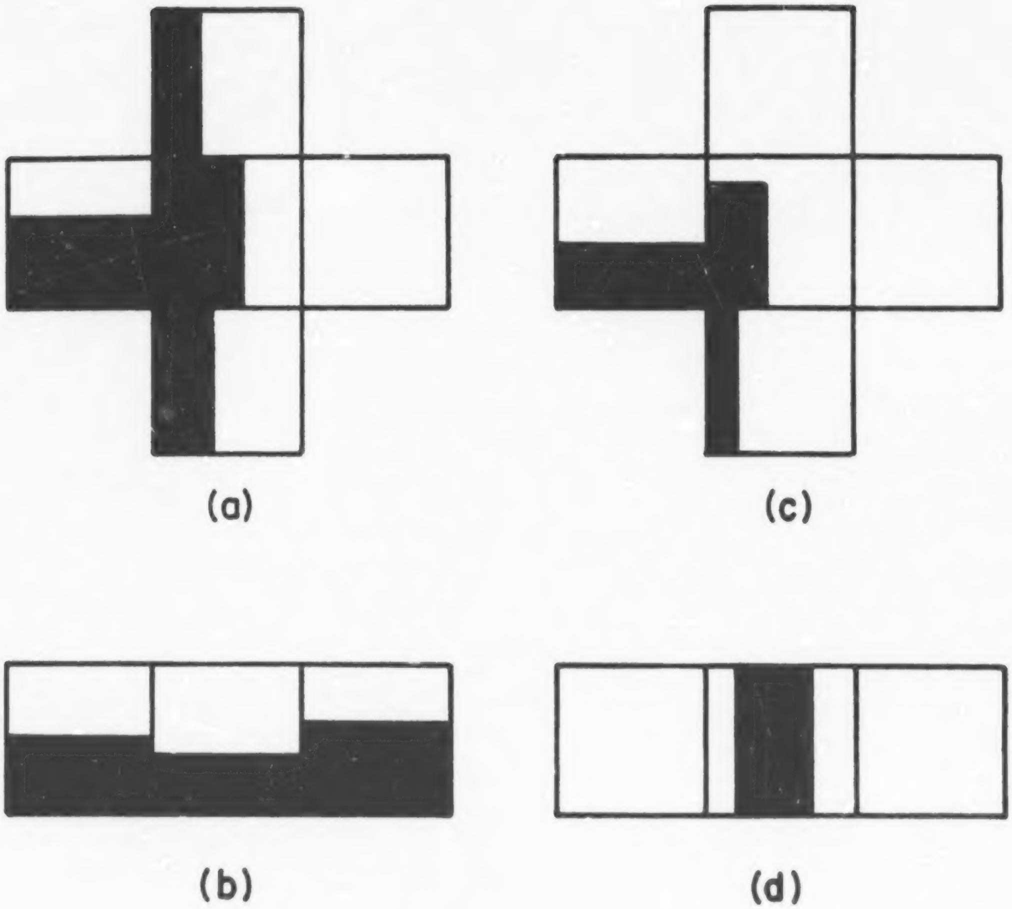

Fig. 3 Classification of interface geometries according to SLIC algorithm.

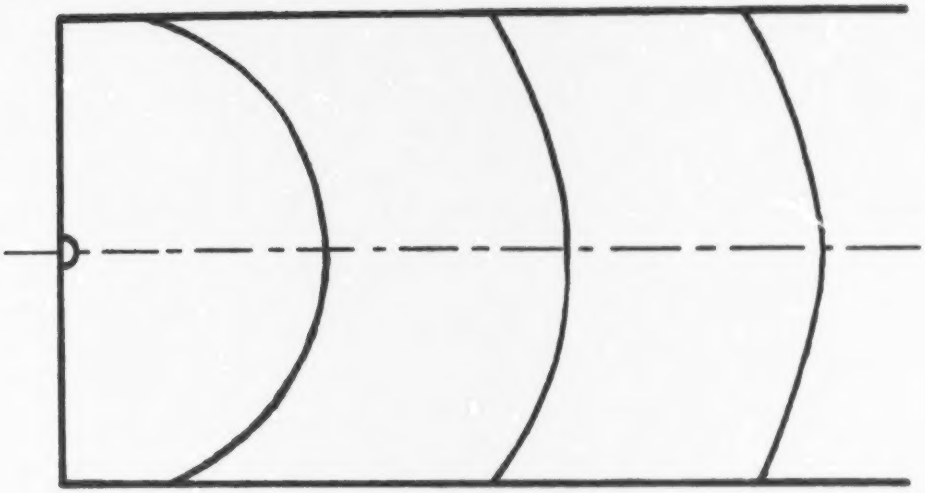

Fig. 4 Illustration of the Huygens principle by flame propagation in a parallel duct.

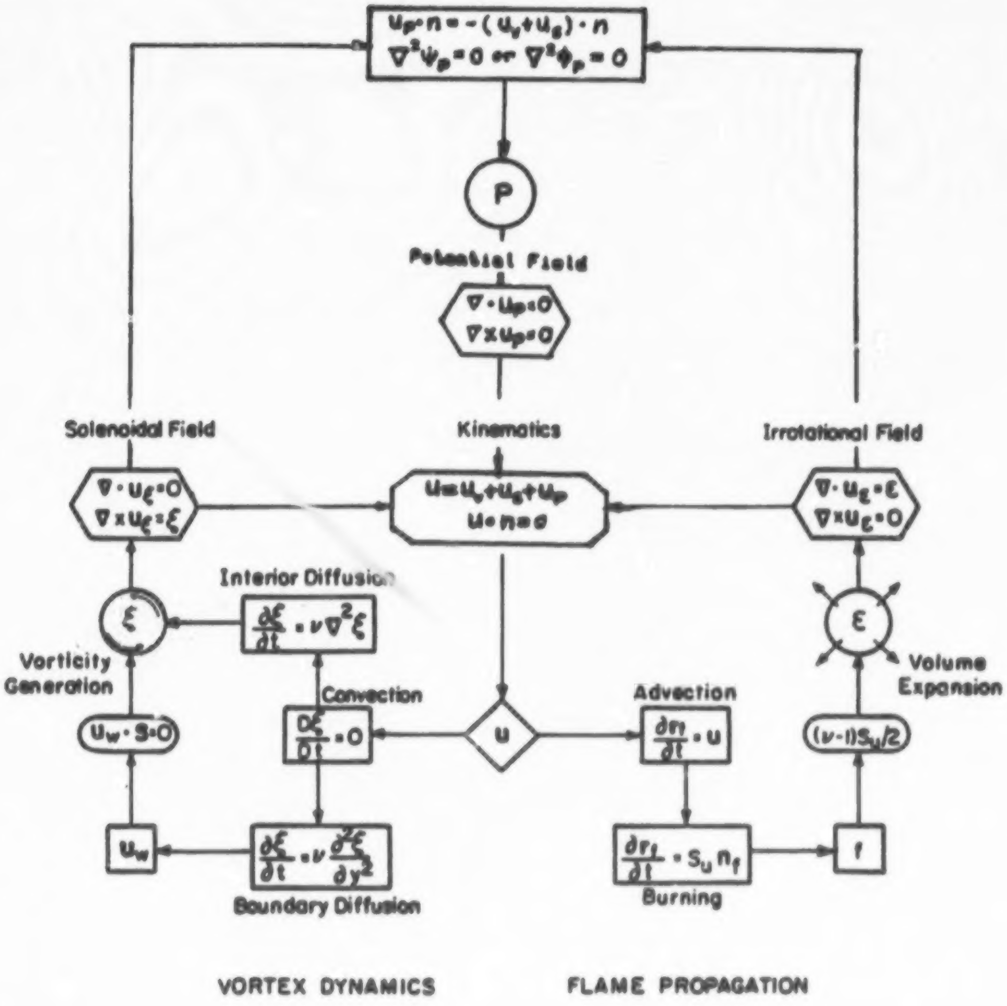
$u_p \cdot n = -(u_v + u_\varepsilon) \cdot n$
$\nabla^2 \psi_p = 0$ or $\nabla^2 \phi_p = 0$
P
Potential Field
$\nabla \cdot u_p = 0$
$\nabla \times u_p = 0$
Solenoidal Field
Kinematics
Irrotational Field
$\nabla \cdot u_\xi = 0$
$\nabla \times u_\xi = \xi$
$u = u_v + u_\varepsilon + u_p$
$u \cdot n = 0$
$\nabla \cdot u_\varepsilon = \varepsilon$
$\nabla \times u_\varepsilon = 0$
Interior Diffusion
ξ
$\frac{\partial \xi}{\partial t} = \nu \nabla^2 \xi$
ε
Vorticity Generation
Convection
Advection
Volume Expansion
$u_w \cdot s = 0$
$\frac{D\xi}{Dt} = 0$
u
$\frac{\partial r_f}{\partial t} = u$
$(\nu - 1) S_u / 2$
u_w
$\frac{\partial \xi}{\partial t} = \nu \frac{\partial^2 \xi}{\partial y^2}$
$\frac{\partial r_f}{\partial t} = S_u n_f$
f
Boundary Diffusion
Burning
VORTEX DYNAMICS
FLAME PROPAGATION

Fig. 5 The overall solution procedures for reacting flows.

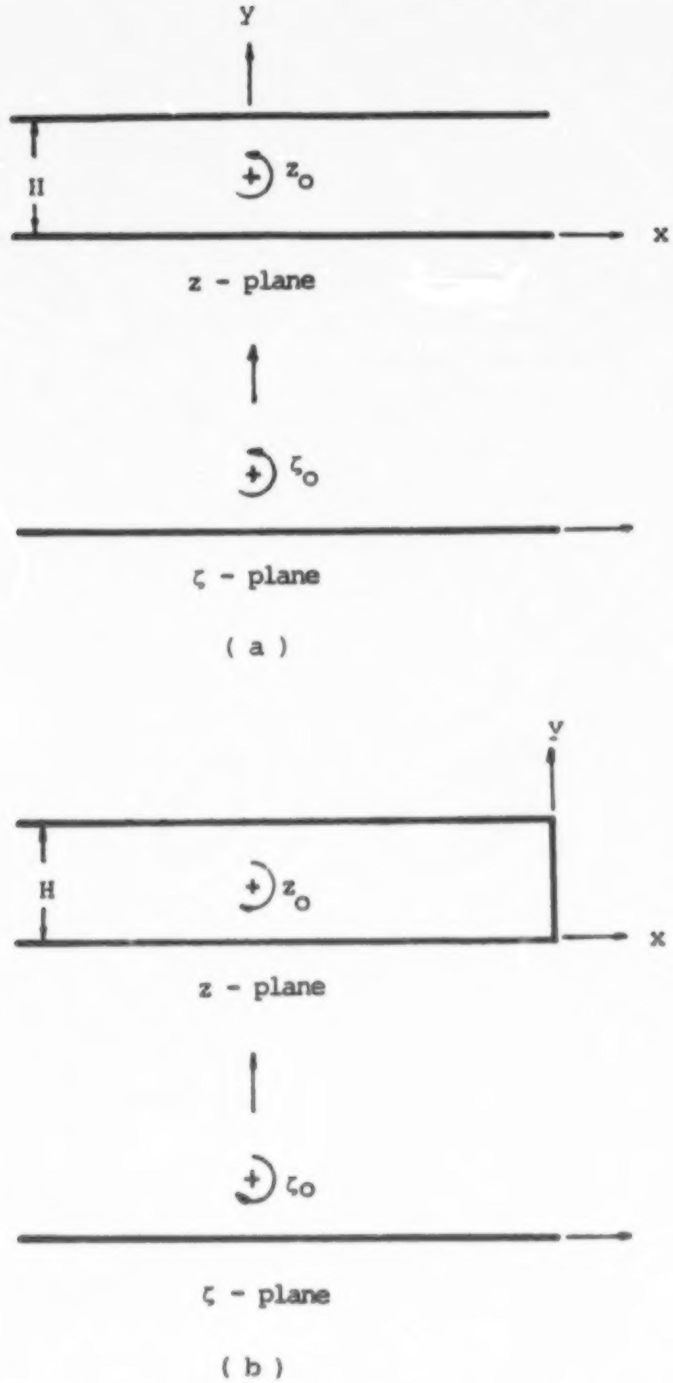
y
z_o
H
x
z - plane
ζ_o
ζ - plane
(a)
y
H
z_o
x
z - plane
ζ_o
ζ - plane
(b)

Fig. 8 (a) The coordinate system of a duct with open ends.

(b) the coordinate system of a duct with one closed end.

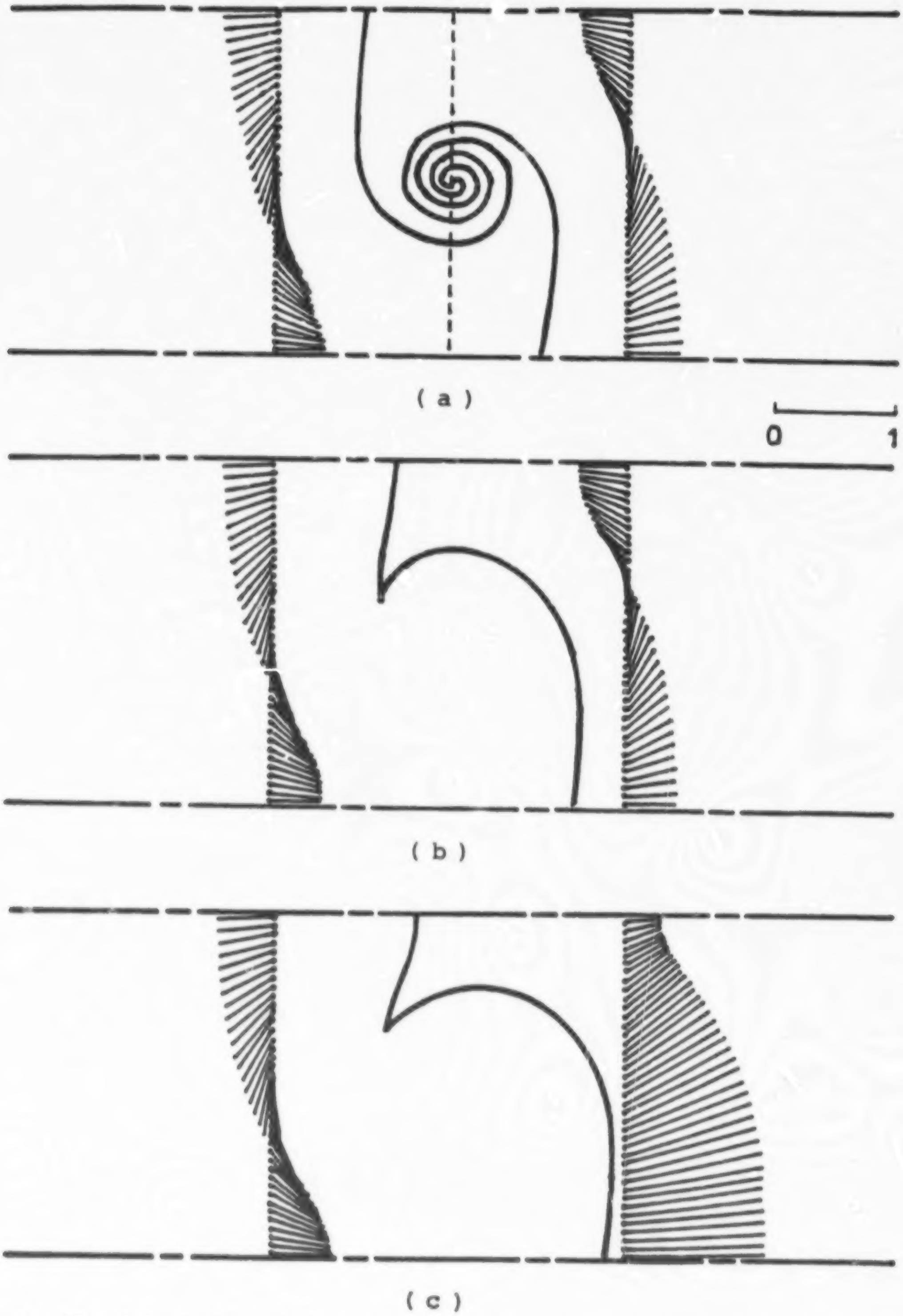

Fig. 7 The deformation of flame fronts and velocity vectors in an open duct due to three fundmental mechanisms of flame propagation.

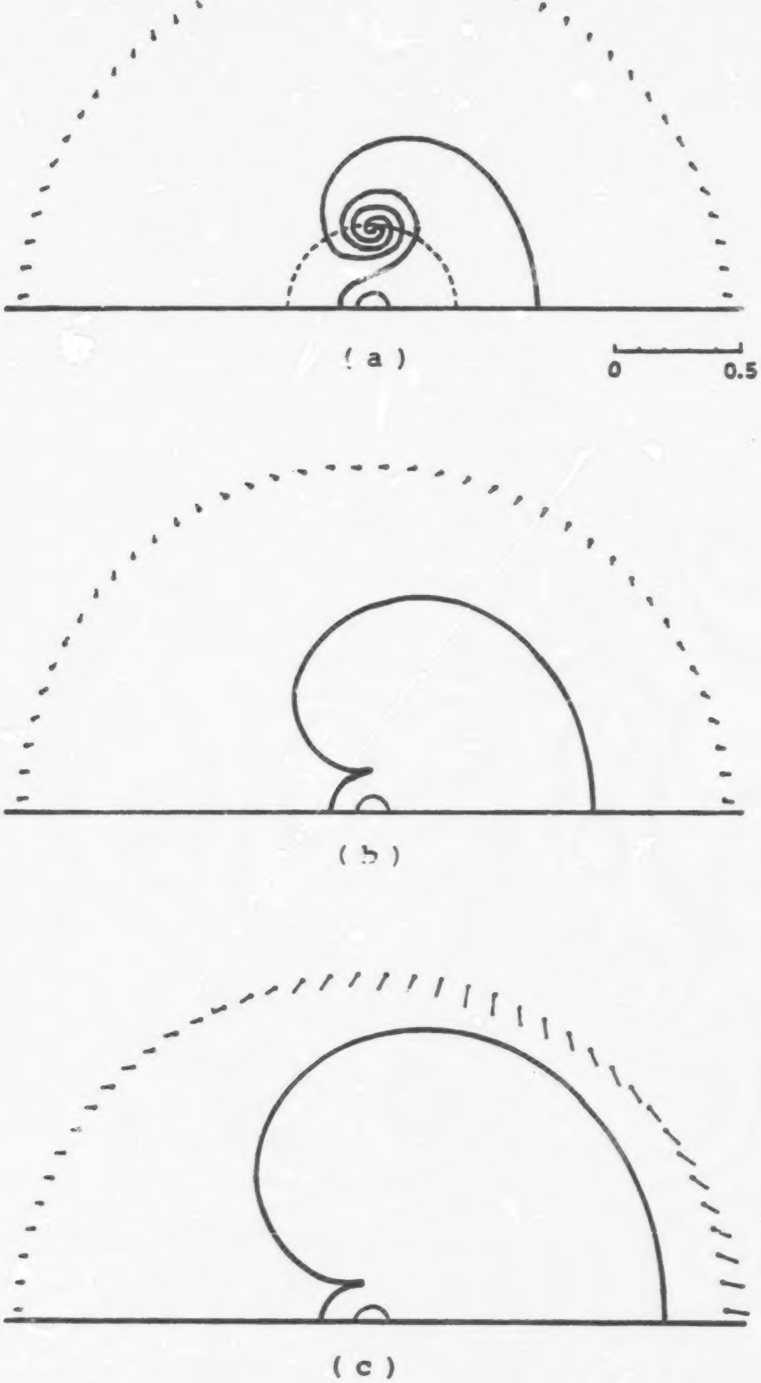

Fig. 8 The correponding plots of Fig. 7 in the transformed plane.

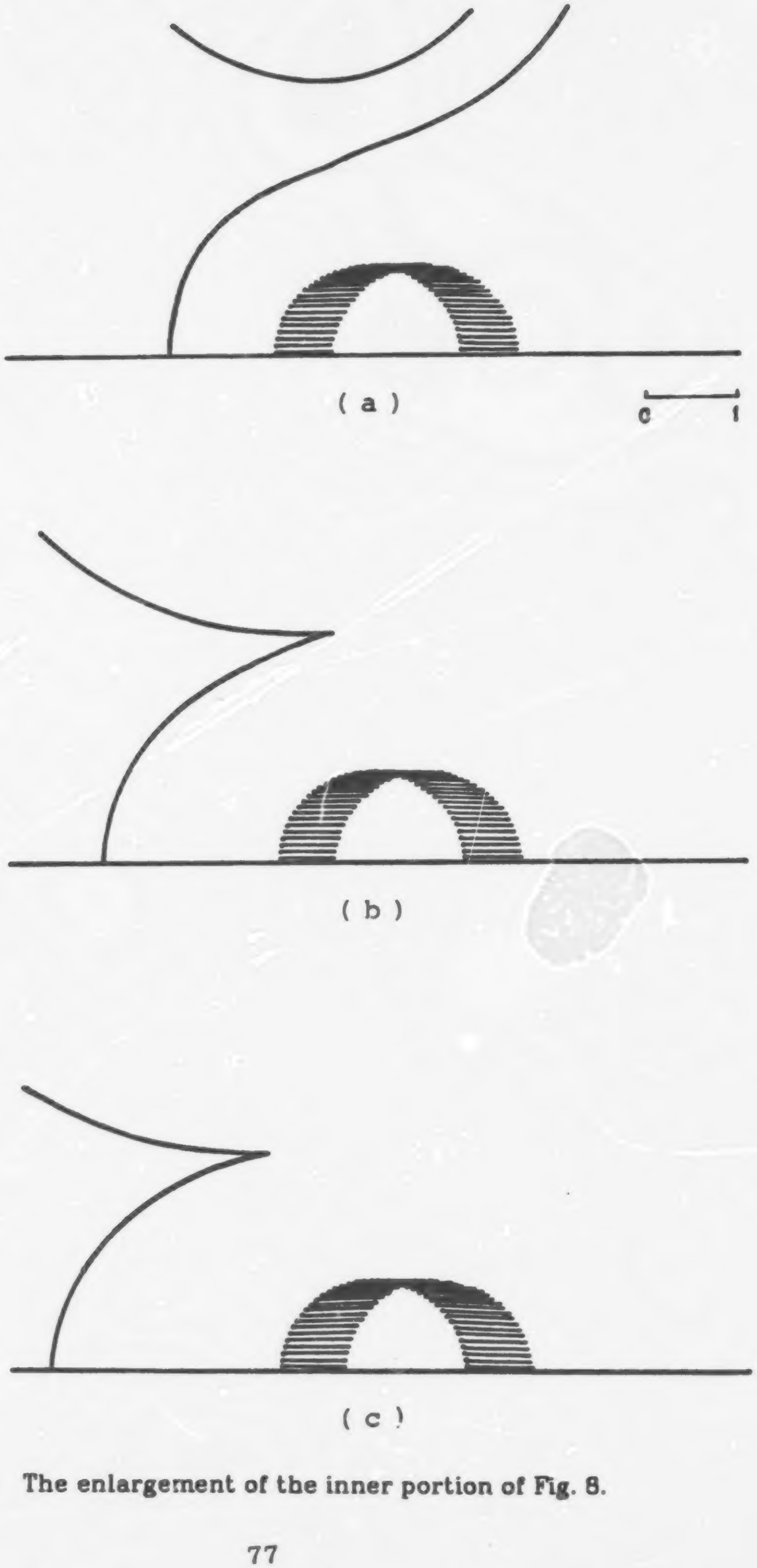

Fig. 9 The enlargement of the inner portion of Fig. 8.

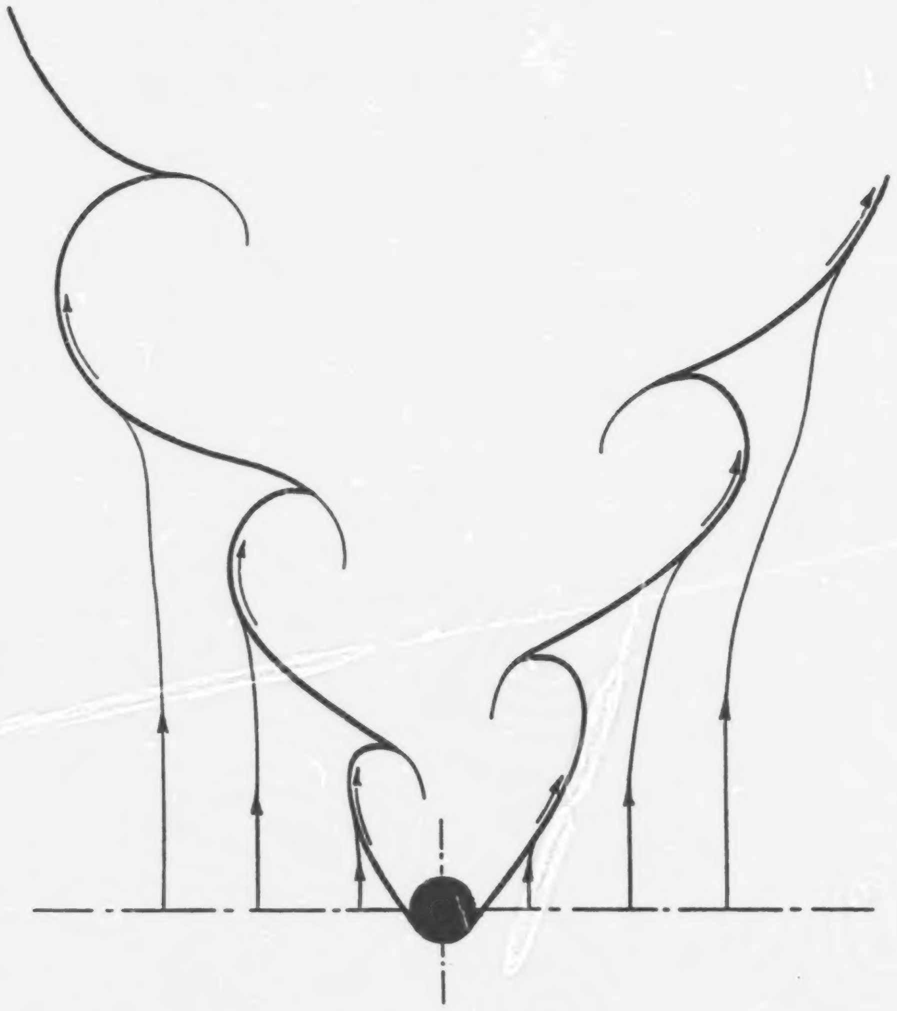

Fig. 10 A phenomenological sketch of flame front stabilized by a circular rod holder.

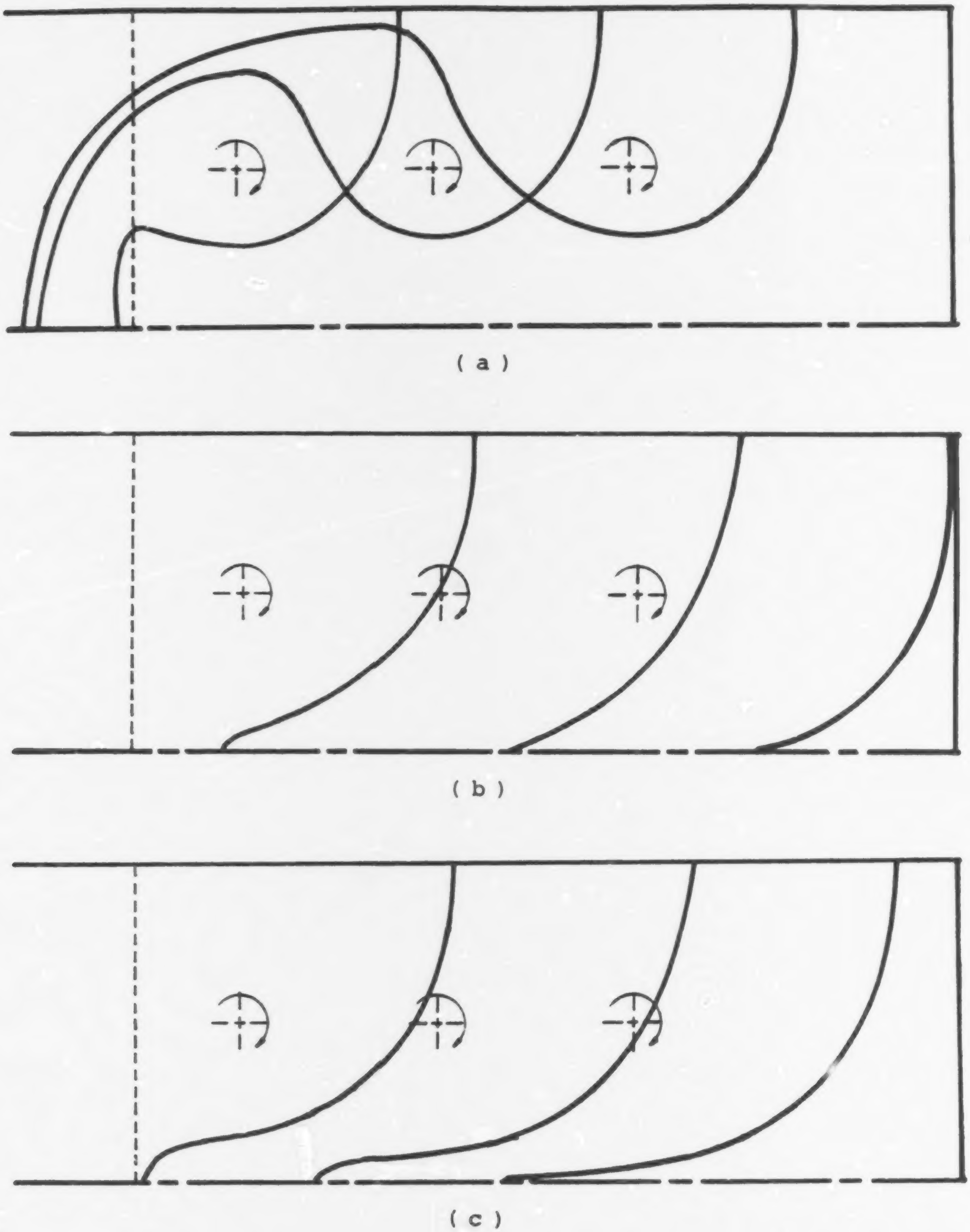

Fig. 11 The deformation of flame fronts in a closed duct at the 40th , 120th and 200th time step.

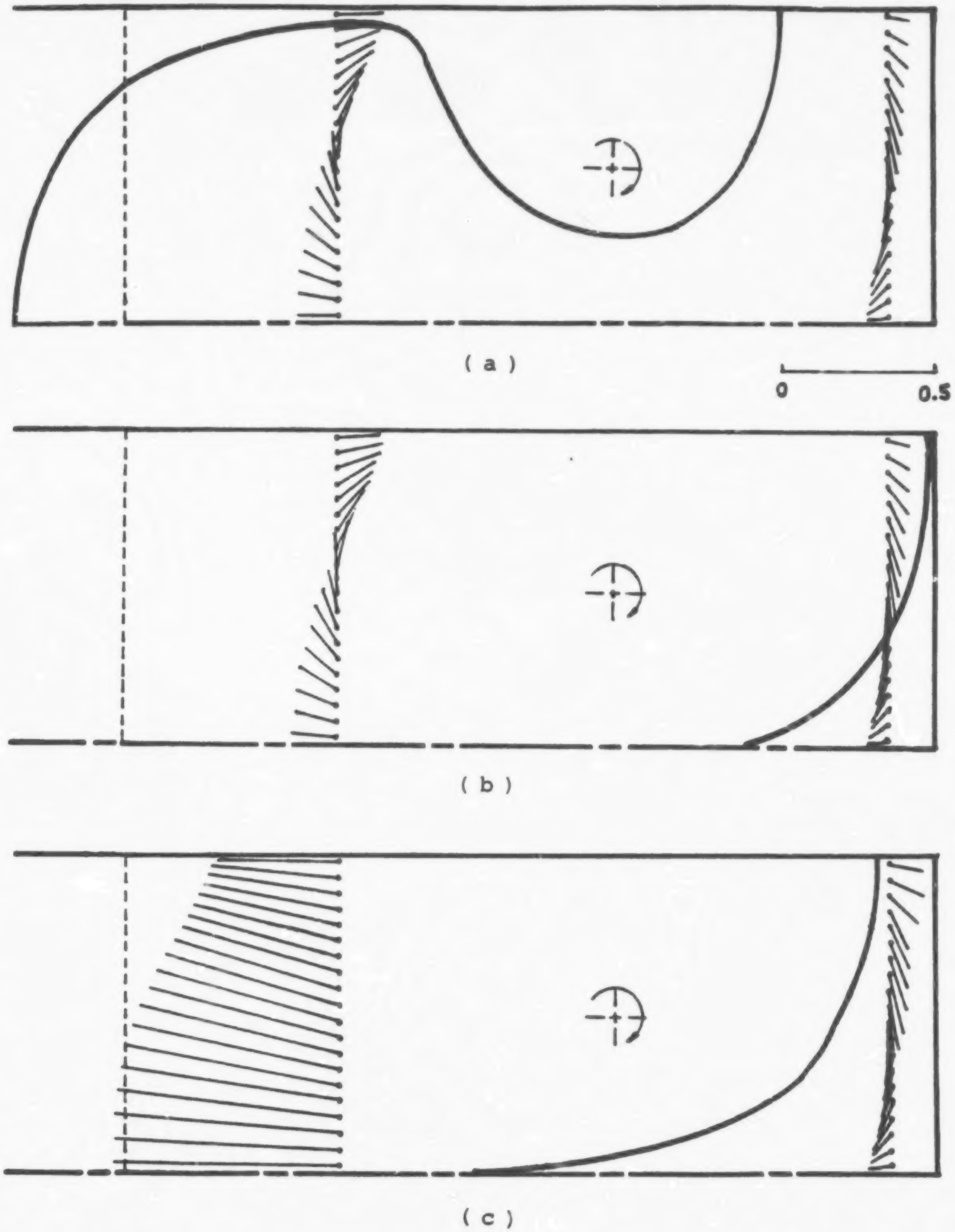

Fig. 12 The flame fronts and velocity vectors at the 200th time step.

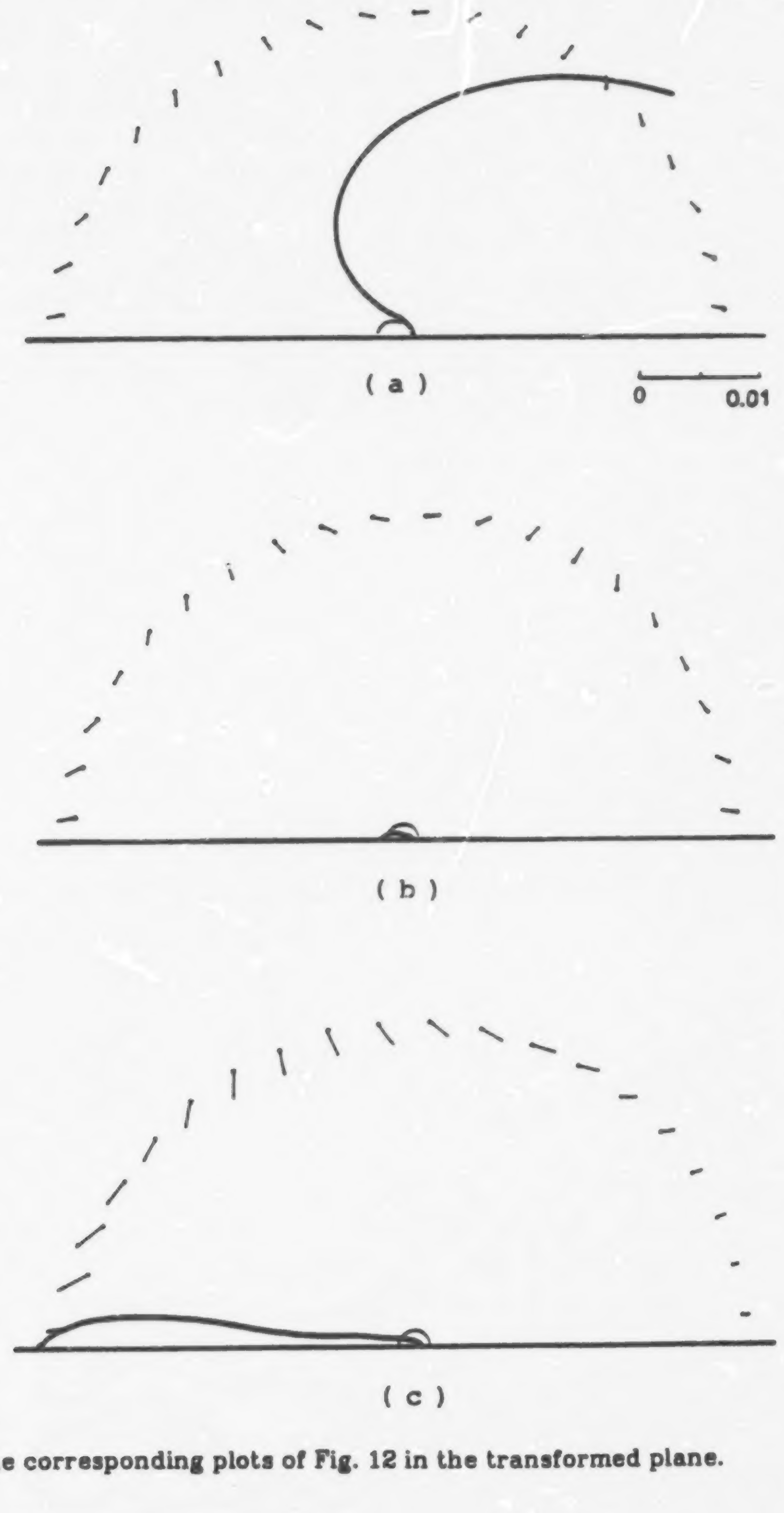

Fig. 13 The corresponding plots of Fig. 12 in the transformed plane.

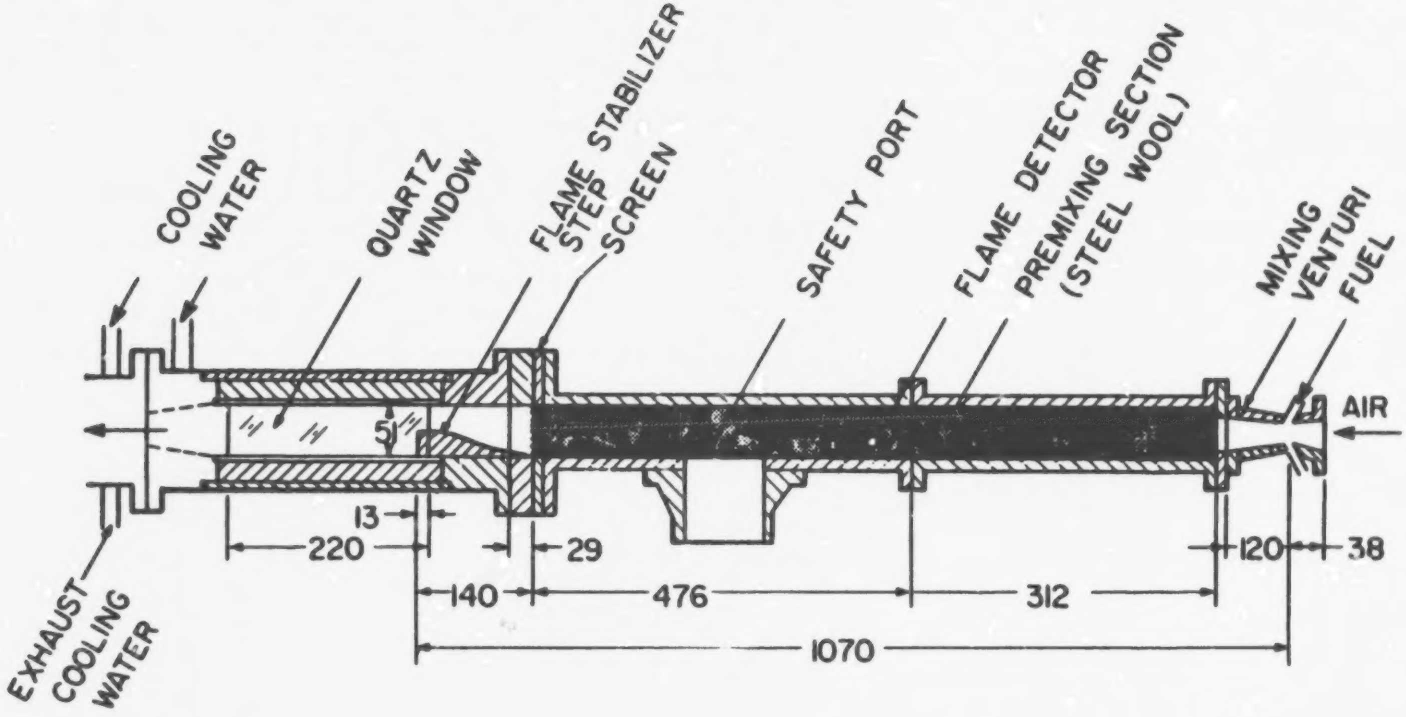
COOLING WATER
QUARTZ WINDOW
FLAME STABILIZER
STEP
SCREEN
SAFETY PORT
FLAME DETECTOR
PREMIXING SECTION (STEEL WOOL)
MIXING VENTURI
FUEL
AIR
51
13
220
29
140
476
312
120
38
1070
EXHAUST COOLING WATER

Fig. 14 The cross section and dimensions of the two-dimensional combustor used by Pitz & Daily (1983).

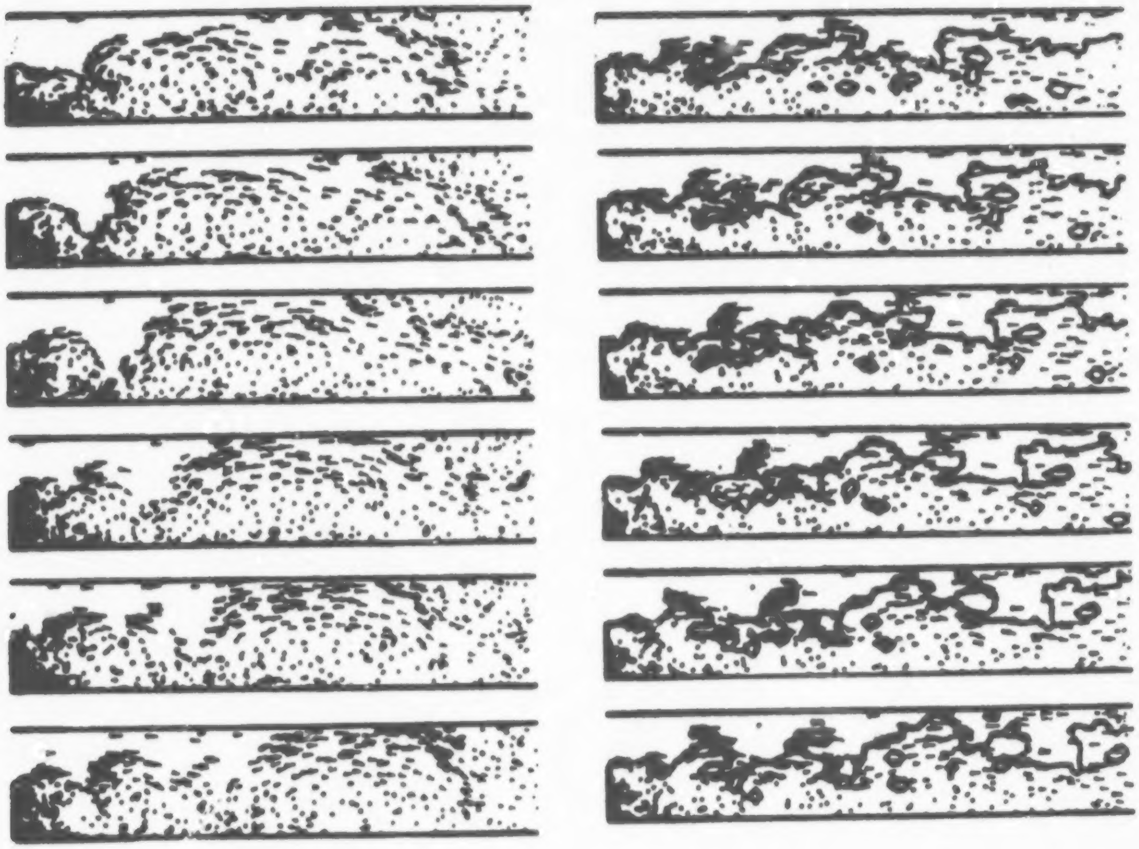

(a) (b)

Fig. 15 The numerical results obtianed by Ghoniem et al (1982) for (a) non-reacting flow, and (b) reacting flow behind a rearward-facing step.

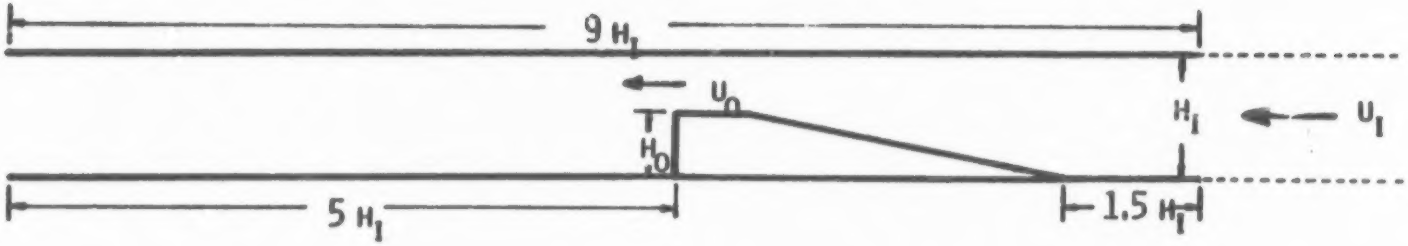
9 H_I
U_O
H_O
H_I
U_I
5 H_I
1.5 H_I

Fig. 16 The configuration of the rearward-facing step combustor used in the numerical simulation.

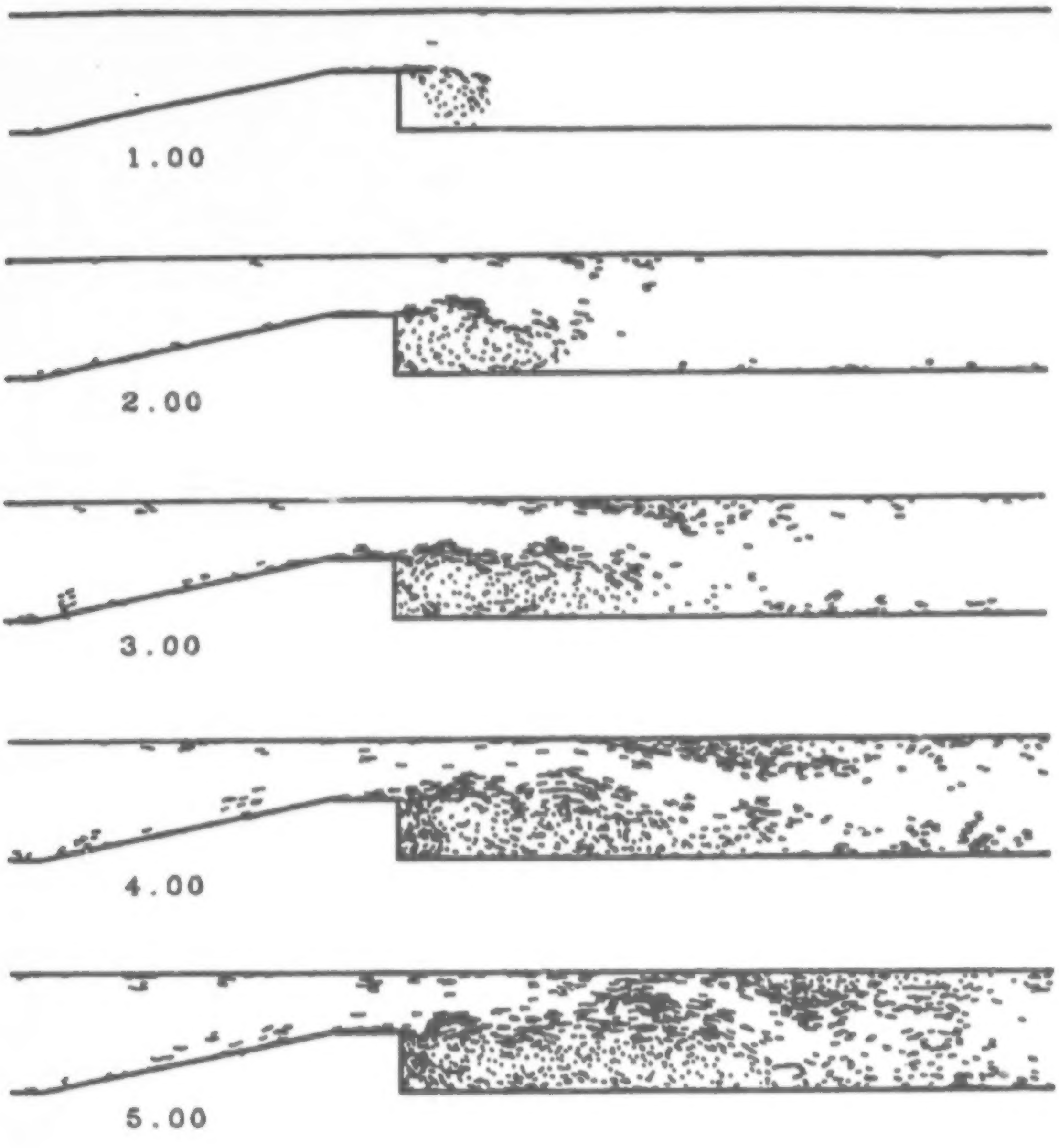
1.00
2.00
3.00
4.00
5.00

Fig. 17.a

Fig. 17 The developing vorticity field of the non-reacting flow at Re = 22,000.

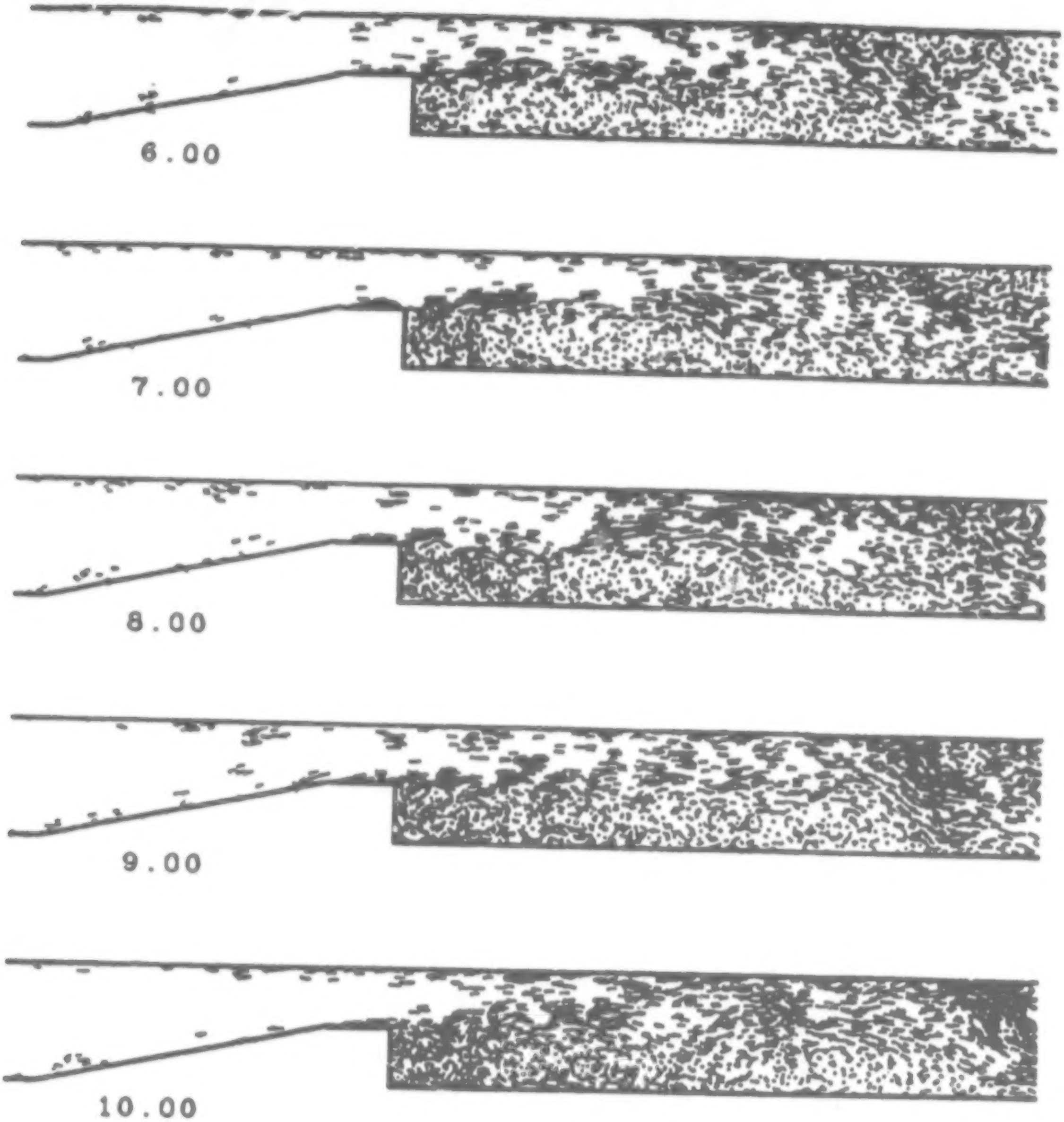

6.00
7.00
8.00
9.00
10.00

Fig. 17.b

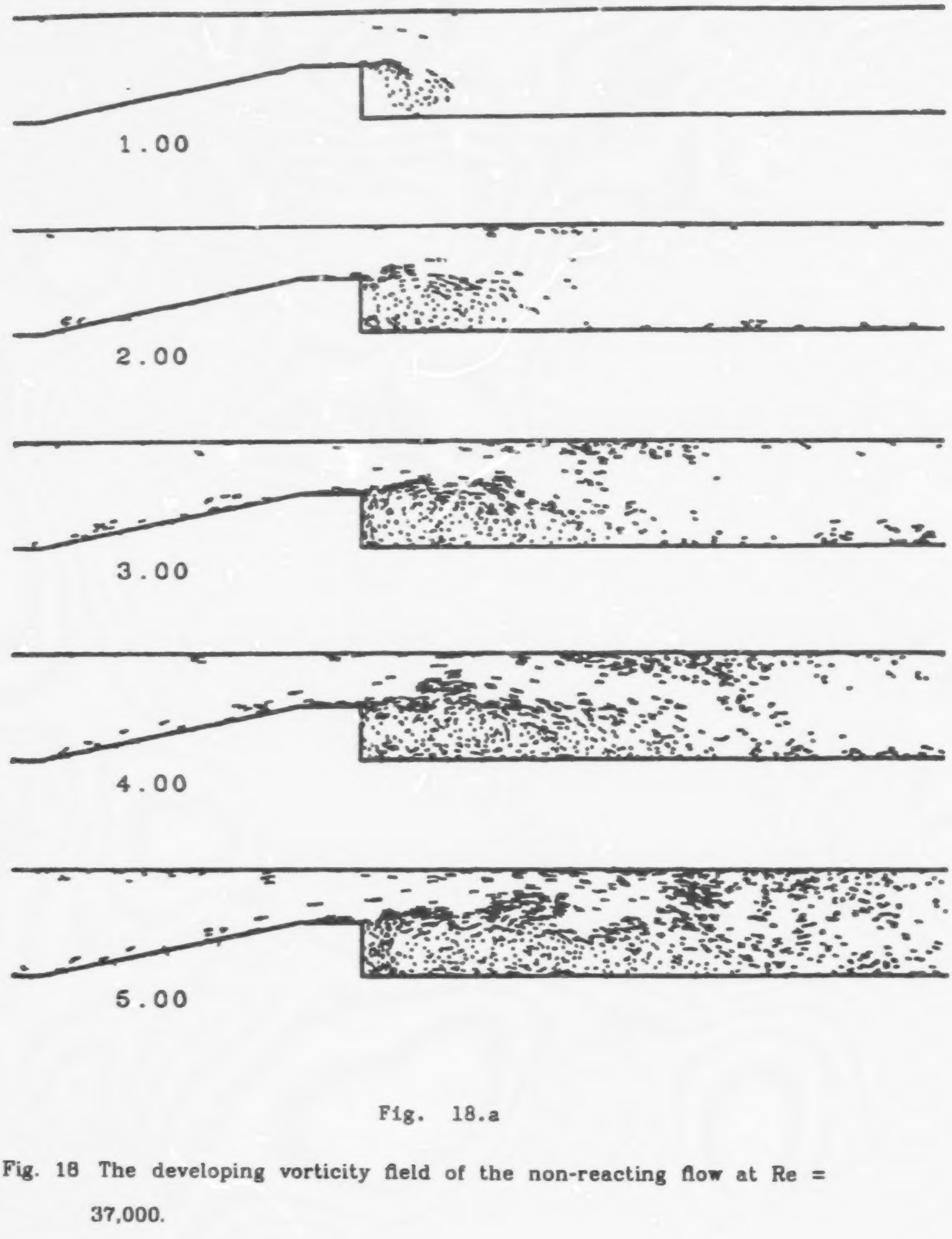

Fig. 18.a

Fig. 18 The developing vorticity field of the non-reacting flow at Re = 37,000.

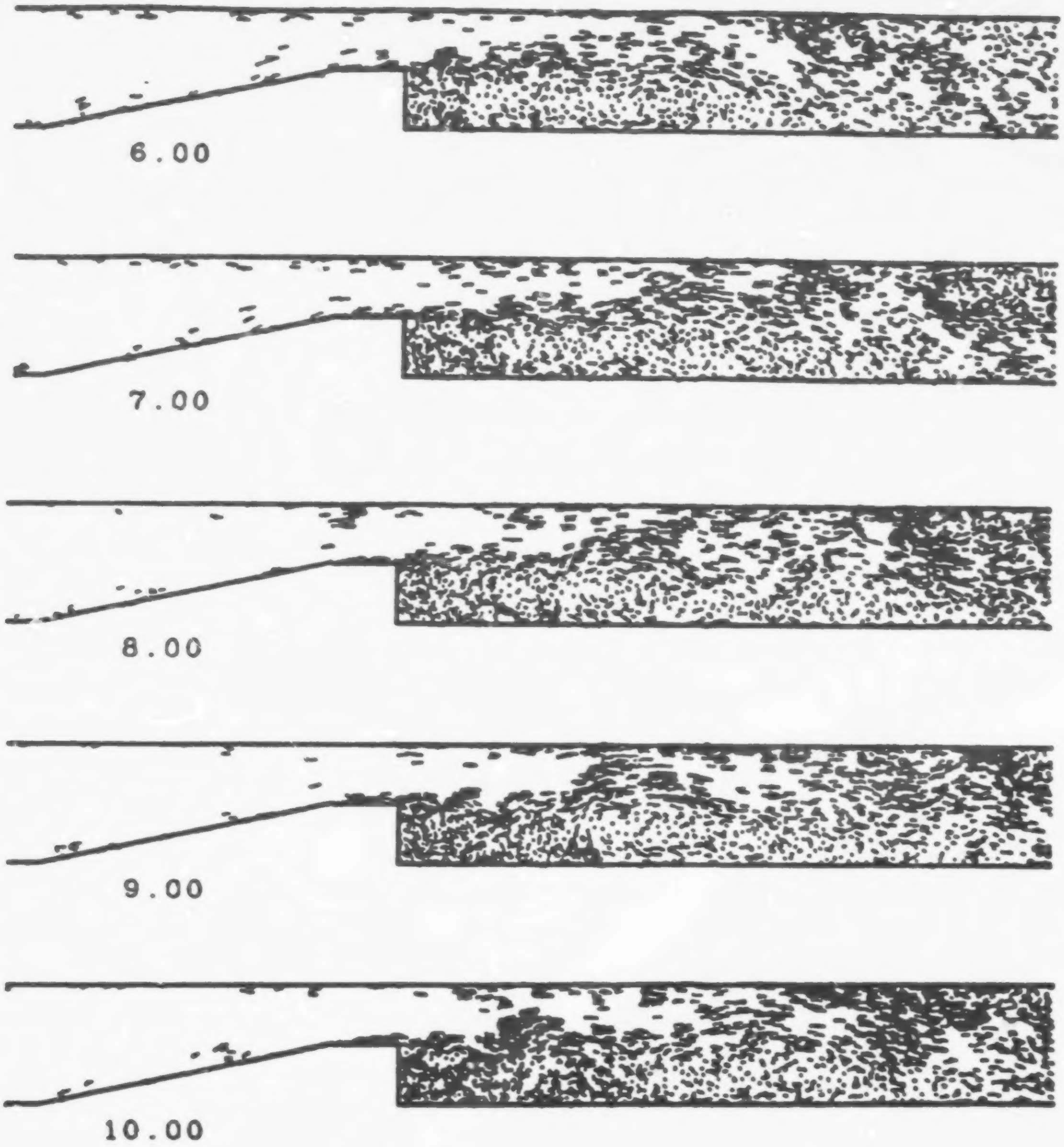

Fig. 18.b

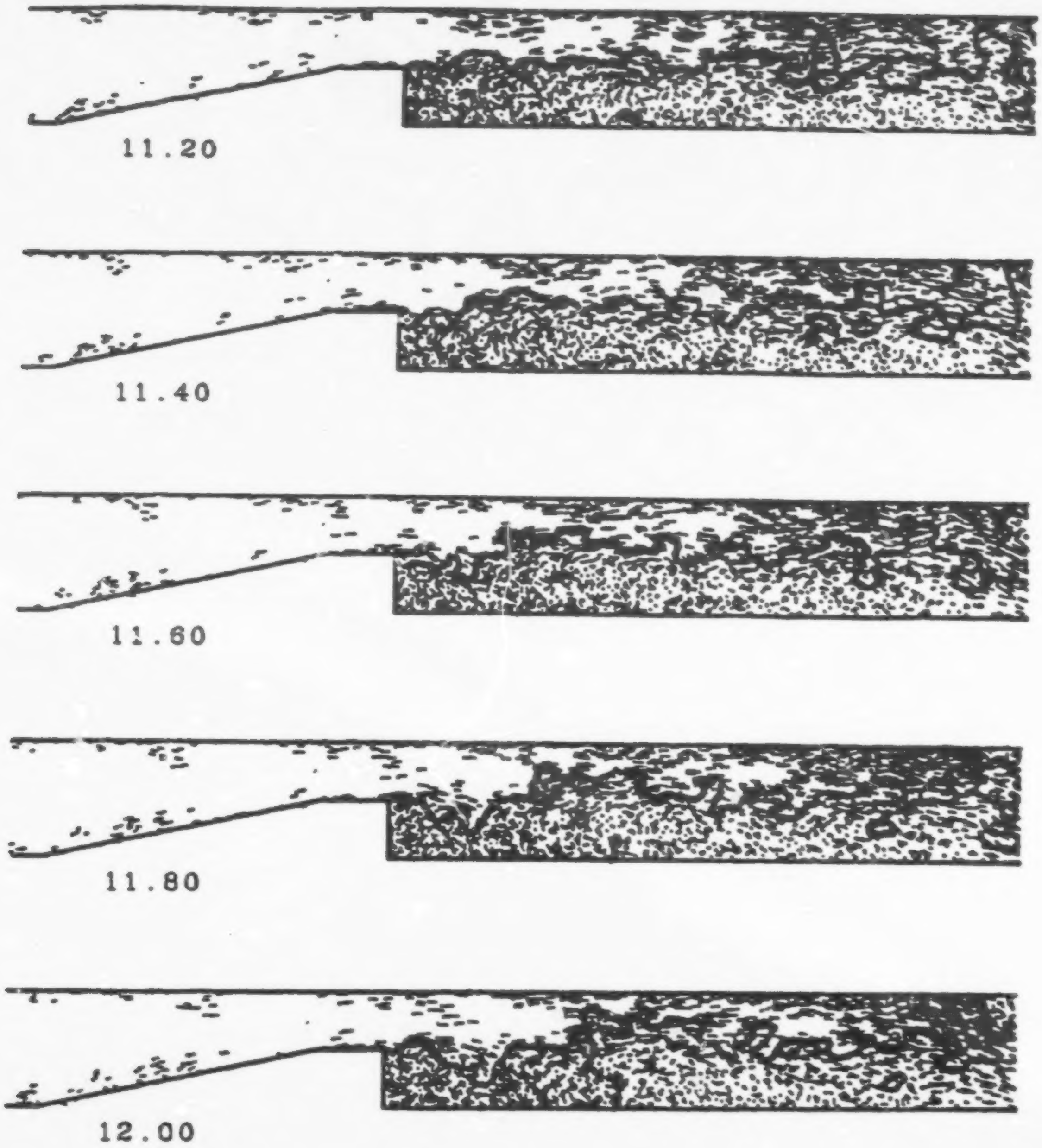
11.20
11.40
11.60
11.80
12.00

Fig. 19 Vorticity fields and flame front contours of the reacting flow at Re = 22,000.

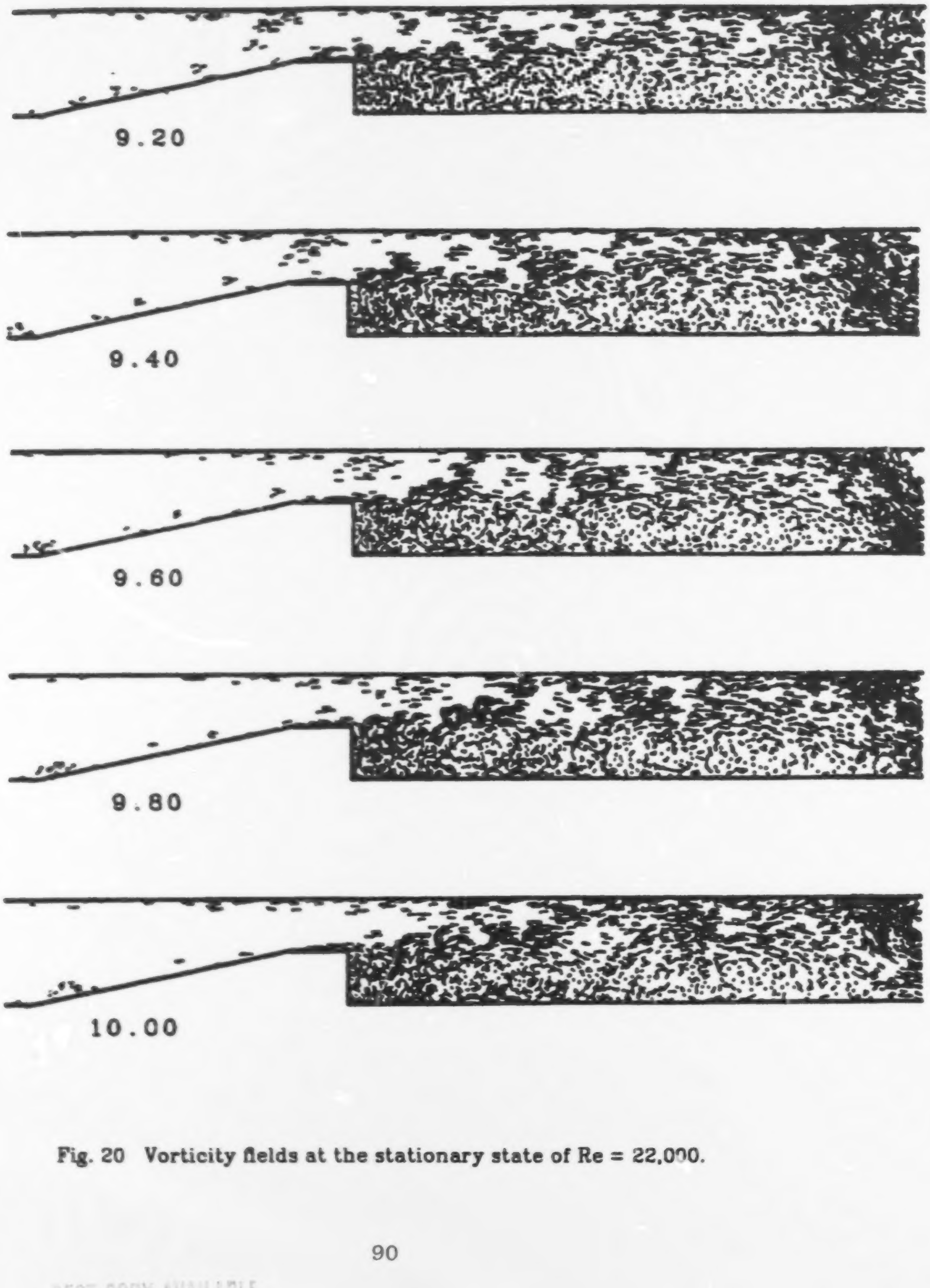
9.20
9.40
9.60
9.80
10.00

Fig. 20 Vorticity fields at the stationary state of Re = 22,000.

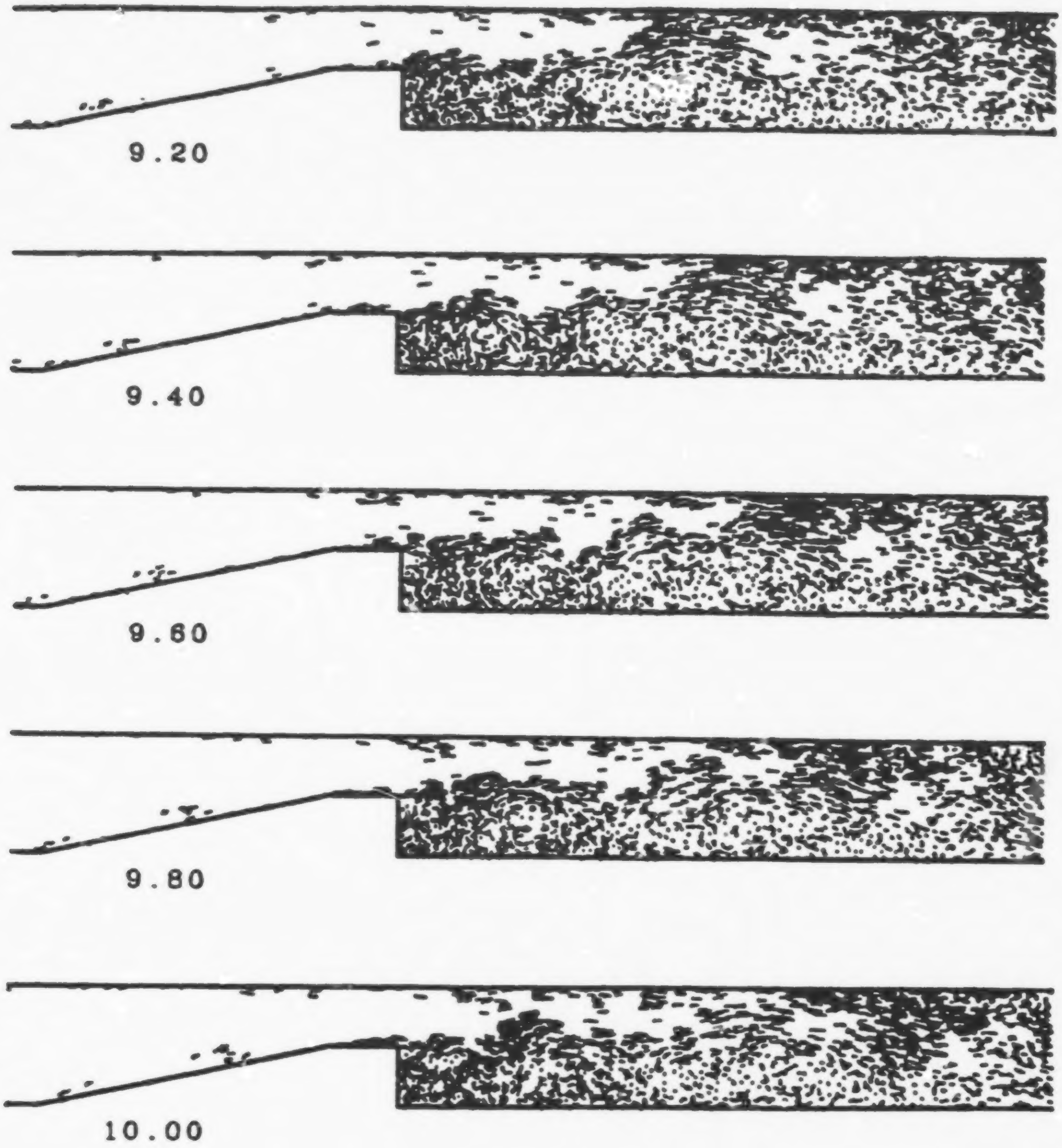
9.20
9.40
9.60
9.80
10.00

Fig. 21 Vorticity fields at the stationary state of Re = 37,000.

a) Non-reacting

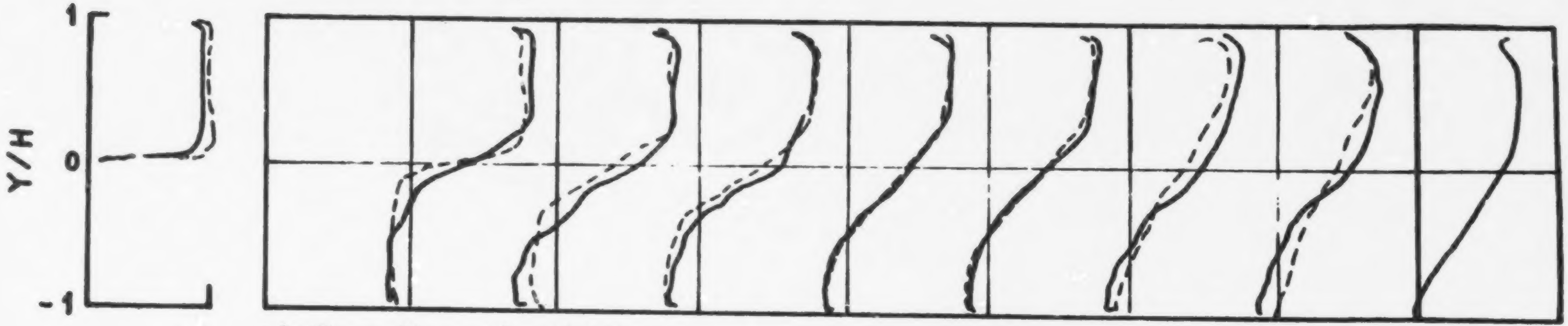

b) Reacting, $\phi = 0.57$

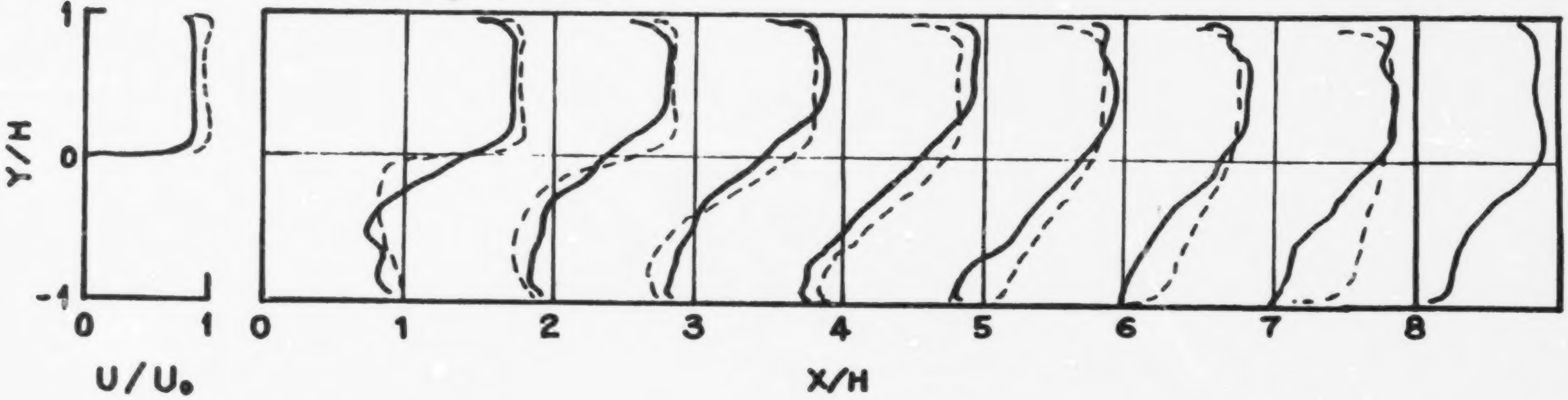

Fig. 22 Averaged streamwise velocity profiles for non-reacting and reacting flows at Re = 22,000.

a) Non-reacting

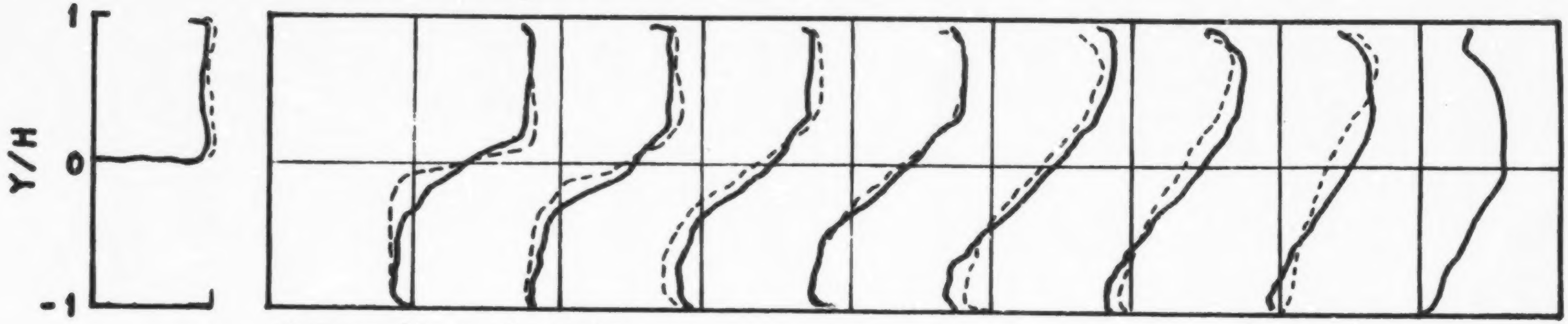

b) Reacting, ϕ= 0.57

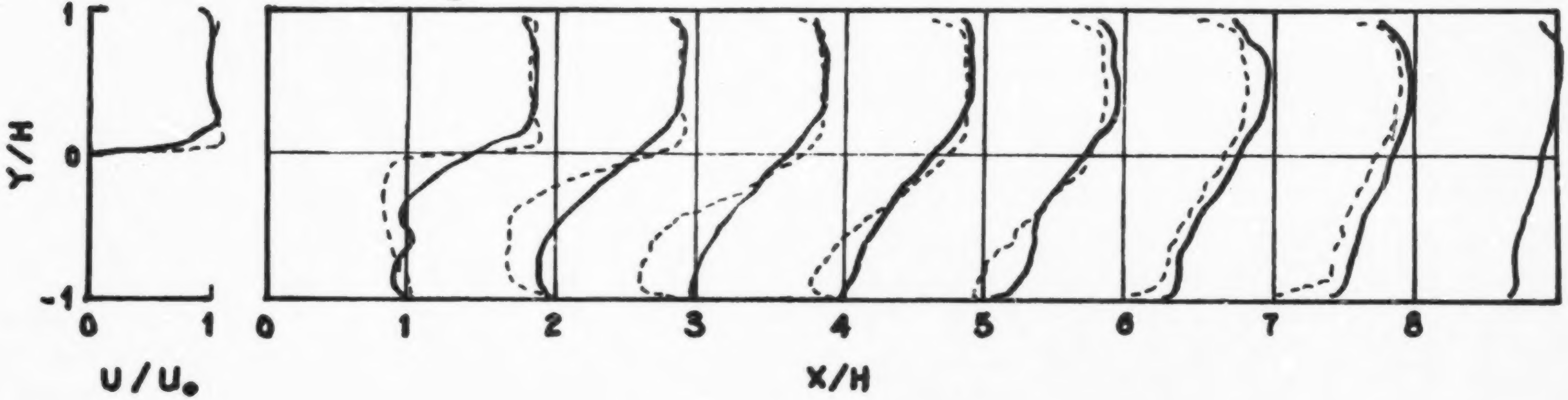

Fig. 23 Averaged streamwise velocity profiles for non-reacting and reacting flows at Re = 37,000.

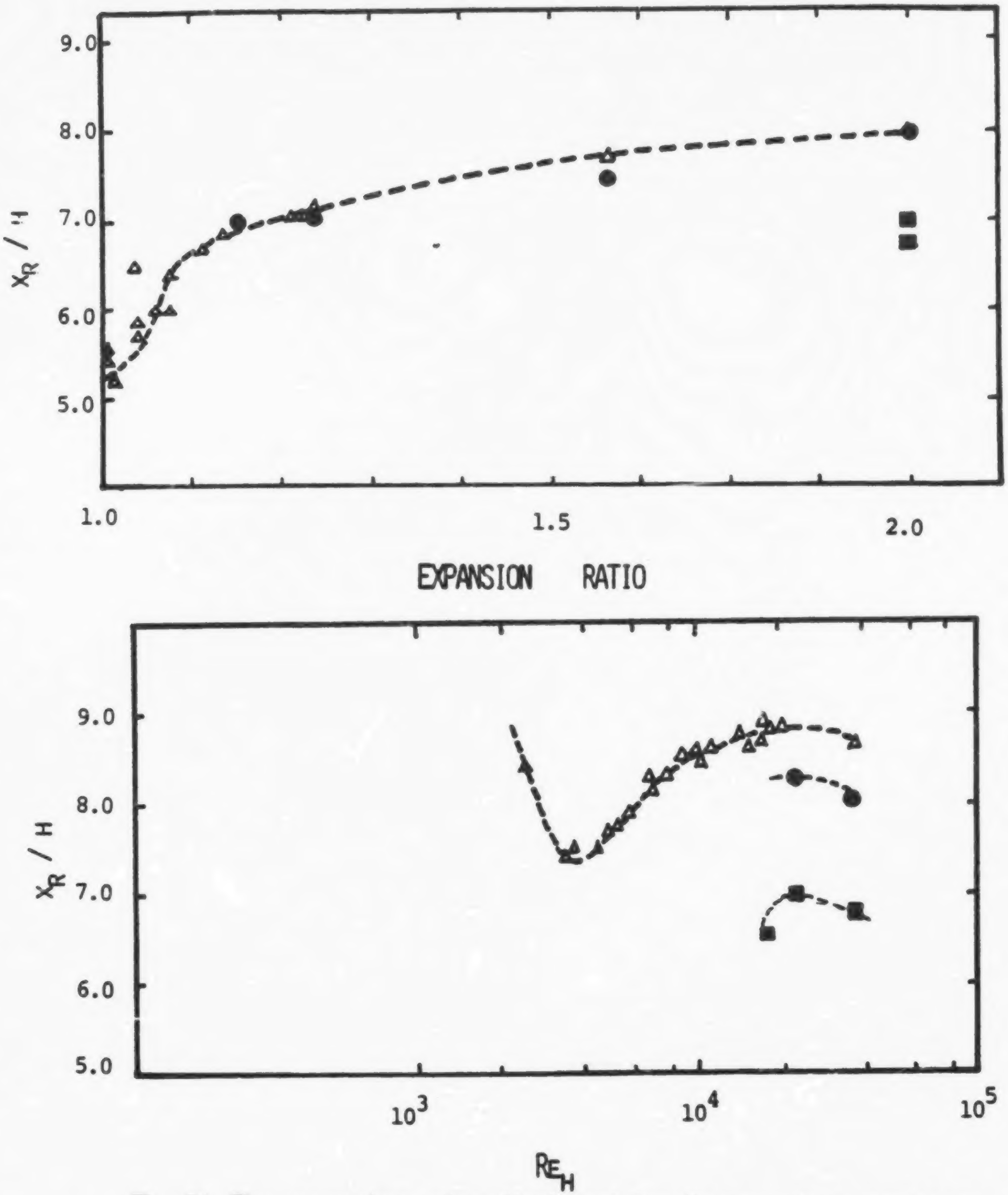

Fig. 24 The comparison of reattachment length: numerical results are represented by dark circles, experimental data are denoted by dark squares, while triangles are the data in the review paper of Durst & Tropea.

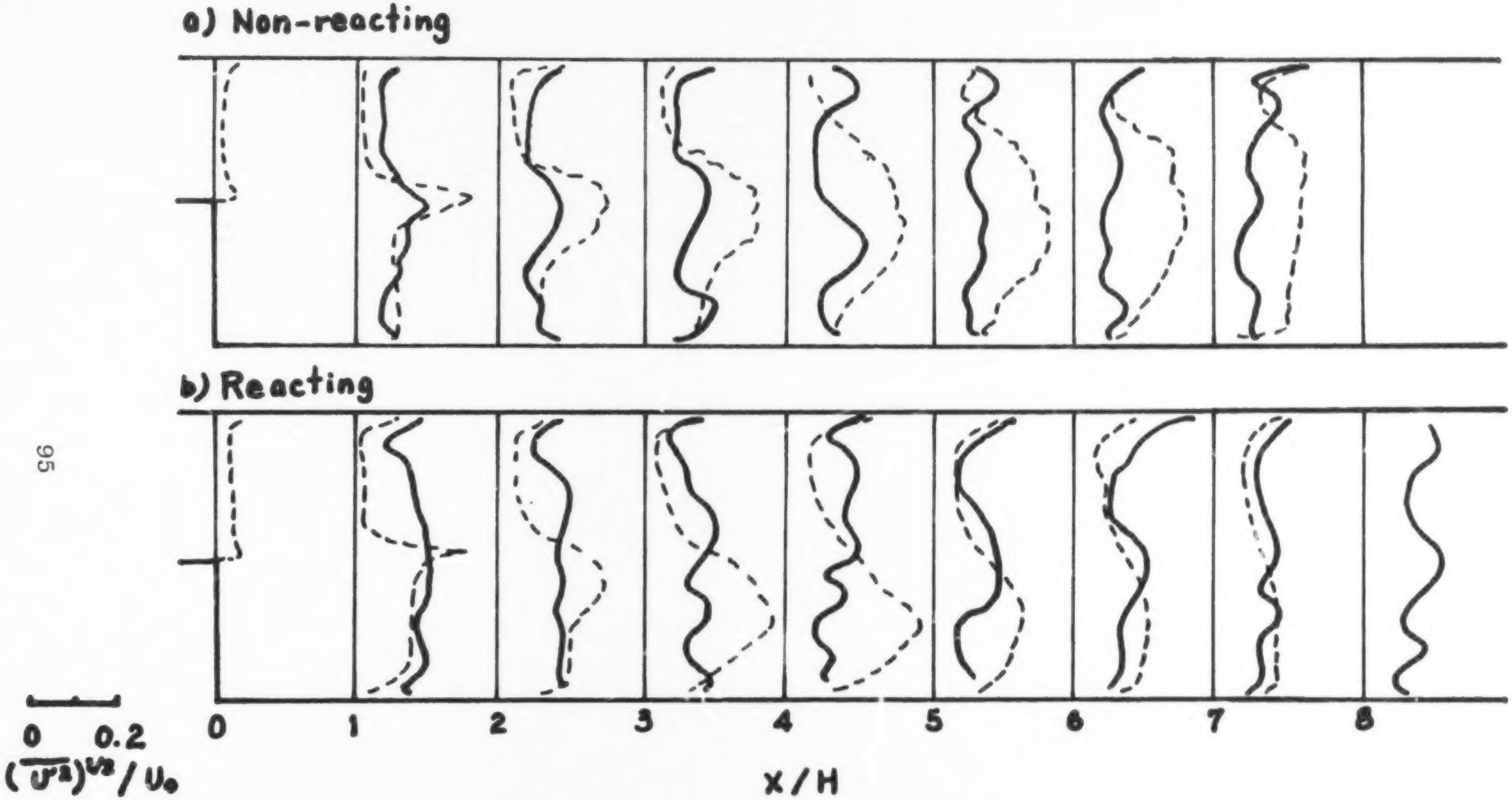

Fig. 25 Streamwise turbulence intensity profiles for nonreacting and reacting flow at Re = 22,000.

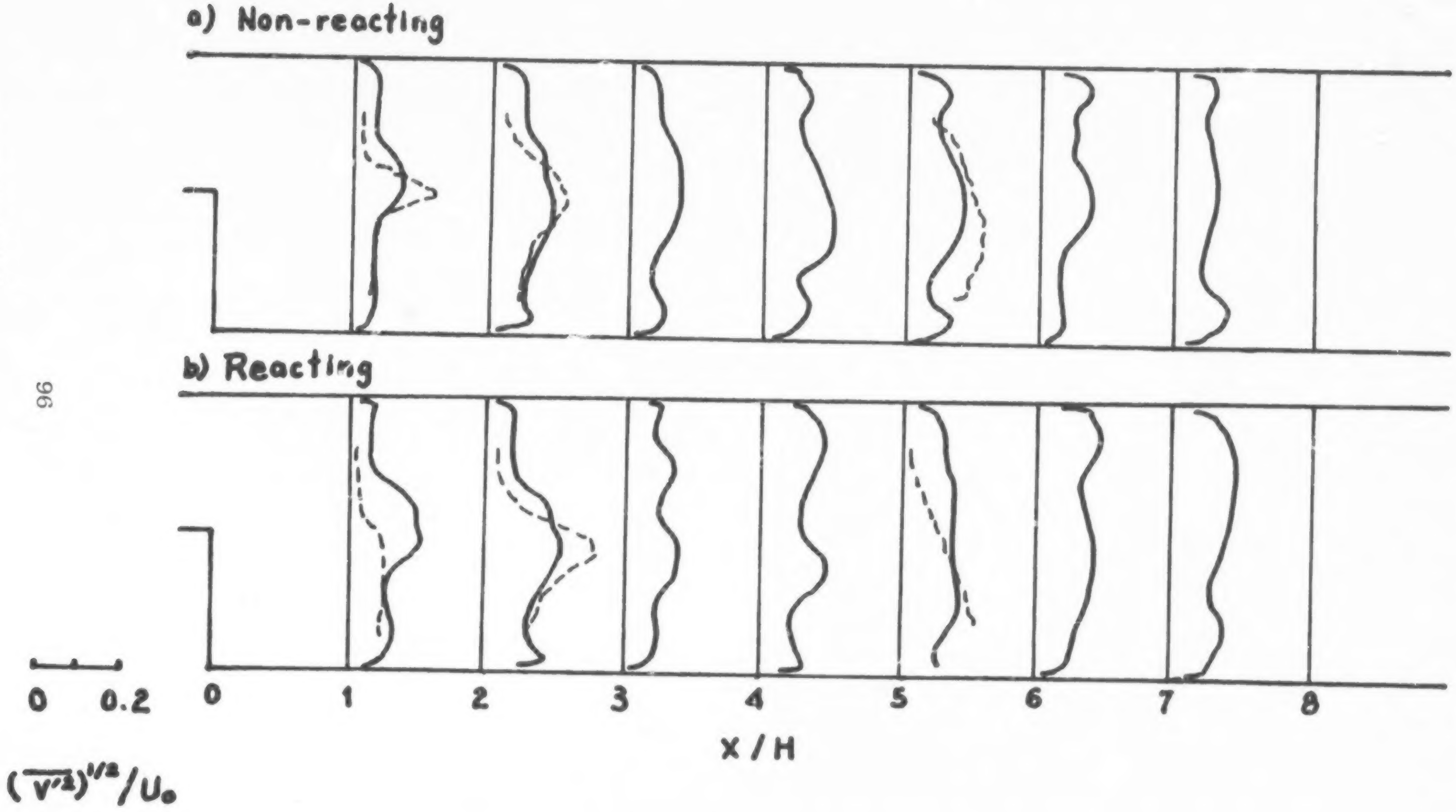

Fig. 26 Transverse turbulence intensity profiles for nonreacting and reacting flow at Re = 37,000.

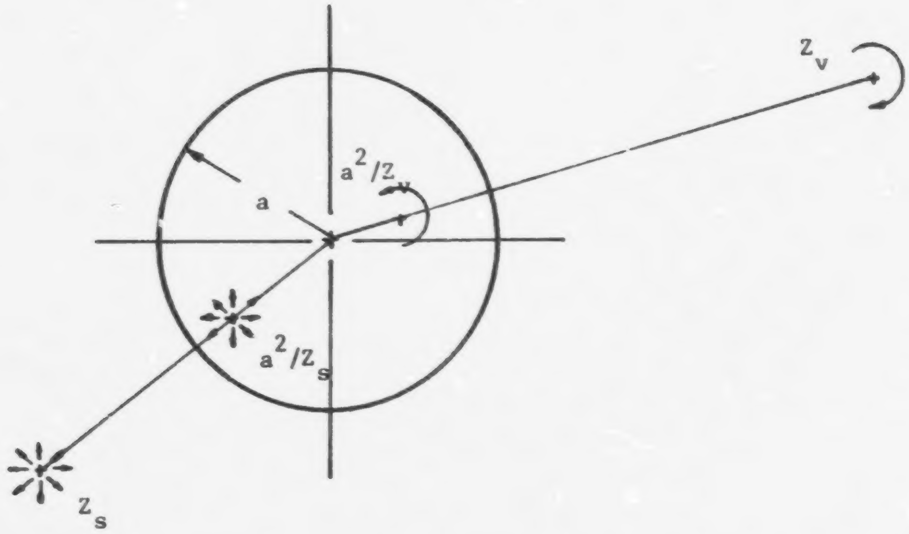
z_v
a^2/z_v
a
a^2/z_s
z_s

Fig. 27 The image system of vortex and source blobs for a flow past a circular cylinder.

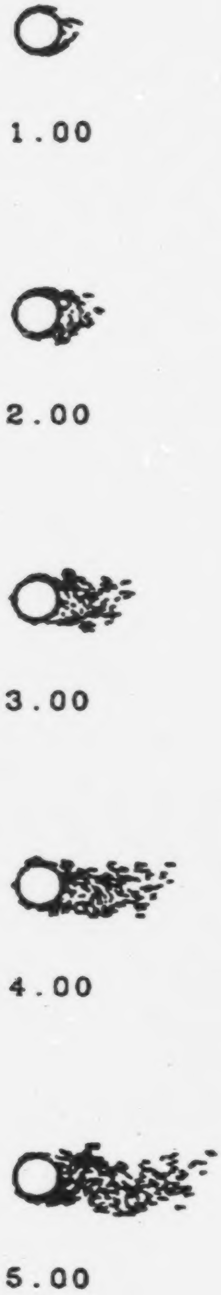

Fig. 28 The developing vorticity field of the wake behind a circular cylinder at Re = 10,000.

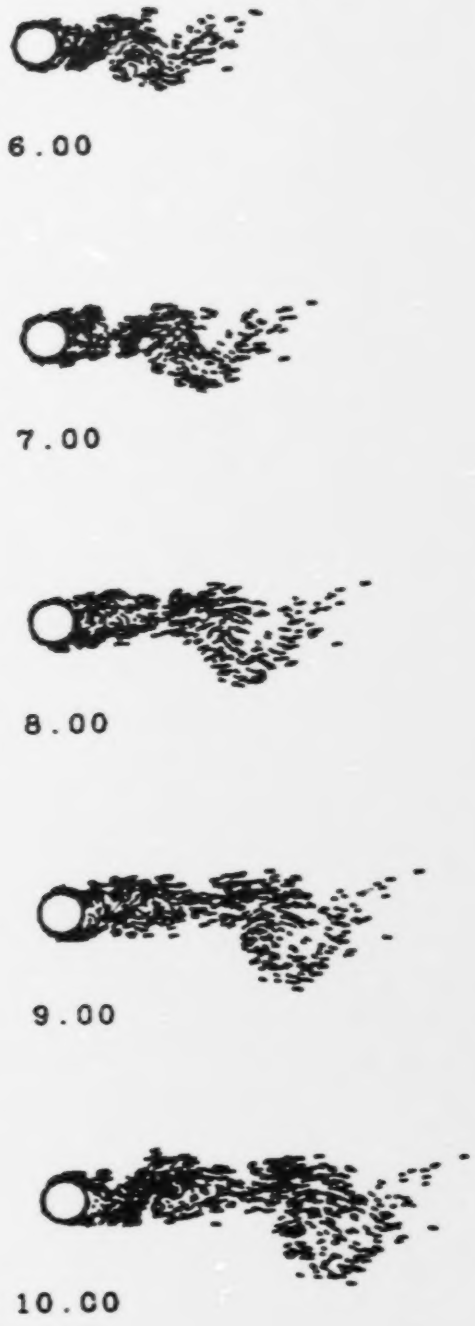

Fig. 28b

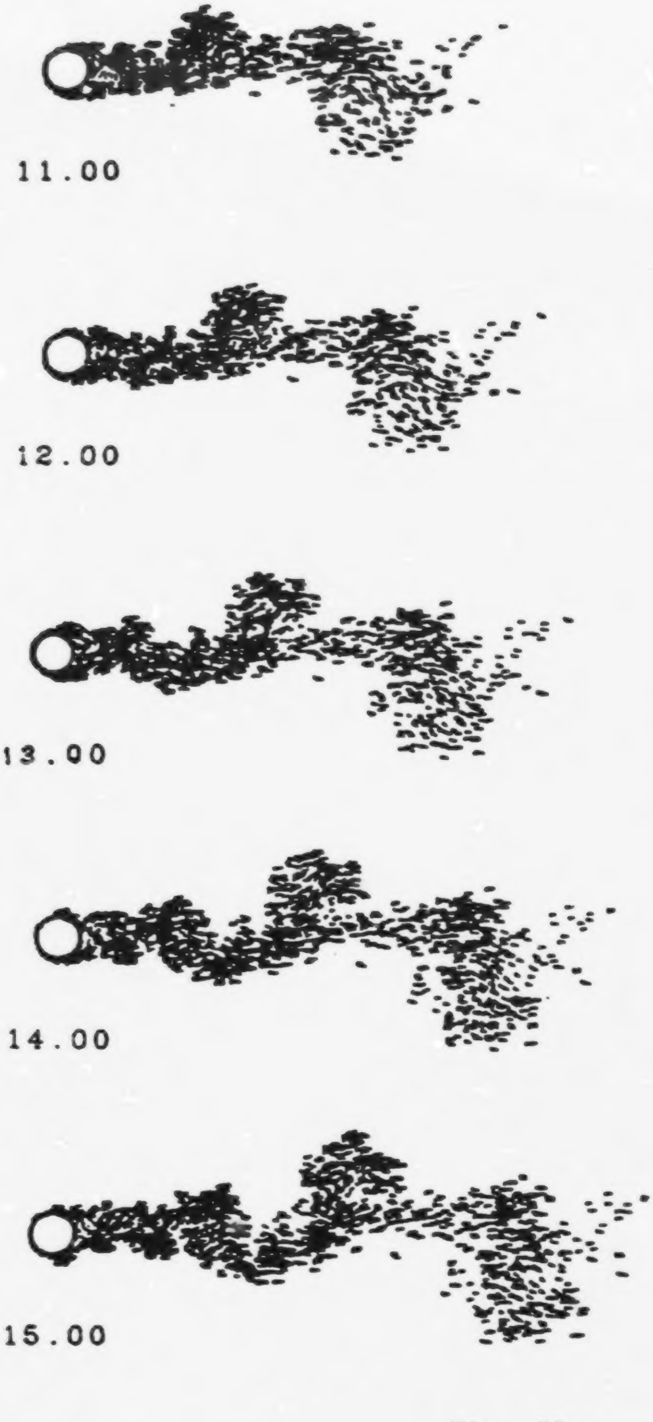

Fig. 28.c

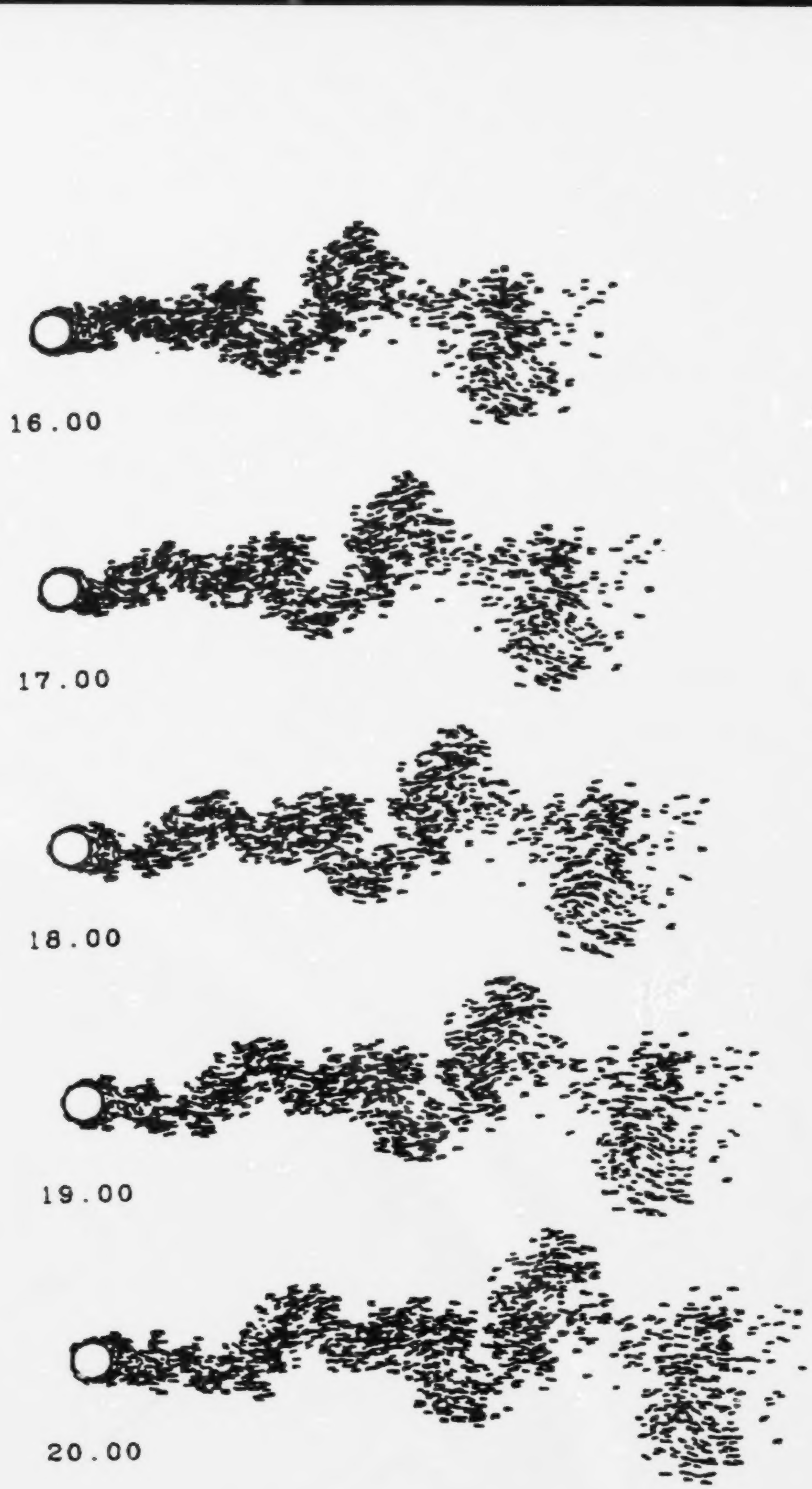
16.00
17.00
18.00
19.00
20.00

Fig. 28.d

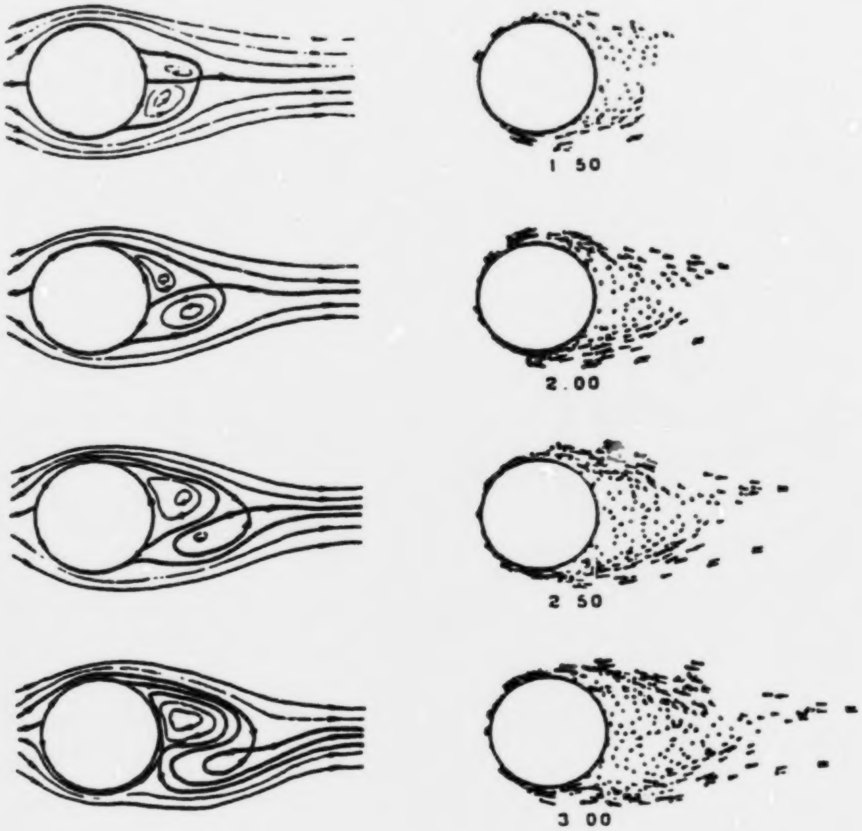
1 50
2.00
2 50
3 00

Fig. 29.a

Fig. 29 The instantaneous streamlines and vorticity field in the formation zone from T = 1.5 to 5.0 at Re = 10^4.

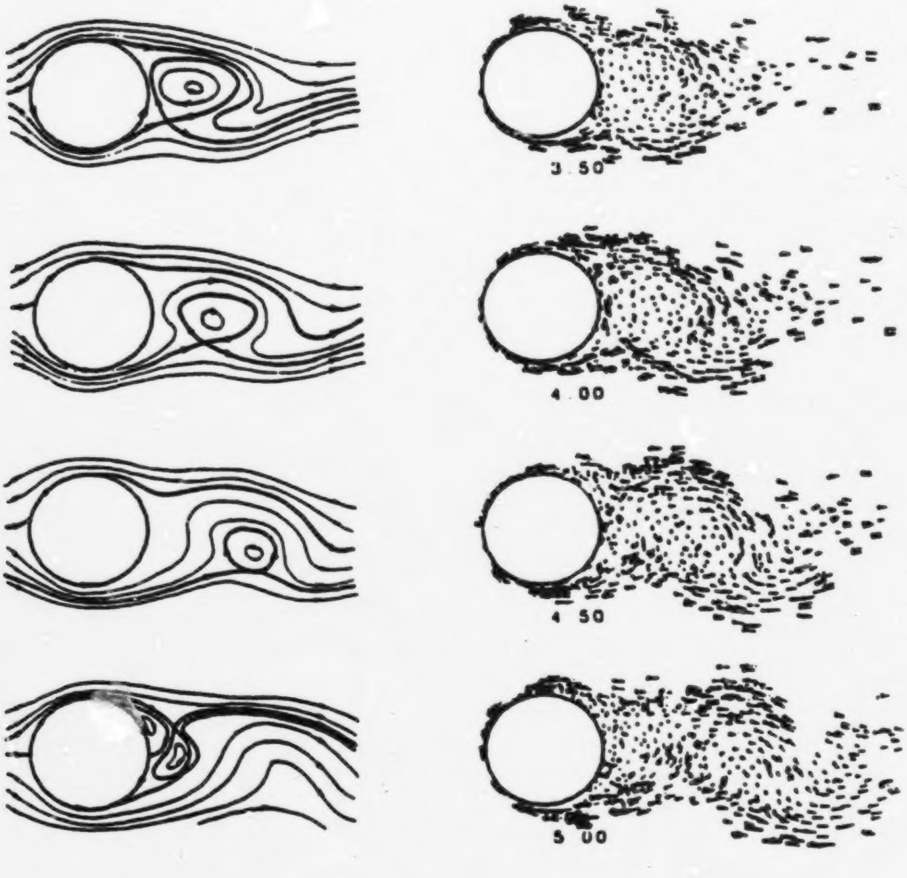
3.50
4.00
4.50
5.00

Fig. 29.b

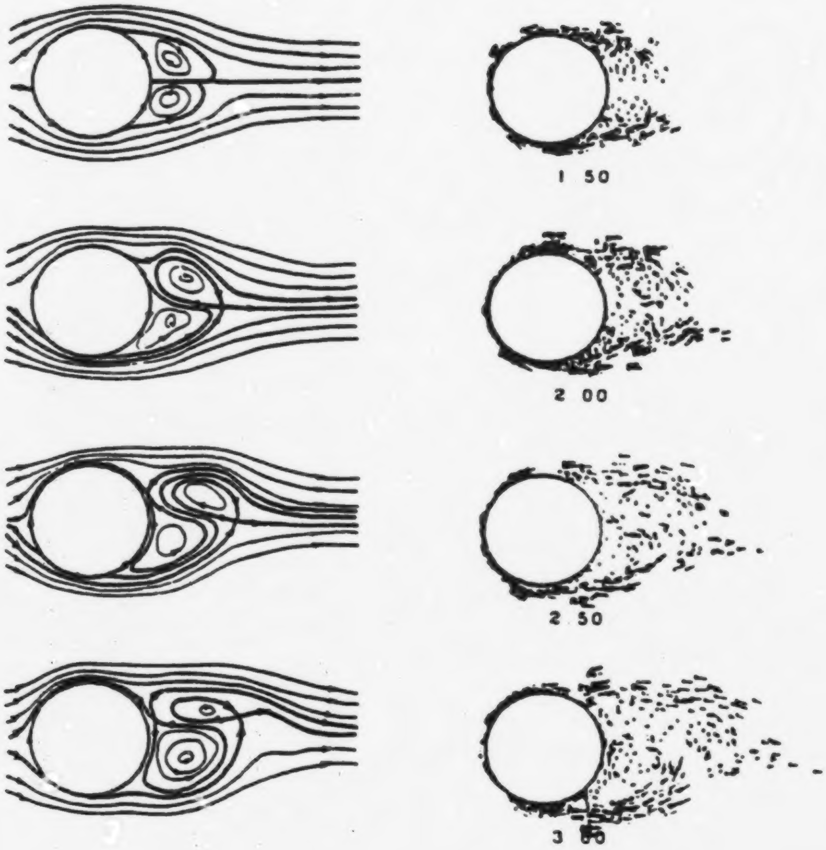
1 50
2 00
2 50
3 00

Fig. 30.a

Fig. 30 The instantaneous streamlines and vorticity field in the formation zone from T = 1.5 to 5.0 at Re = 10^5.

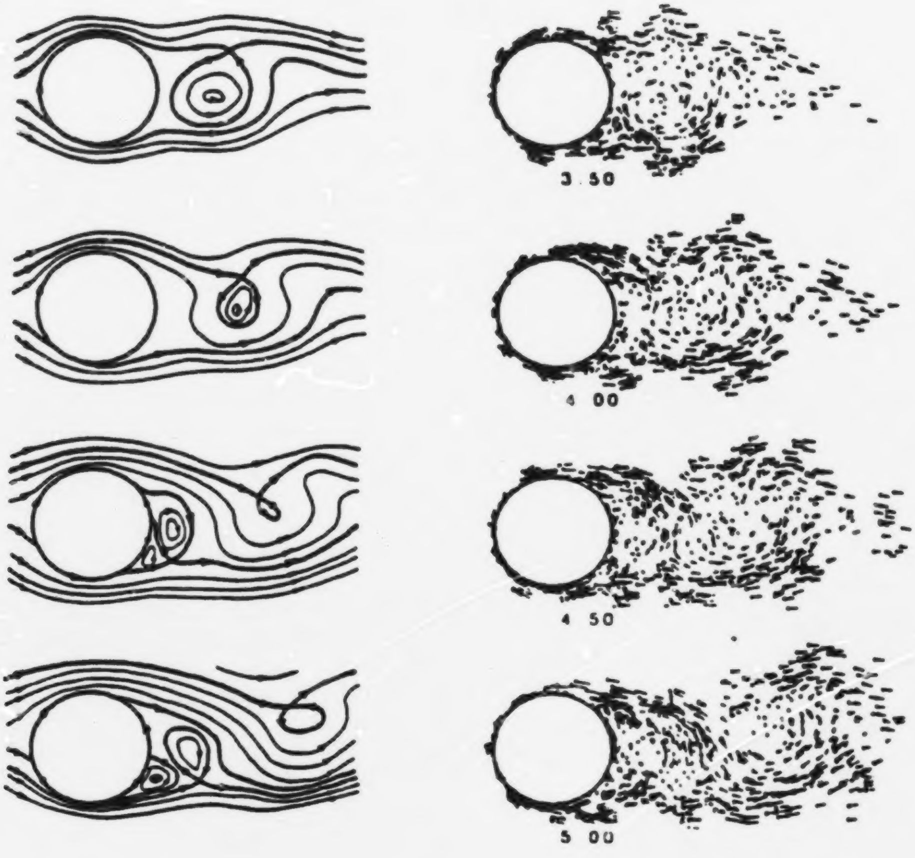
3.50
4.00
4.50
5.00

Fig. 30.b

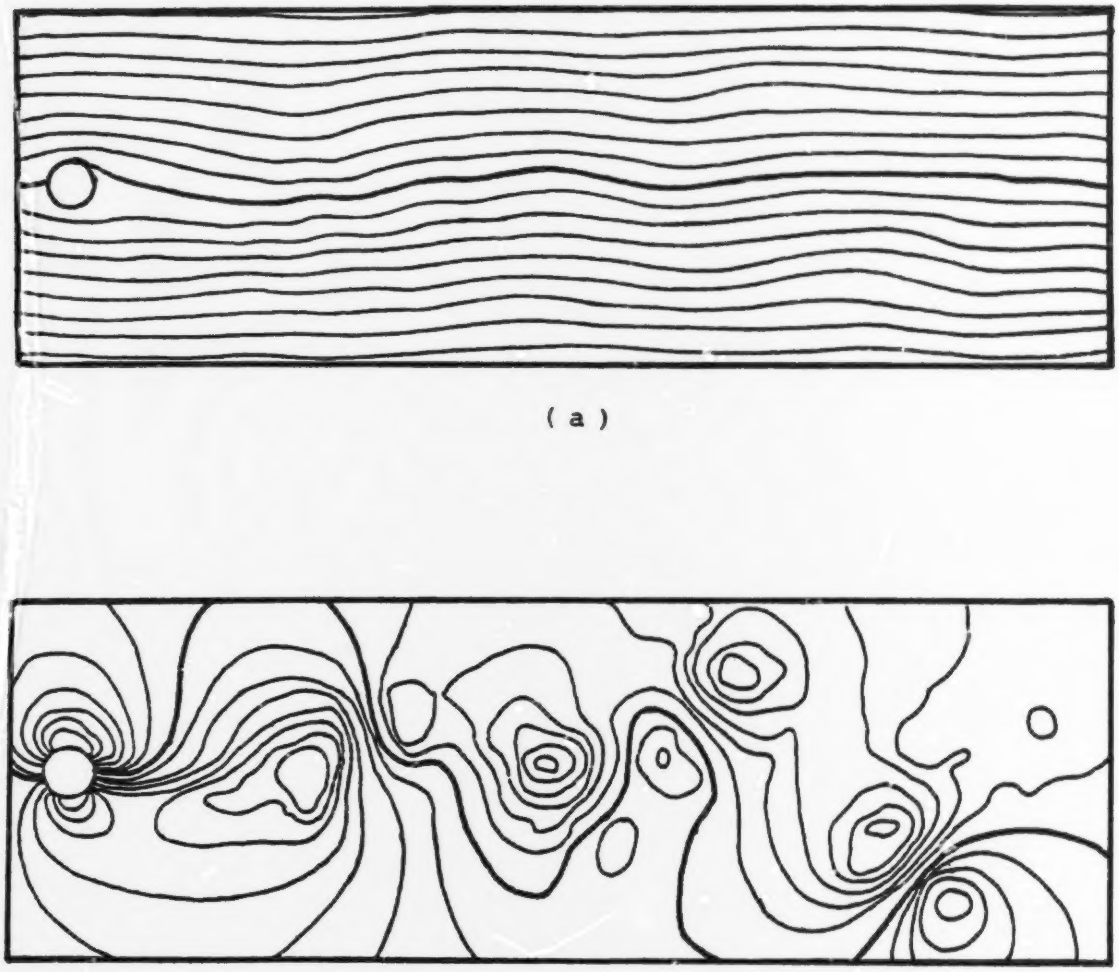

(a)

(b)

Fig. 31 (a) The streamline pattern of Re = 10^4 at T = 20.0 as a uniform flow past the cylinder.

(b) the streamline pattern of Re = 10^4 at T = 20.0 as the cylinder moves toward the fluid at a uniform velocity to the left.

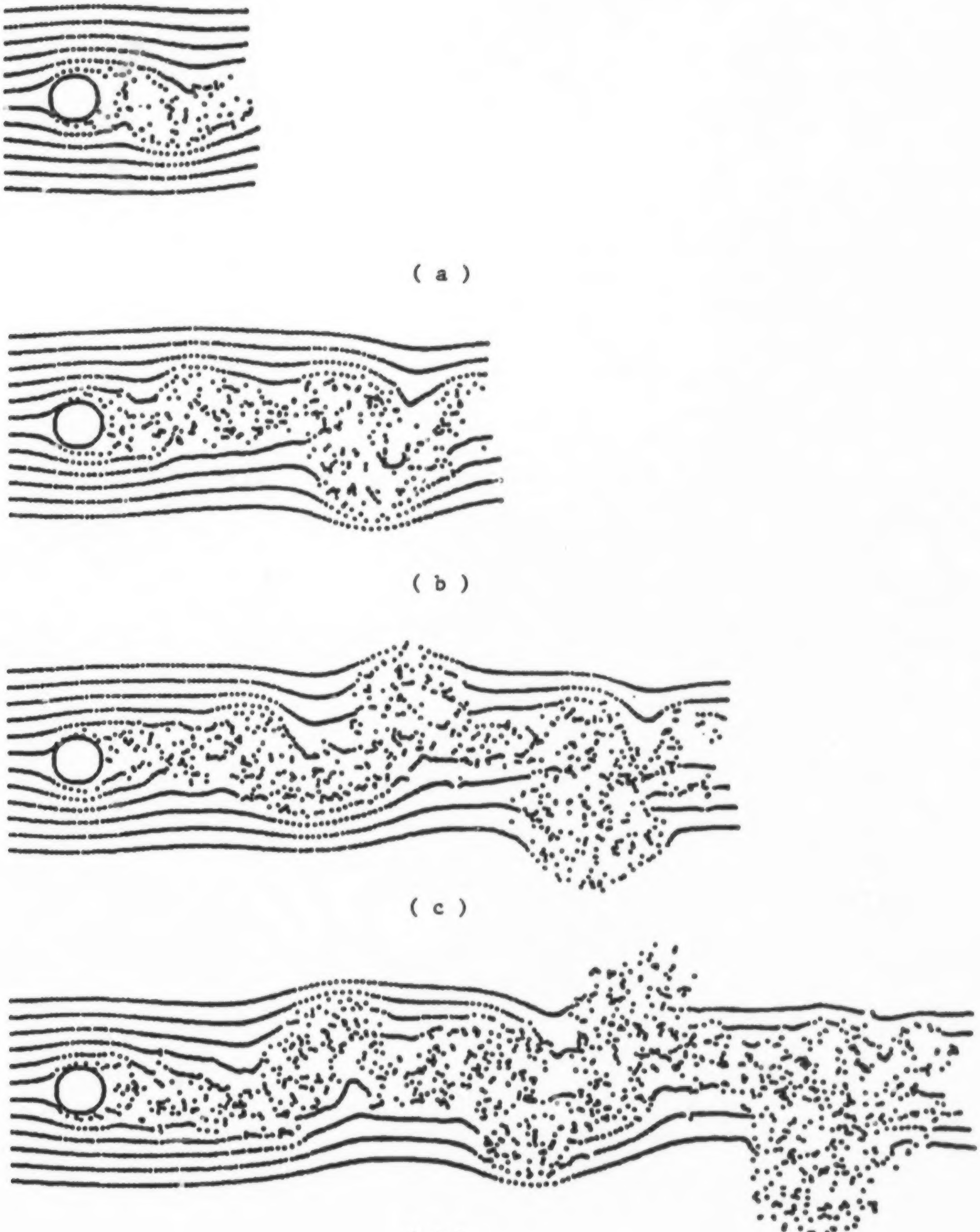

Fig. 32 Streaklines at T = (a) 5, (b) 10, (c) 15, and (d) 20, respectively.

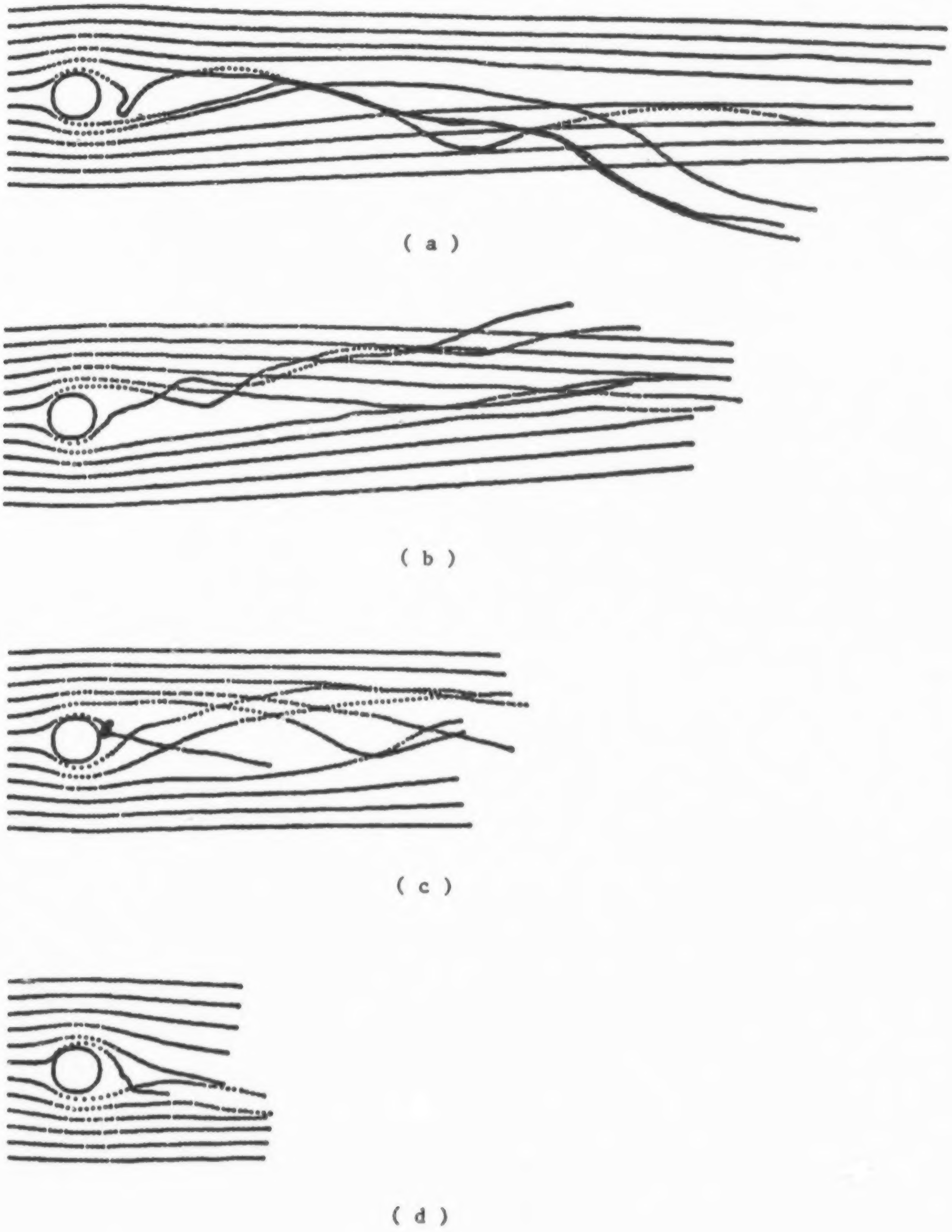

Fig. 33 Particle pathlines from T = (a) 0, (b) 5, (c) 10, and (d) 15 to T = 20, respectively.

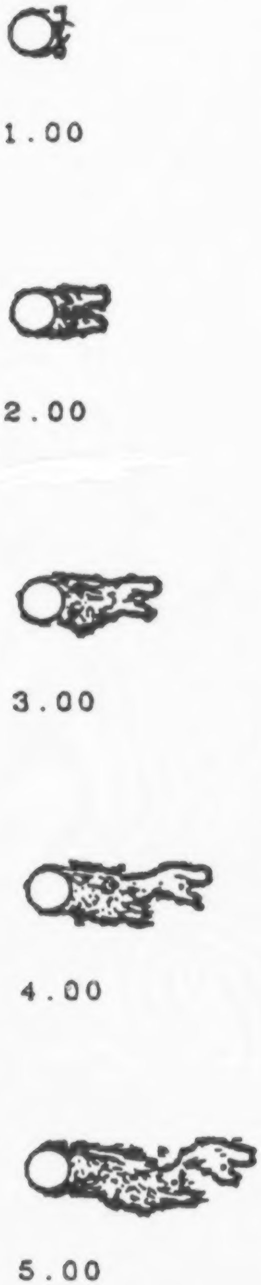
1.00
2.00
3.00
4.00
5.00

Fig. 34 Flame front contours and vorticity fields of the reacting flow stabilized by a circular cylinder at Re = 10,000.

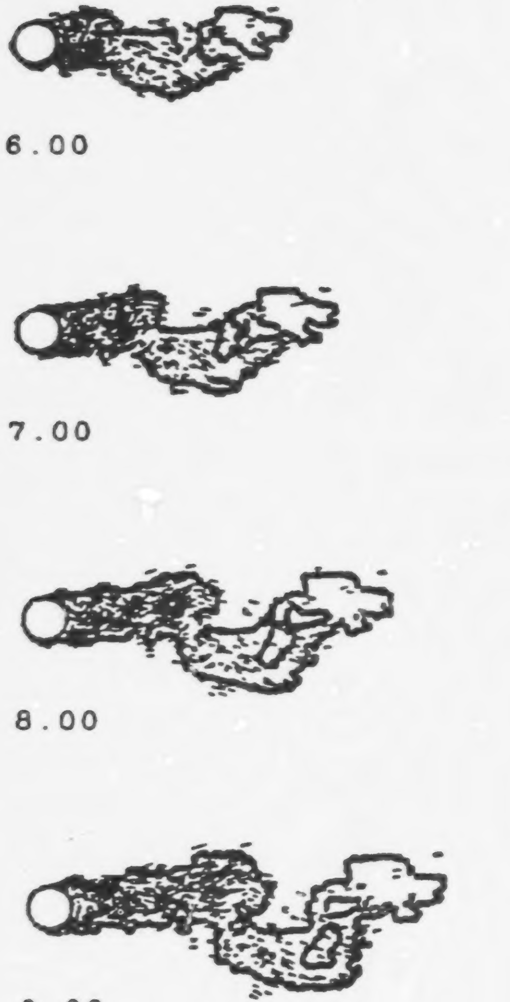

6.00

7.00

8.00

9.00

10.00

Fig. 34.b

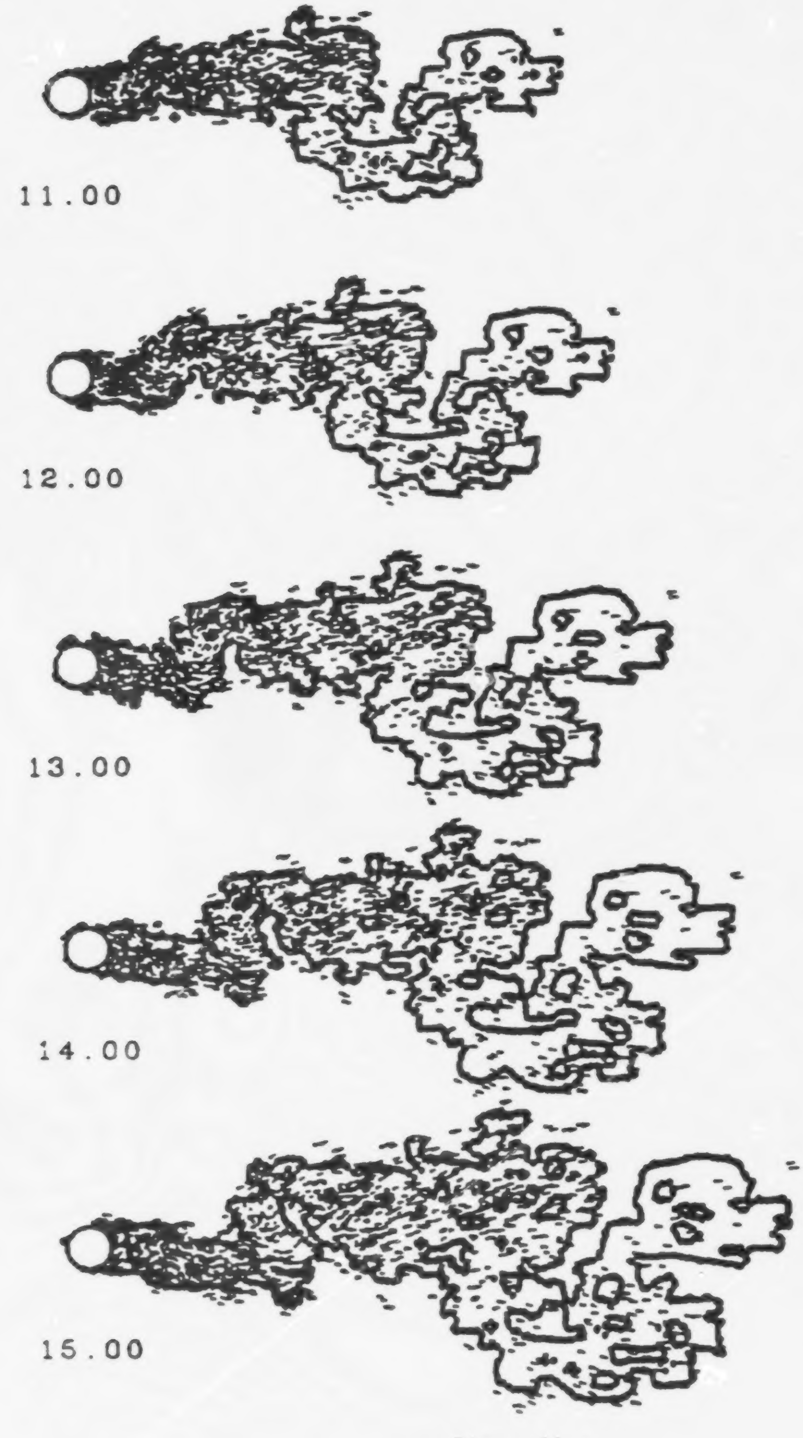

Fig. 34.c

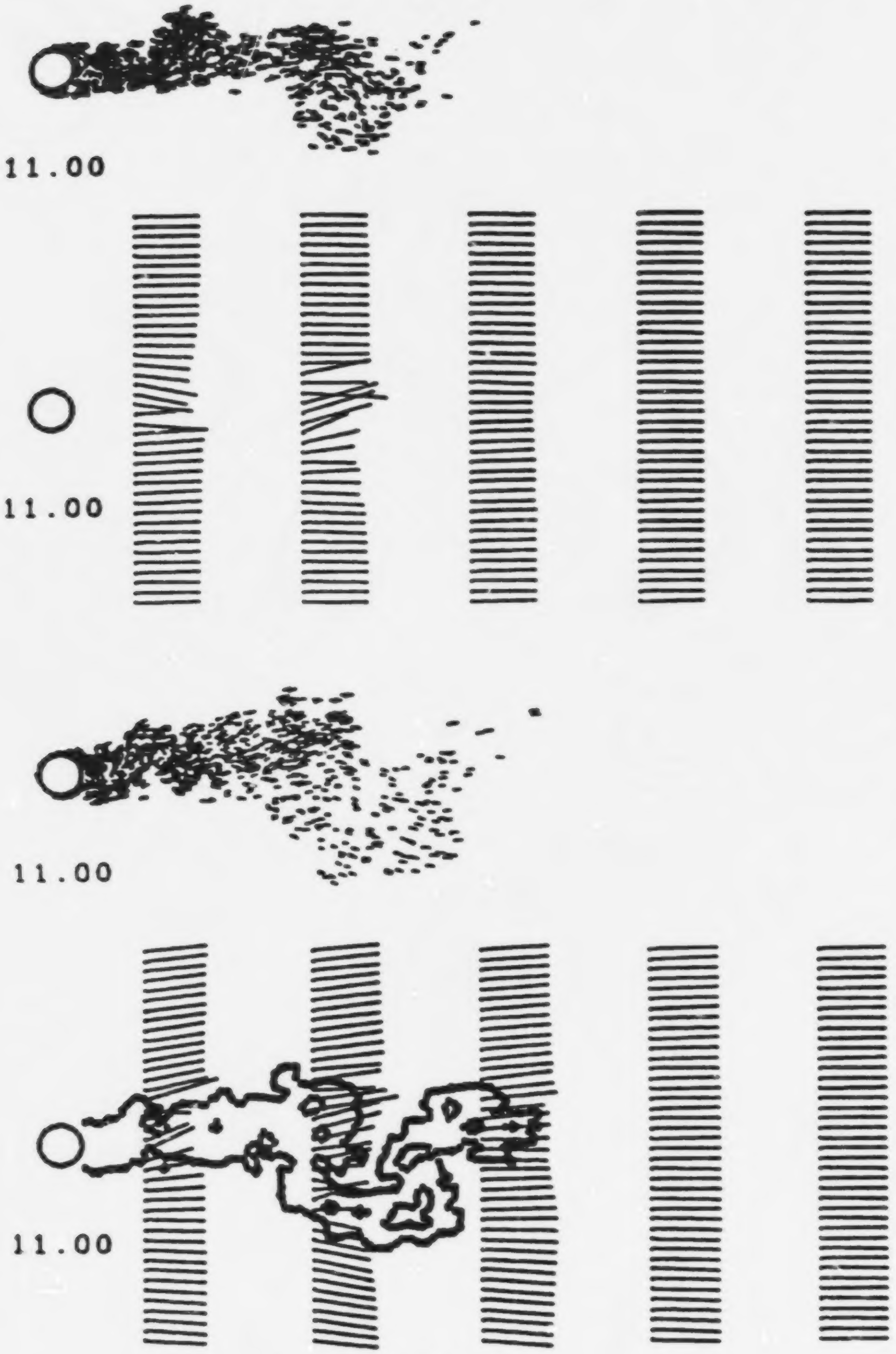

Fig. 35.a

Fig. 35 Comparison of velocity vectors and vorticity fields between non-reacting and reacting case for T = (a) 11.0, (b) 12.0, (c) 13.0, (d) 14.0, and (e) 15.0 respectively.

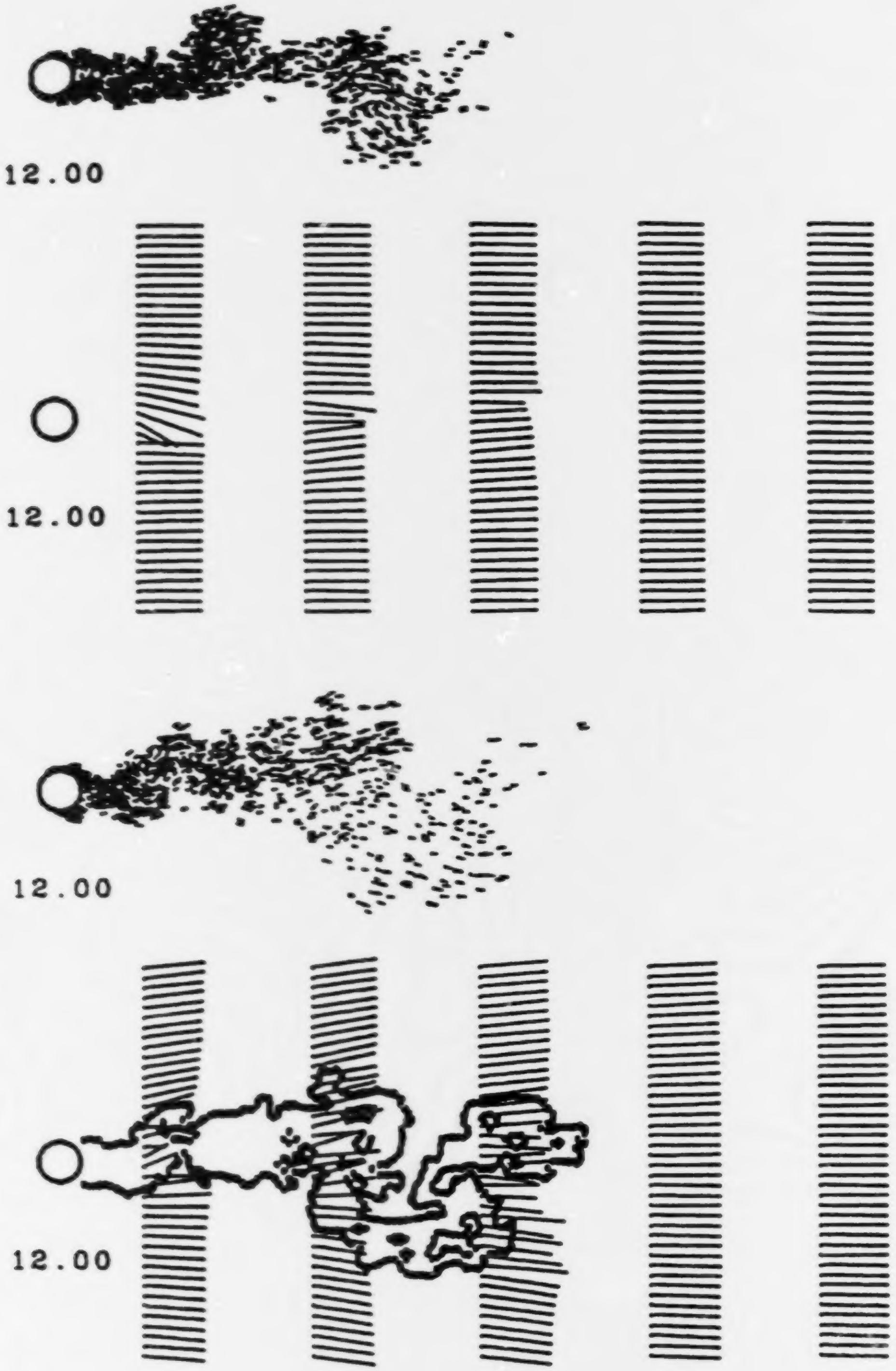
12.00
12.00
12.00
12.00

Fig. 35.b

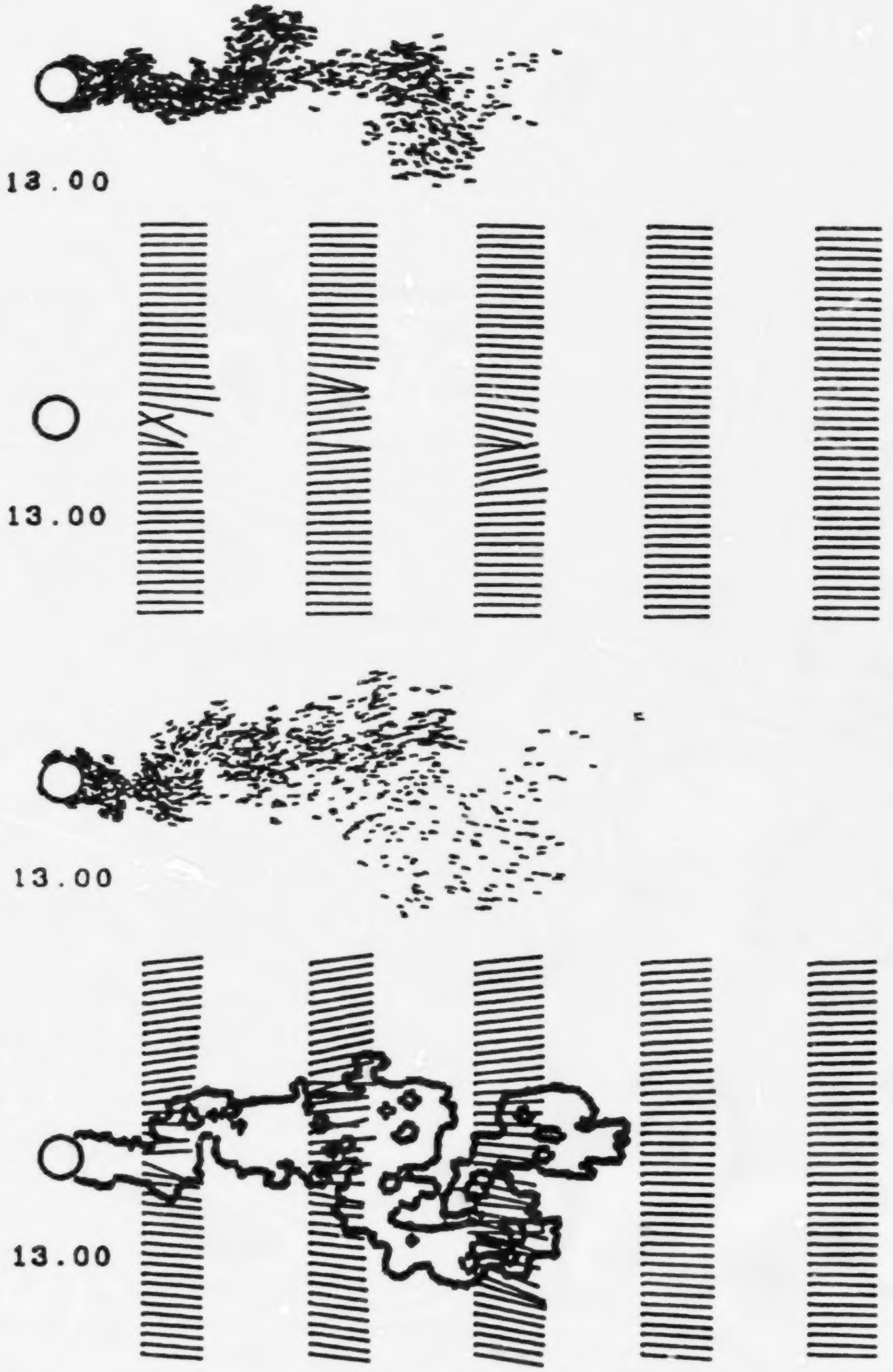
13.00
13.00
13.00
13.00

Fig. 35.c

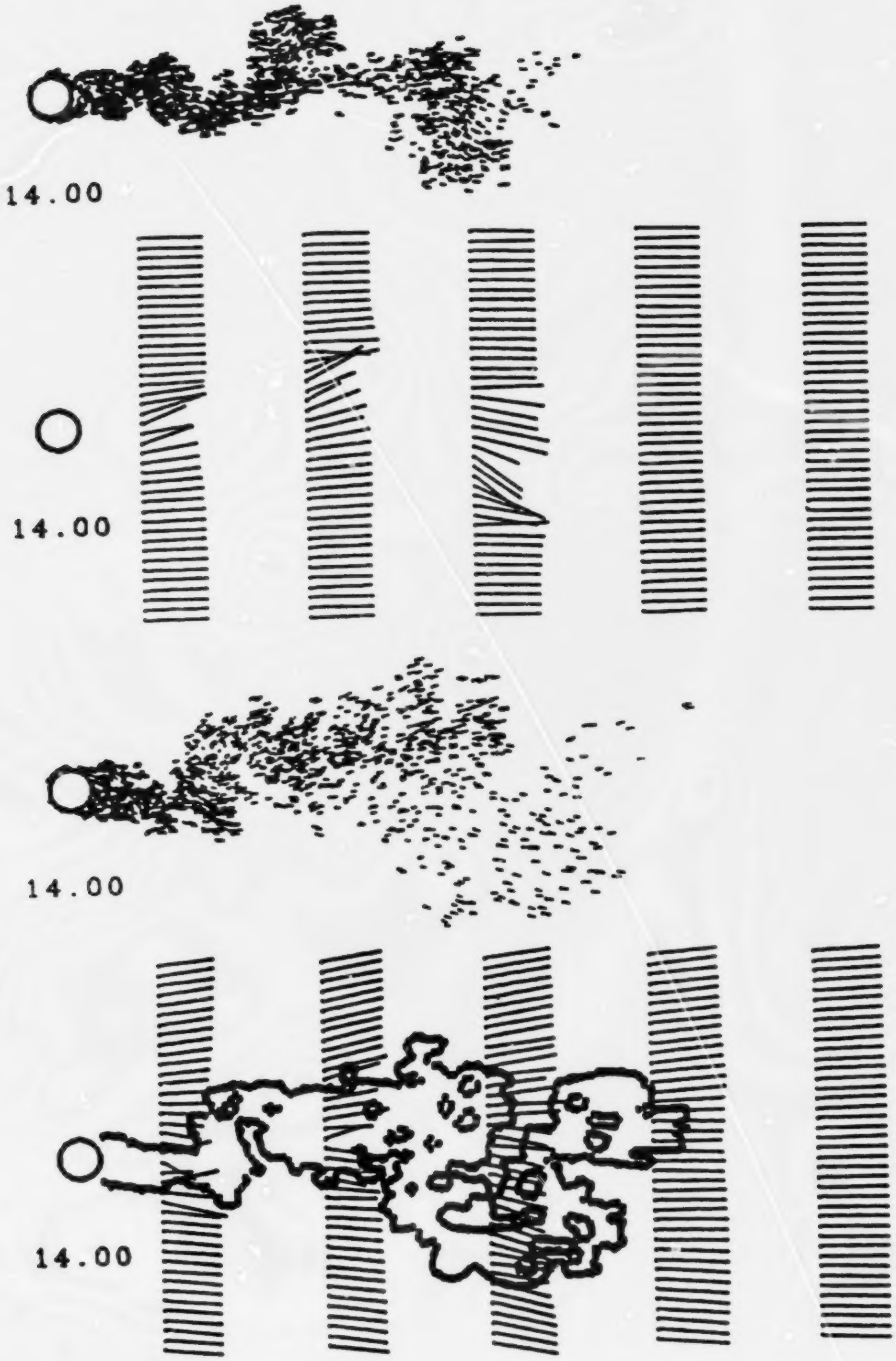

Fig. 35.d

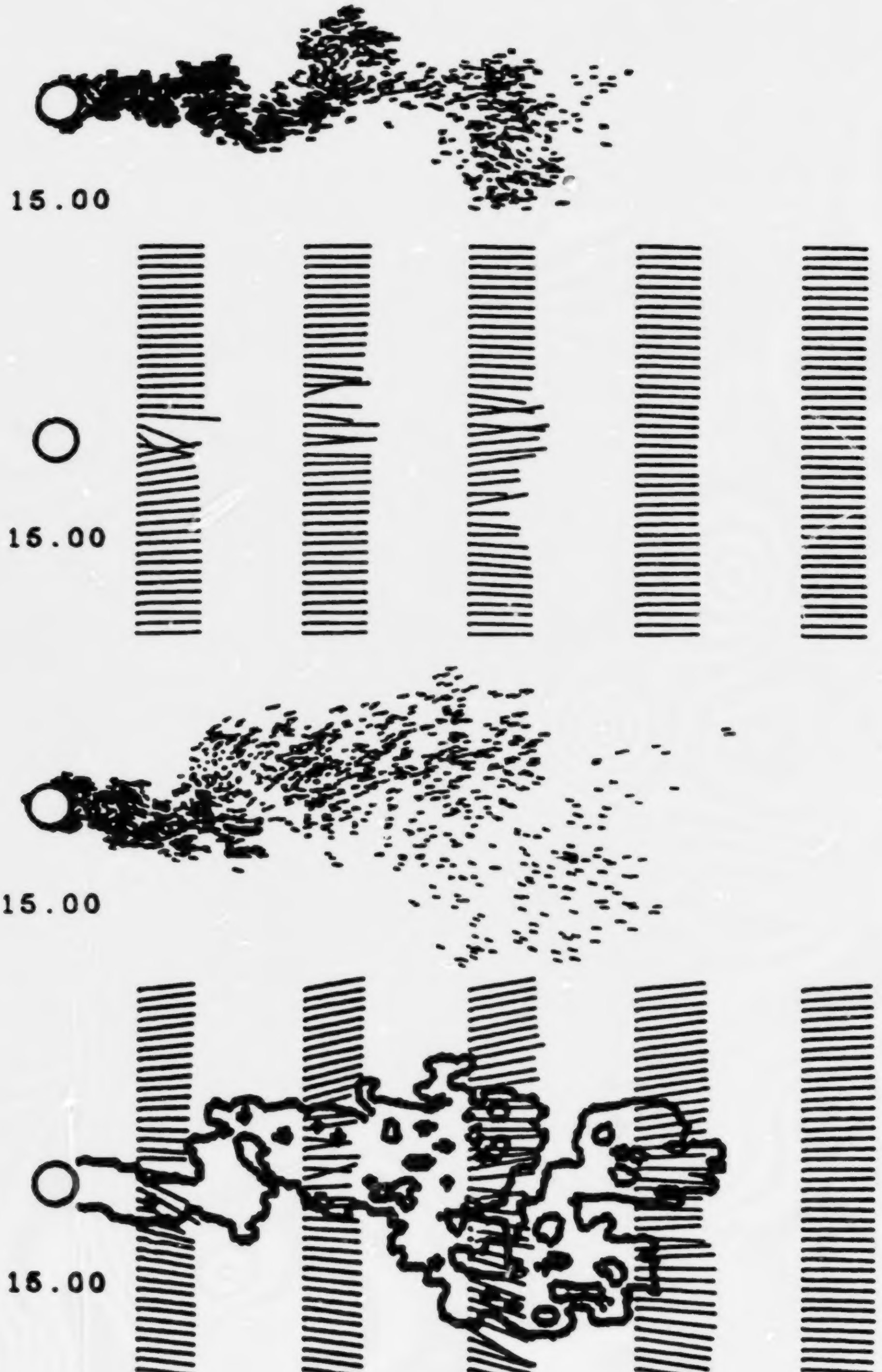

Fig. 35.e

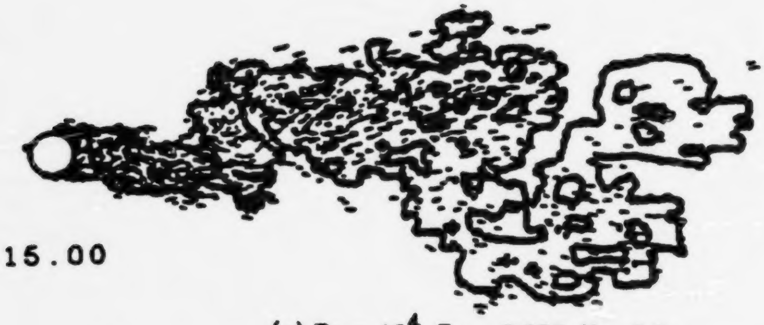

(a) Re = 10^4, Su = 0.020, V = 8.0;

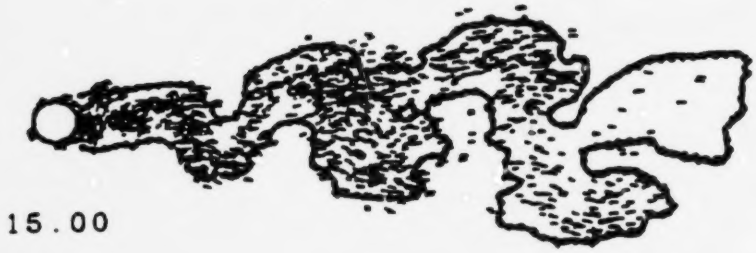

(b) Re = 10^4, Su = 0.025, V = 8.0;

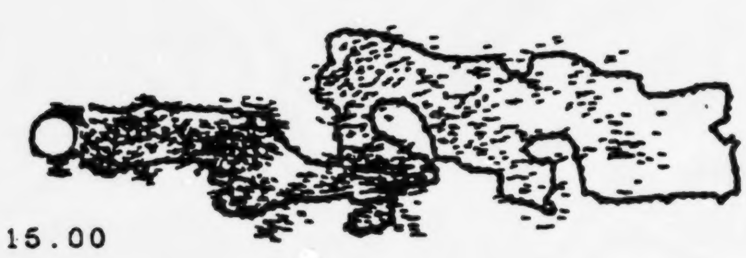

(c) Re = 10^3, Su = 0.025, V = 8.0;

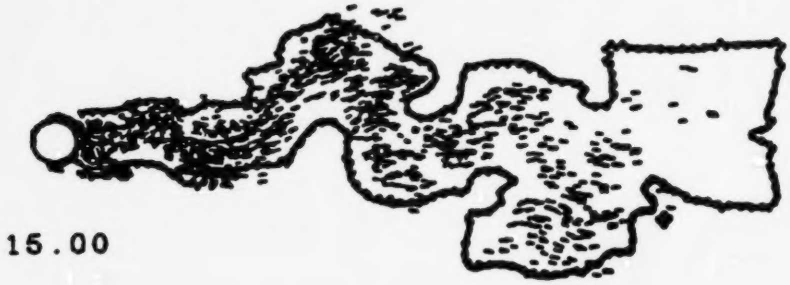

(d) Re = 10^4, Su = 0.040, V = 8.0;

Fig. 36 Flame front contours of different cases at T = 15.0 .

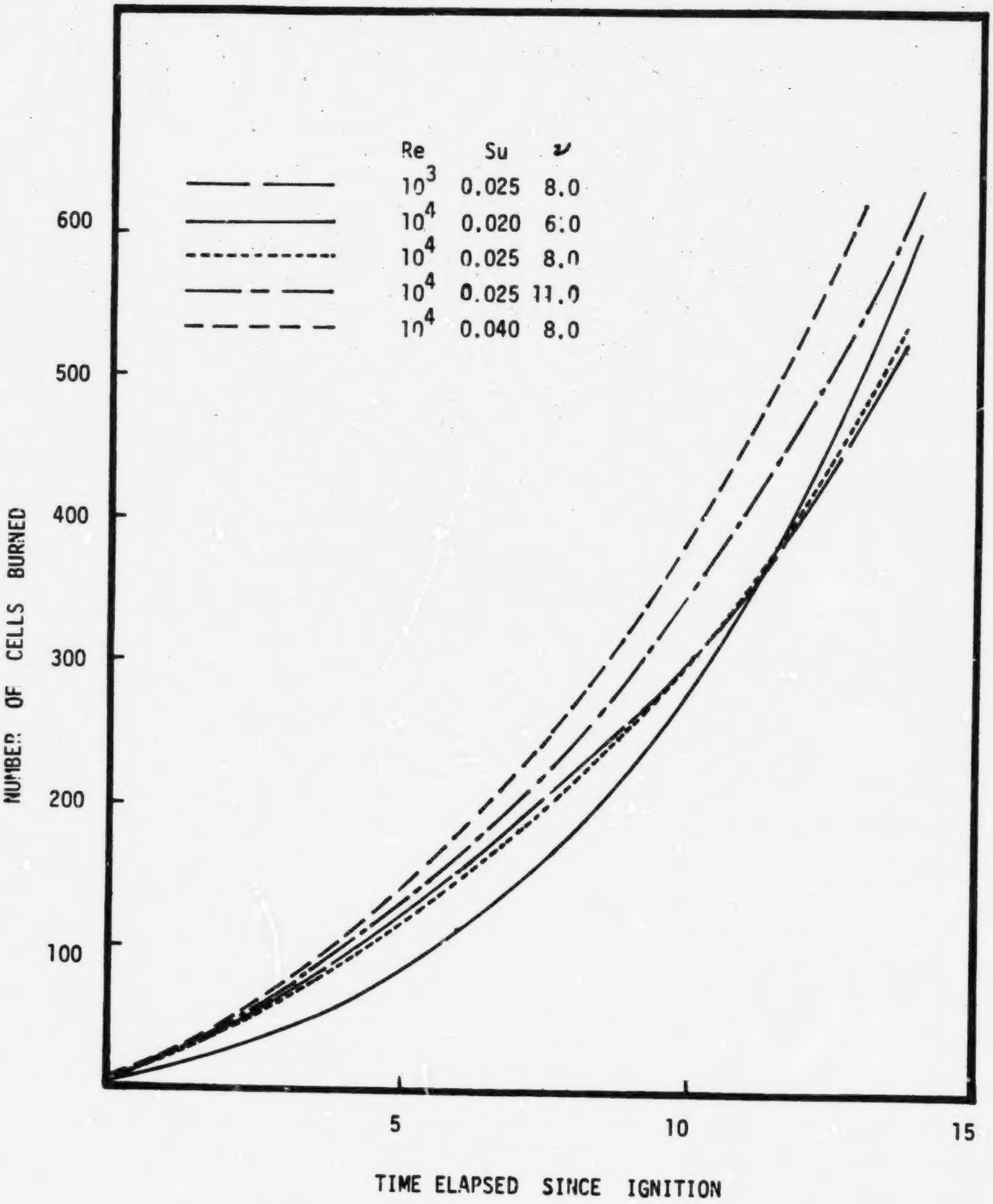

Fig. 37 Reaction rates of different reacting flows as a function of time.

References

Ashurst, W.T., Durst, F., and Tropea, C. 1980, "Two-Dimensional Seperated Flow : Experiment and Discrete Vortex Dynamics Simulation", AGARD Report, 24, 1-13.

Ashurst, W.T. 1981, "Vortex Simulation of a Model Turbulent Combustor", Prog. Astronaut. Aeronaut., 76, 259-273.

Baker, G.R. 1979 ,"The Cloud-in-Cell Technique Applied to the Roll Up of Vortex Sheets", J. Comput. Phys., 31, 76-95.

Bray, K.N.C., Libby, P.A. and Moss, J.B. 1984, "Scalar Length Scale Variations in Premixed Turbulent Flame", 20th Symposium (International) on Combustion, Ann Arbor, Michigan.

Brigg, M., Mellor, G., and Yamada, Y. 1976, "A Second-Moment Turbulence Model Applied to Fully Separated Flows", in Turbulence in Internal Flows, ed. by S.N.B. Murthy, Hemishere Pub. Co., Washington.

Buzbee, B.L., Golub, G.H. and Nielson, C.W. 1970, SIAM J. Numer. Anal., 7, 627.

Cantwell, B. and Coles, D. 1983, "An Experimental Study of Entrainment and Transport in the Turbulent Near Wake of a Circular Cylinder", J. Fluid Mech., 136, 321-374.

Cheer, A.Y. 1983, "A Study of Incompressible 2-D Vortex Flow Past a Circular Cylinder", SIAM J. Sci. Stat. Comp., 685-705.

Chen, D.-Y., A.F. Ghoniem and A.K. Oppenheim 1983 "Experimental and

Theoretical Study of Combustion Jet Ignition", NASA Report, CR-168139, 130pp.

Cheng, R.K. and Ng, T.T. 1983, "Velocity Statistics in Premixed Turbulent Flames", Comb. and Flame, 52, 185-202.

Chorin, A.J. 1973, "Numerical Studies of Slightly Viscous Flow", J. Fluid Mech. 57, 785-596.

Chorin, A.J. 1978, "Vortex Sheet Approximatation of Boundary Layers", J. comput. Phys. 27, 428-442.

Chorin, A.J., Hughes, T.J.R., McCracken, M.F. & Marsden, J.E. 1978, "Product Formulas and Numerical Algorithms" ,Communs. Pure Appl. Math. 31, 205-256.

Chorin, A.J. 1980, "Flame Advection and Propagation Algorithms", J. Comput. Phys., 35, 1-11.

Christiansen, J.P. 1973, "Numerical Simulation of Hydrodynamics by the Method of Point Vortices", J. Comput. Phys. 13, 363-379.

Clements, R.R. 1973, "An Inviscid Model of Two-Dimensional Vortex Shedding", J. Fluid Mech., 57, 2, 321-336.

Dai, Y.W., Ghoniem, A.F., Sherman, F., and Oppenheim, A.K. 1983, "Numerical Modeling of Turbulent Flow in a Channel", NASA Report CR-168278, 63pp.

Dandekar, K.V. and Gouldin, F.C. 1982, "Temperature and Velocity Measurements in Premixed Turbulent Flames", AIAA J., 20, 5, 652-660.

Davis, R.W. and Moore, E.F. 1982, "A Numerical Study of Vortex Shedding from

Rectangles", J. Fluid Mech., 116, 475-506.

Dorr, F.W. 1970, "The Direct Solution of the Discrete Poisson Equation on a Rectangle", SIAM Review, 12, 2, 248-263.

Durst, F., Tropea, C. 1981, "Turbulent, Backward-Facing Step Flows in Two-Dimensional Ducts and Channels"

Eaton, J.K., Johnston, J.P. 1981, "A Review Of Research on Subsonic Turbulent Flow Reattachment", AIAA J., 19, 9, 1093-1100.

El-Benhawy, Y., Sivasegram, S., and Whitelaw, J.H. 1983 "Premixed, Turbulent Combustion of a Sudden-Expansion Flow", Comb. & Flame, 50, 153-165.

Ellis, O.C. de C. 1928, "Flame Movement in Gaseous Explosive Mixtures (part 7)", Fuel: a Journal of Fuel Science, 7, 6, 502-508.

Etheridge, D.W. and Kemp, P.H. 1978, "Measurement of Turbulent Flow Downstream of a Rearward-Facing Step", J. Fluid Mech., 86, 3, 545-566.

Frankel, S.P. 1950, "Convergence Rates of Iterative Treatments of Partial Differential Equations", Math. Table and Other Aids to Comput., 4, 65-75.

Fromm, J.E. and Harlow, F.H. 1963, "Numerical Solution of the Problem of Vortex Sheet Development", Phys. Fluids, 6, 975.

Ganji, A.R. and Sawyer, R.F. 1980, "An Experimental Study of The Flow Field of a Two-Dimensional Premixed Turbulent Flame", AIAA J., 18, 817-824.

Gerrard, J.H. 1966, "The Mechanics of the Formation Region of Vortices Behind Bluff Bodies", J. Fluid Mech., 25, 401-413.

Ghoniem, A.F., Chorin, A.J. & Oppenheim, A.K. 1982, "Numerical Modeling of Turbulent Flow in a Combustion Tunnel", Phil. Trans. R. Soc. Lond. A 304, 303-325.

Giovannini, A. 1984, Private Communication.

Guenoche. H. 1964, "Flame Propagation in Tubes and in Closed Vessels", Non-steady Flame Propagation, ed. Markstein, G.H., Pergamon Press, New York.

Hald, O.H. 1979, "Convergence of Vortex Methods for Euler's Equations, II.", SIAM J. Numer. Anal. 16, 5, 726-755.

Hess, J.L. and Smith, A.M.O. 1967, "Calculation of Potential Flow About Arbitrary Bodies", Prog. in Aero. Science 8, 1-138

Hsiao, C.C., Ghoniem, A.F., Chorin, A.J. and Oppenheim, A.K. 1984, "Numerical Simulation of a Turbulent Flame Stabilized Behind a Rearward-Facing Step", the 20th Symposium (International) on Combustion, The Combustion Institute, Pittsburgh, PA.

Keller, J.O., Vaneveld, L., Krochlet, D., Hubbard, G.L., Ghoniem, A.F., Daily, J.W. and Oppenheim, A.K. 1982, "Mechanisms of Instabilities Leading to Flashback", AIAA J. 20, 2, 254-262.

Kellogg, O.D. 1929, "Foundations of Potential Theory" , Dover, New York.

Kilham, J.K. and Kirmani, N. 1979, 17th Symposium (International) on Combustion, The Combustion Institute, Pittsburgh, PA.

Landau, L.D. 1944, "On the Theory of Slow Combustion", J. Exp. Theor. Phys., 14, 240-249.

Leonard, A. 1980, "Vortex Methods for Flow Simulation", J. Comp. Phys. 37, 3, 289-335.

Majda, A. and Sethian, J. 1984. "The Derivation and Numerical Solution of the Equations for Zero Mach Number Combustion", LBL Report, LBL-17289.

McDonald, H. 1979, "Combustion Modeling in Two and Three Dimensions - Some Numerical Considerations", Prog. Energy Combustion Science, 5, 97-122.

Mellor, A.M. and Ferguson, C.R. 1980, "Pratical Problems in Turbulent Reacting Flow", Turbulent Reacting Flows, ed. by P. Libby and F. Williams, Springer-Verlag, 45-64.

Milne-Thomson, L.M. 1971, "Theoretical Hydrodynamics".

Noh, W.T. & Woodward, P. 1976, "SLIC(Simple Line Interface Calculation)", Proc. 5th Int. Conf. Numer. Math. Fluid. Mechanics, 330-339, Berlin: Springer-Verlag.

Oppenheim, A.K. & Ghoniem, A.F. 1983, "Aerodynamic Features of Turbulent Flames", AIAA 21st Aerospace Sciences Meeting, Reno, Nevada.

Papilou, P.S. and Lykoudis, P.S. 1974, "Turbulent Vortex Streets and the Entrainment Mechanism of the Turbulent Wake", J. Fluid Mech., 62, 11-31.

Paris, J. & Whitaker, S. 1965, "Confined Wakes: A Numerical Solution of the Navier-Stokes Equations", American Inst. of Chem. Engr. J. 11, 6, 1033-1041.

Peaceman, D.W. & Rachford, H. H. Jr 1955, "The Numerical Solution of Parabolic and Elliptic Differential Equations", J. Soc. Indust. Applied Math. 3, 1, 28-41.

Peters, N. and Williams, F.A. 1980, "Coherent Structures in Turbulent Combustion", The Role of Coherent Structures in Modeling Turbulence and Mixing, ed. by J. Jimenez, Lecture Notes in Physics, 136, Springer-Verlag.

Petersen, R.E. and Emmons, H.W. 1961, "Stability of Laminar Flames", Phys. Fluids, 4, 456-464.

Pitz, R.W. and Daily, J.W. 1983, "Experimental Study of Combustion in a Turbulent Free Shear Layer Formed at a Rearward-Facing Step", AIAA J. 21, 11, 1565-1570.

Roache, P.J. 1971, "A Direct Method for the Discretized Poisson Equation", SC-RR-70-579, Sandia Laboratories, Albuguergue, New Mexico.

Rosenhead, L. 1931, "The Formation of Vortices From a Surface of Continuity", Proceedings of the Royal Society, London, A, 134, 170-192.

Sand, I.O. 1984, "The Potential Flow in a Channel with Cavity", CMI Ref No. 843403-3, R. Norwegian Council for Scien. and Indus. Research, Bergen, Norway.

Shepherd, I.G., Moss, J.B., and Bray, K.N.C. 1982 ,"Turbulent Transport in a Confined Premixed Flame", 19th Symposium (international) on Combustion, 423-431, The Combustion Institute, Pittsburgh.

Sivashinsky, G.I. 1976, "On a Distorted Flame Front as a Hydrodynamic Discontinuity", ACTA Astronautica, 3, 11-12, 889-918.

Sivashinsky, G.I. 1979, "Hydrodynamic Theory of Flame Propagation in an

Enclosed Volume", ACTA Astronautica, 6, 5-6, 631-646.

Sivashinsky, G.I. 1982, "Instabilities, Pattern Formation, and Turbulence in Flames", LBL Report, LBL-14133.

Susuki, T., Hirano, T. and Tsuji, H. 1979, 17th Symposium (International) on Combustion, The Combustion Institute, Pittsburgh, PA.

Swarztrauber, P. 1975, "Efficient Fortran Subprograms for the Solution of Elliptic Partial Differential Equations", NCAR Report, TN-109+IA.

Takagi, T., Shin, H. and Ishio, A. 1980, "Local Laminarization in Turbulent Flames", Combustion & Flames, 37, 163-170.

Takami, H. 1964, "A Numerical Experiment with Discrete Vortex Approximation, with Reference to the Rolling Up of a Vortex Sheet", AFOSR, 64, 1536.

Tennekes, H. & Lumley, J.L. 1972, "A First Course in Turbulence", MIT Press, Cambridge, Mass.

Theodorsen, T. 1932, "Theory of Wing Sections of Arbitrary Shape", NACA Report No. 411.

Walterick, R.E., Jagoda, J.E., Richardson, C.R.J., de Groot, W.A., Strahle, W.C. and HUbbartt, J.E. 1984, "Experimental and Computation on Two-Dimensional Turbulent Flow Over a Backward Facing Step", AIAA-84-0013, AIAA 22nd Aerospace Sciences Meeting, Reno, Nevada.

Williams, F.A. 1974, "A Review of Some Theoretical Consideration of Turbulent Flame Structure", AGARD REP 43rd Meetings, Liege, Belgium, II, 1-125.

Wright, F.H. and Zukoski, E.E. 1960, "Flame Spreading from Bluff-Body

Flameholder", 8th Symposium (International) on Combustion, 933-944, Reinhold Publishing Co., NY.

Yoshida, A. and Tsuji, H. 1984, "Mechanism of Flame Wrinkling in Turbulent Premixed Flames", 20th Symposium (International) on Combustion, The Combustion Institute, Pittsburgh, PA.

*U.S. GOVERNMENT PRINTING OFFICE: 1986-646-114-20419

1. Report No. NASA CR-175005	2. Government Accession No.	3. Recipient's Catalog No.

4. Title and Subtitle Aerodynamic Properties of Turbulent Combustion Fields	5. Report Date November 1985
	6. Performing Organization Code
7. Author(s) Chia-Chun Hsiao and A.K. Oppenheim	8. Performing Organization Report No. None
	10. Work Unit No.
9. Performing Organization Name and Address University of California, Berkeley Berkeley, California 94720	11. Contract or Grant No. NAG 3-131
12. Sponsoring Agency Name and Address National Aeronautics and Space Administration Washington, D.C. 20546	13. Type of Report and Period Covered Contractor Report
	14. Sponsoring Agency Code 505-36-22

15. Supplementary Notes

Final Report. Project Manager, Cecil J. Marek, Altitude Wind Tunnel Project Office, NASA Lewis Research Center, Cleveland, Ohio 44135.

16. Abstract

Flow fields involving turbulent flames in premixed gases under a variety of conditions are modeled by the use of a numerical technique based on the random vortex method to solve the Navier-Stokes equations and a flame propagation algorithm to trace the motion of the front and implement the Huygens principle, both due to Chorin. A successive over-relaxation hybrid method is applied to solve the Euler equation for flows in an arbitrarily shaped domain. The method of images, conformal transformation, and the integral-equation technique are also used to treat flows in special cases, according to their particular requirements. Salient features of turbulent flame propagation in premixed gases are interpreted by relating them to the aerodynamic properties of the flow field. Included among them is the well-known cellular structure of flames stabilized by bluff bodies, as well as the formation of the characteristic tulip shape of flames propagating in ducts. In its rudimentary form, the mechanism of propagation of a turbulent flame is shown to consist of (i) rotary motion of eddies at the flame front, (ii) self-advancement of the front at an appropriate normal burning speed, and (iii) dynamic effects of expansion due to exothermicity of the combustion reaction. An idealized model is used to illustrate these fundamental mechanisms and to investigate basic aerodynamic features of flames in premixed gases. The case of a confined flame stablized behind a rearward-facing step is given particular care and attention. Solutions are shown to be in satisfactory agreement with experimental results, especially with respect to global properties such as the average velocity profiles and reattachment length. Velocity fluctuations are found to compare quite well with experimental data, exhibiting discrepancies which can be plausibly ascribed to three-dimensional effects and the scarcity of the numerical data sample. The unconfined turbulent flow behind a circular flameholder is calculated to study the detailed mechanism of flame stabilization. The process of vortex shedding and the development of the Von Karman vortex street at a high Reynolds number are described in terms of the vorticity field and the instantaneous streamline pattern. Although the flame front is stabilized on the outer contours of eddies, the classical alternating large scale structure of the wake is destabilized by the expansion due to the exothermicity of combustion. The parametric study of flame propagation indicates that the flame spread and the burning rate are relatively insensitive to the Reynolds number in the range under consideration, whereas the product of the normal burning speed and the normalized density ratio increment across the front, expressing the action of the flame as a velocity source, is of crucial importance.

17. Key Words (Suggested by Author(s)) Vorticity; Turbulent combustion; Premixed; Random vortex method; Computation	18. Distribution Statement Unclassified - unlimited STAR Category 07

19. Security Classif. (of this report) Unclassified	20. Security Classif. (of this page) Unclassified	21. No. of pages 135	22. Price* A07

*For sale by the National Technical Information Service, Springfield, Virginia 22161

127.